Published by Institute of Physics Publishing for SISSA
Received: *May 8, 2007*
Accepted: *June 2, 2007*
Published: *June 15, 2007*

Dirichlet sigma models and mean curvature flow

Ioannis Bakas and Christos Sourdis

Department of Physics, University of Patras,
GR-26500 Patras, Greece
E-mail: bakas@ajax.physics.upatras.gr,
sourdis@pythagoras.physics.upatras.gr

Abstract: The mean curvature flow describes the parabolic deformation of embedded branes in Riemannian geometry driven by their extrinsic mean curvature vector, which is typically associated to surface tension forces. It is the gradient flow of the area functional, and, as such, it is naturally identified with the boundary renormalization group equation of Dirichlet sigma models away from conformality, to lowest order in perturbation theory. D-branes appear as fixed points of this flow having conformally invariant boundary conditions. Simple running solutions include the paper-clip and the hair-pin (or grim-reaper) models on the plane, as well as scaling solutions associated to rational (p, q) closed curves and the decay of two intersecting lines. Stability analysis is performed in several cases while searching for transitions among different brane configurations. The combination of Ricci with the mean curvature flow is examined in detail together with several explicit examples of deforming curves on curved backgrounds. Some general aspects of the mean curvature flow in higher dimensional ambient spaces are also discussed and obtain consistent truncations to lower dimensional systems. Selected physical applications are mentioned in the text, including tachyon condensation in open string theory and the resistive diffusion of force-free fields in magneto-hydrodynamics.

Keywords: Renormalization Group, Sigma Models, Differential and Algebraic Geometry, D-branes.

JHEP06(2007)057

© SISSA 2007

Contents

JHEP06(2007)057

1. Introduction

The theory of geometric flows is a modern subject of common interest in physics and mathematics. In abstract terms, one is led to consider continuous deformations of geometric quantities defined on Riemannian manifolds (of fixed topology) starting from some initial data and evolve it under a given set of parabolic equations with respect to the flow variable t, called time. When the driving term of the deformation is provided by the curvature, in various forms, the corresponding geometric evolutions are called curvature flows. These are naturally divided into two distinct classes, intrinsic and extrinsic curvature flows, depending on whether one deforms the metric on a Riemannian manifold $\mathcal{M}$ by its Ricci curvature or a submanifold $\mathcal{N}$ embedded in $\mathcal{M}$ by the associated extrinsic curvature. Since extrinsic geometry is more elementary than intrinsic geometry, as the simple example of planar curves illustrates, one expects that extrinsic curvature flows have longer history in science, as they do. The mathematical motivation for introducing geometric flows varies from one type to the other and the same also applies to their physical origin and diverse applications. However, what makes them worth studying is the undisputed fact that such a simple minded framework, based on geometric analysis, had far reaching consequences and led to ground breaking results in recent years.

The main qualitative feature of curvature flows is their tendency to dissipate any possible deviations from canonical geometries associated to fixed point configurations with special curvature. It is typical that intrinsic flows will deform the metrics towards constant curvature metrics, if they exist on a given Riemannian manifold. Likewise, extrinsic flows will deform the embedded submanifolds towards special configurations with prescribed extrinsic curvature, e.g., minimal submanifolds and generalizations thereof. This behavior is expected from parabolic equations on Riemannian manifolds, since they share common properties with the heat equation; actually, the latter is a local linear approximation to the late stage evolution of geometries in the vicinity of the fixed points. These particular properties have turned geometric flows into a valuable tool for addressing a variety of long standing problems in differential geometry, such as the geometrization of manifolds in low dimensions, and many others. In practice, one should device suitable systems of flows for a given class of geometric data and follow their evolution towards configurations with prescribed curvature. In all cases there are many technical obstacles related to the possible formation of singularities along the flows, and their mathematical classification, which affect the long time behavior of solutions and need to be accounted for complete study.

The prime example of intrinsic curvature flow is the celebrated Ricci flow that deforms metrics by their Ricci curvature tensor. It first arose in the physics literature as renormalization group equation for the coupling constant of non-linear sigma models defined in two dimensions, [1]. In this case, the deformation variable t is the logarithm of the world-sheet length scale of the field theory and the metric of the target space -viewed as generalized coupling- receives counter-terms that are computable by the perturbative renormalizability of the two-dimensional quantum field theory. Then, in this context, the Ricci flow describes the response of the target space metric to different energy (and hence

JHEP06(2007)057

length) scales of the quantum theory to lowest order in perturbation theory, [2]. When the renormalization group equation of sigma models is applied to spaces of positive curvature, it implies, in particular, that the quantum theory becomes asymptotically free in the ultra-violet regime, thus justifying the use of perturbative calculations at high energies. This is analogous to the asymptotic freedom exhibited by non-Abelian gauge theories in four space-time dimensions, [3], which, after all, motivated the study of renormalization group flows in toy quantum field theories, such as non-linear sigma models in two dimensions.

The derivation of the beta function equations for non-linear sigma models played a prominent role in the development of string theory, since fixed points of the Ricci flow are selected by the requirement of conformal invariance on the world-sheet. Generalizations in the presence of dilaton and anti-symmetric tensor fields were also considered in the literature, [4 – 6], thus leading to coupled systems of beta function equations for the massless modes of closed strings which can be derived from an effective gravitational action in target space. Critical string theory in curved spaces is only concerned with the existence and construction of fixed point solutions to these equations. However, it was realized in recent years that the problem of tachyon condensation in closed string theory can be studied as off-shell process involving trajectories between different fixed points, via the renormalization group equations, in the weak gravitational regime. Thus, genuine running solutions of the Ricci flow, and its generalizations, are of great interest for exploring the problem of vacuum selection in closed string theory.

The Ricci flow was introduced independently in the mathematics literature as new analytic tool to attack Poincaré's conjecture and related geometric problems in three dimensions, [7]; in this context it also became known as Hamilton-Ricci flow. Since then there have been may important developments which are summarized in ref. [8, 9], together with the complete list of original contributions to the subject. Quite recently, Hamilton's programme was brought to completion by solving the long standing geometrization problem of compact 3-manifolds by the Ricci flow, [10], in all generality; see also ref. [11] for an overview of this subject. The classification of singularities that may arise in the process and the introduction of appropriate entropy functionals for the Ricci flow have played important role in these studies. However, their relations to physics have not been entirely clarified so far. It also remains to understand in general mathematical terms the structure of the generalized Ricci flows, in the presence of anti-symmetric tensor fields, and their relevance to the formation of singularities. Finally, instanton corrections to the beta function equations of non-linear sigma models, [12], which are quite customary in physics and usually affect the nature of the infra-red fixed points, are still awaiting for their proper mathematical interpretation in the context of geometric analysis by Ricci flow. Non-trivial infra-red fixed points are known to exist by adding topological torsion terms with $\theta = \pi$ in sigma models, [13].

The prime example of extrinsic curvature flow is provided by the mean curvature flow of hypersurfaces that deform by their extrinsic mean curvature vector in the ambient space. It first arose in the physics literature as idealized (two-dimensional) model for the motion of grain boundaries in an annealing piece of metal, [14], by drawing analogies with the motion of soap bubbles and interfaces due to their surface tension; see also ref. [15]

JHEP06(2007)057

for a similar model for the development of a surface groove by evaporation-condensation mechanism. The subject was subsequently generalized and put on firm mathematical base in ref. [16]. Later, it flourished and became a whole area of intense study in mathematics up to the present time; see, for instance, the recent textbooks [17 – 19] and references therein. The mean curvature flow arises, in its original formulation, as gradient flow for the area functional of a hypersurface embedded in a fixed Riemannian manifold and as such it encompasses minimal surfaces among its critical points. Thus, it offers a new analytic tool in the framework of geometric analysis for studying minimal submanifolds, such as geodesics curves, and various isoperimetric problems associated with them. The structure of the singularities that may form on the way and the construction of entropy functionals for this flow are some of the main technical problems which are well investigated by now, as for the Ricci flow.

Apart from its intrinsic mathematical interest, the mean curvature flow has several physical applications serving as local model for the evolution of interfaces and the dendritic crystal growth, [20], the formation of labyrinthine patterns in ferro-fluids, [21], the rendezvous problem for mobile autonomous robots, [22], and others that will be discussed in due course. There are also some variants of this flow, which will not be examined in this paper, that have led to ground breaking results in the mathematical theory of general relativity, [23]. However, what has been lacking, up to this day, was an account of the mean curvature flow in quantum field theory analogous to the Ricci flow.

The primary aim of the present work is to describe in detail the field theoretic manifestation of the mean curvature flow, and some of its generalizations, as boundary renormalization group equations for Dirichlet sigma models defined on two-dimensional regions with boundary, [24]. This connection was first pointed out in ref. [25] but without offering the details. Thus, it turns out that the renormalization group analysis of sigma models with embedded branes in their target space provide a natural field theoretic framework to address and interpret many important results that have been derived in the mathematics literature on the mean curvature flow. At the same time, new ideas can be brought in mathematics by implementing the perturbative and non-perturbative aspects of quantum field theories with boundaries in the modern trends and studies. In this context, the mean curvature flow is tautonymous to the boundary renormalization group flow, to lowest order in perturbation theory, whereas the fixed points of the flow, which correspond to conformally invariant boundary conditions, are the familiar D-branes in target space. Running solutions become applicable to the problem of tachyon condensation in open string theory and to the Kondo effect of screening magnetic impurities by conduction electrons in metals.

There has been considerable activity in recent years on boundary renormalization group flows and related quantum field theory problems, [26 – 31]. Most of the existing work concerns the construction of integrable quantum field theories of boundary interactions and their target space and world-sheet interpretation. These are based on mini-superspace models of the complete boundary flow, which is defined, in all generality, as dynamical system in the infinite dimensional space of all possible embedded configurations $\mathcal{N}$ in a given background $\mathcal{M}$. The ambient space can be arbitrary, having its own renormalization group flow, but to simplify matters only models with boundary interactions on Ricci flat

JHEP06(2007)057

target spaces have been considered so far. Even the simplest case of boundary interactions in the quantum field theory of two free bosons, represented by embedded curves in R^2, is quite rich and has not been fully explored yet. Specific proposals were made in this context for the exact form of the boundary quantum states of the so called semi-classical circular, paper-clip and hair-pin curves in R^2, which take into account perturbative as well as instanton corrections, but their validity has only been tested in special limits. Boundary states associated to more general trajectories of the renormalization group flow do not seem tractable, to this day, due to the absence of systematic framework connecting the world-sheet with the target space description of deforming branes. The exact characterization of fixed points, satisfying appropriate Virasoro constraints, [32], or (in some cases) extended conformal world-sheet symmetries, is also a difficult problem that has not been brought to the same level of understanding as for the bulk conformal field theories. Finally, the existence and construction of non-trivial infra-red fixed points, which take into proper account non-perturbative effects, as in the case of sigma models with $\theta = \pi$ terms, have not been investigated in all generality (see, however, ref. [26]–[31] for results in some special cases). Thus, it is only fair to say that the subject of boundary interactions and associated flows in quantum field theory is still at its infancy, in many respects, and any new insight cannot do less but contribute further to its development.

Here, we will concentrate entirely on the target space description of running branes, as they arise in the semi-classical regime, examine general features of the mean curvature flow and obtain exact solutions. Although several of these solutions are known in the mathematics literature, there has been no proper mention or use in quantum field theory apart from some notable cases. Apart from bridging this gap, new solutions will also be constructed and studied in detail. Most results will be limited to two dimensions, where the mean curvature flow assumes its simplest - yet quite non-trivial - form for embedded or more generally immersed curves in R^2. However, generalizations to curved spaces in two or higher dimensions will also be in focus, in which case the metric of the ambient space may also deform according to the Ricci flow. This combination of intrinsic and extrinsic curvature flows is quite natural from the physics point of view, as derived from the generalized system of beta function equations for non-conformal sigma models with non-conformal boundary conditions. It should be contrasted to the form of the mean curvature flow appearing in the mathematics literature, where the metric of the ambient space is usually fixed once and for all.

Further generalizations entail the inclusion of anti-symmetric tensor fields and Abelian gauge fields, which substitute the area functional of the mean curvature flow by the corresponding Dirac-Born-Infeld action, [33 – 35]. The presence of fluxes supports the existence of new solutions and alters the structure of the fixed points, as in the case of Ricci flow. In this context, the beta function of the gauge field also finds its proper place in mathematics in terms of the so called (Abelian) Yang-Mills flow. Thus, the sigma model approach to the closed and open sectors of string theory provide a unifying framework for studying all these different kind of geometric flows. In the general case one has to consider the coupled system of beta function equations for all massless modes of the string. The addition of fluxes will be addressed properly in future works.

JHEP06(2007)057

The presentation of the material is organized as follows. In section 2, the theory of Dirichlet sigma models is summarized and their boundary renormalization group equation is identified with the mean curvature flow. In section 3, the flow is considered on the two-dimensional plane and various forms are derived in view of the applications. Entropy functionals and their relevance to the structure of singularities are discussed. In section 4, several running solutions on the plane are introduced and studied in detail; they include special curves that evolve by translations, rotation or scaling, as well as other configurations that provide consistent mini-superspace truncations of the general evolution equations. Some of these solutions have already appeared in the physics literature, but several others, like the Abresch-Langer curves (to be discussed later), have not yet found a proper place; they may serve as (p, q) models for boundary interactions in an appropriate setup. In section 5, a thorough analysis of the (in)stability modes associated to special solutions is performed and general results on the eigenvalues of the linearized operators are obtained in terms of supersymmetric quantum mechanics. Then, geometric transitions between different configurations are envisaged for various curves. In section 6, generalizations of the mean curvature flow are considered on two-dimensional curved spaces. The simplest examples are provided by curves embedded in the Euclidean black hole background, with the familiar cigar shape, which is a Ricci soliton. Other examples include curve shortening problems on simple backgrounds that also deform by the Ricci flow, such as the sphere and its axially symmetric sausage-like variations. In section 7, we consider the mean curvature flow of surfaces in R^3 and then specialize to cylindrical branes as well as branes of revolution. Their evolution is reduced to an effective curve shortening problem on the plane. Finally, in section 8, we present the conclusions and list directions for further work.

There are also three appendices included at the end for completeness. Appendix A summarizes the embedding equations of hypersurfaces in Riemannian geometry and provides the appropriate definitions. Appendix B compares the mean curvature flow to other systems of evolution equations for planar curves and draws connections to integrable systems. Appendix C reviews the emergence of the mean curvature flow from magnetohydrodynamics by dimensional reduction of the resistive diffusion of force-free magnetic fields. Several exact solutions discussed in the paper can be re-interpreted in this context and enjoy astrophysical applications.

Parts of this paper can be considered as review of the main mathematical results on the mean curvature flow, but even in those cases there are supplementary details and alternative viewpoints that are of interest in physical applications. We hope that their systematic presentation will prove useful in many respects. The world-sheet description of various solutions, the role of non-perturbative effects in the characterization of the exact boundary states, as well as the addition of fluxes will be left to future publications.

2. Dirichlet sigma models

Consider a two-dimensional sigma model associated to maps of a two dimensional surface Σ into a general Riemannian manifold $\mathcal{M}$ with local coordinates X^μ and metric $G_{\mu\nu}(X)$. It serves as classical model for string propagation in target space $\mathcal{M}$ of dimension m,

JHEP06(2007)057

whereas Σ is the two-dimensional world-sheet that is generally assumed to have boundary $\partial\Sigma$. For practical purposes, Σ is taken to be a disc with connected boundary $\partial\Sigma = S^1$; more complicated world-sheets, such as the annulus, may also be considered if higher loop string corrections are to be included in the study. Furthermore, (some of) the target space coordinates X^μ are taken to satisfy Dirichlet boundary conditions, i.e.,

$$X^\mu \mid_{\partial\Sigma} = f^\mu(y^A)\,, \tag{2.1}$$

where y^A are local coordinates in an n-dimensional submanifold $\mathcal{N}$ of $\mathcal{M}$. These boundary conditions ensure that the variations of the sigma model fields along the world-sheet boundary, $\delta X^\mu \mid_{\partial\Sigma}$, are tangent to $\mathcal{N}$. According to this, there are $m-n$ Dirichlet conditions imposed on the fields, in general, thus defining $\mathcal{N}$ as classical brane embedded in $\mathcal{M}$. Then, the embedding equations (2.1) follow the general theory of Riemannian geometry as outlined in appendix A. The extrinsic curvature of the classical branes $\mathcal{N}$, as well as the Ricci curvature of the ambient space $\mathcal{M}$, are arbitrary at this point, but they will be shortly constrained by quantum mechanical requirements if conformal invariance on Σ is to be maintained to lowest order in perturbation theory.

2.1 Ricci and mean curvature flows

With these explanations in mind, the corresponding Dirichlet sigma model is defined by the classical action

$$S = \frac{1}{4\pi\alpha'}\int_\Sigma d^2z\; G_{\mu\nu}(X)\delta^{ab}\partial_a X^\mu \partial_b X^\nu + \frac{1}{2\pi\alpha'}\oint_{\partial\Sigma} d\tau\; G_{\mu\nu}(X)V^\mu(X)\partial_n X^\nu \tag{2.2}$$

using conformally flat coordinates on Σ. Here, τ denotes the parameter along the world-sheet boundary and ∂_n is the derivative operator normal to it. The boundary contribution to the usual two-dimensional action allows for the coupling of arbitrary vector fields in target space that are perpendicular to the submanifold $\mathcal{N}$. Thus, as it is customary, $G_{\mu\nu}(X)$ is considered as generalized bulk "coupling constant" of the two-dimensional sigma model and $V^\mu(X)$ as the corresponding generalized boundary "coupling constants". There are $m-n$ independent vector fields V^μ of $\mathcal{M}$ that can couple to the normal derivatives of the fields X^μ at $\partial\Sigma$. Note the additional possibility to consider n fields coupled to the tangent derivatives of the coordinate fields y^A in $\mathcal{N}$ along the world-sheet boundary $\partial\Sigma$. They naturally form the components of a U(1) gauge field that lives on the brane; together with the anti-symmetric tensor field they may be used to provide flux generalizations of the present framework. Here, these additional fields are set to zero, thus only considering pure metric sigma models with embedded branes of arbitrary codimension. Throughout the paper, the signature of the world-sheet and of the target space will be assumed Euclidean.

Two-dimensional sigma models, with or without Dirichlet branes, are perturbatively renormalizable quantum field theories. First, there is the bulk renormalization group flow of the target space metric that follows from the standard computation of the metric beta function, [2],

$$\beta(G_{\mu\nu}) = R_{\mu\nu} \tag{2.3}$$

JHEP06(2007)057

to lowest order in perturbation theory. It is valid when all components of the curvature are small for otherwise higher order curvature terms arising from higher orders in perturbation theory become increasingly important. Such corrections will be excluded here, thus taking the lowest order result at face value. According to this analysis, sigma models are not scale invariant, in general, since their target space metric depends on the energy scale of the quantum field theory. In particular, identifying the logarithm of the world-sheet scale with the deformation variable t, one obtains the bulk renormalization group equation

$$\frac{\partial G_{\mu\nu}}{\partial t} = -R_{\mu\nu} + \nabla_\mu \xi_\nu + \nabla_\nu \xi_\mu \,, \tag{2.4}$$

by also including the possibility to perform arbitrary reparametrizations along the flow generated by a vector field ξ^μ. As such, it coincides with the general form of the (unnormalized) Ricci flow for $G_{\mu\nu}(X;t)$. The fixed points of this flow, $R_{\mu\nu} = \nabla_\mu \xi_\nu + \nabla_\nu \xi_\mu$, are in accordance to the scale invariance of the world-sheet theory for all vector fields ξ_μ. Note that the renormalization of the bulk metric is inert to the existence of embedded branes in target space.

A special instance of these equations arises for gradient vector fields, $\xi_\mu = -\partial_\mu \Phi$, in which case $\Phi(X)$ assumes the role of the dilaton associated to anomalous transformation law of the target space coordinates of sigma models, $\delta_\epsilon X^\mu = \epsilon \partial^\mu \Phi$, under Weyl transformations of the world-sheet metric, $\delta_\epsilon \gamma_{ab} = \epsilon \gamma_{ab}$. Recall, in this context, that the dilaton field $\Phi(X)$ enters into the bulk sigma model action as

$$S_{\rm bulk} = \frac{1}{4\pi\alpha'} \int_\Sigma d^2 z \, \sqrt{\det \gamma} \left(G_{\mu\nu}(X) \gamma^{ab} \partial_a X^\mu \partial_b X^\nu + \alpha' R[\gamma] \Phi(X) \right) \tag{2.5}$$

in order to ensure that the two-dimensional theory will remain renormalizable if the world-sheet metric γ is not flat, having non-vanishing curvature $R[\gamma]$. Then, the dilaton has its own beta function which together with the metric beta function yield the modified system of renormalization group equations of the bulk theory,

$$\frac{\partial}{\partial t} G_{\mu\nu} = -\beta(G_{\mu\nu}) = -R_{\mu\nu} - 2\nabla_\mu \nabla_\nu \Phi \,, \tag{2.6}$$

$$\frac{\partial}{\partial t} \Phi = -\beta(\Phi) = -(\partial_\mu \Phi)(\partial^\mu \Phi) + \frac{1}{2} \nabla^2 \Phi + \frac{26-m}{6\alpha'} \,. \tag{2.7}$$

The last term above accounts for the central charge of the model and it can be arranged so that it cancels in critical string theory. Here, the central terms will be kept, since the dimension m is arbitrary.

In any case, these beta functions satisfy m differential identities derived from the non-renormalization condition of the trace of the energy-momentum tensor of the sigma model, [36],

$$\partial_\mu \beta(\Phi) = (\partial^\nu \Phi) \beta(G_{\mu\nu}) + \frac{1}{2} \nabla^\nu \left(\beta(G_{\mu\nu}) - \frac{1}{2} G_{\mu\nu} G^{\lambda\rho} \beta(G_{\lambda\rho}) \right) , \tag{2.8}$$

which is valid for all t to lowest order in α'. Weyl invariance of the two-dimensional theory is only achieved at the fixed points of the modified $(G_{\mu\nu}, \Phi)$ flow; it should be compared to

JHEP06(2007)057

the weaker condition of scale invariance that was considered earlier. At the fixed points of the background metric flow, $\beta(G_{\mu\nu}) = 0$, equation (2.8) implies that $\beta(\Phi)$ is constant on $\mathcal{M}$ and can be set equal to zero without loss of generality. Thus, Weyl invariance implies $\beta(G_{\mu\nu}) = 0 = \beta(\Phi)$ simultaneously. Finally, note that the dilaton flow is also inert to the existence of branes in target space, as for the metric.

For sigma models with branes in their target space one also has to consider the dependence of the embedding equations (2.1) on the energy scale of the two-dimensional quantum field theory. This calculation was first performed in all generality in ref. [24], where it was found that the deformations of Dirichlet branes, as described by the one-parameter family of functions $f^\mu(y^A; t)$ that may depend on the logarithmic world-sheet length scale t, are driven by their extrinsic curvature vector to lowest order in perturbation theory. The analysis is performed by first considering the variation of the classical action (2.2) leading to the following set of compatible boundary conditions,

$$f^\mu_{,A} G_{\mu\nu} \partial_n X^\nu = 0\,, \qquad V^\mu = 0\,, \tag{2.9}$$

with respect to the embedding equations of $\mathcal{N}$ into $\mathcal{M}$. If one expands around such a reference configuration, denoted by $\bar{X}^\mu$, V^μ will decouple completely from the computation. However, if one considers quantum corrections, there will be counter-terms for V^μ that can be computed by regulating divergences of the relevant graphs with a short distance cutoff ϵ. Starting with the reference configuration $\bar{X}^\mu$, with $\bar{X}^\mu = f^\mu(\bar{y}^A)$ on $\partial\Sigma$ and introducing normal coordinates in target space and on the brane, as usual, the counter-term assumes the form

$$\Delta S = -\frac{1}{2\pi} \oint_{\partial\Sigma} d\tau\; G_{\mu\nu} \left(g^{AB} K^\sigma_{AB} \hat{n}^\mu_\sigma\right) \partial_n \bar{X}^\nu (\log\, \epsilon)\,, \tag{2.10}$$

to lowest order in perturbation theory, and changes V^μ accordingly.

Thus, to this order, the associated beta function for the boundary coupling is

$$\beta(V^\mu) = -g^{AB} K^\sigma_{AB} \hat{n}^\mu_\sigma\;. \tag{2.11}$$

Here, and above, the right-hand side involves the trace of the second fundamental form K^σ_{AB} of the brane with respect to the induced metric g^{AB} on it, $\hat{n}^\mu_\sigma$ is a complete basis of unit normal vectors to the brane in $\mathcal{M}$ and σ labels the transverse directions. In turn, one arrives at the following boundary renormalization group equation for the embedding conditions (2.1),

$$\frac{\partial f^\mu}{\partial t} = H^\sigma \hat{n}^\mu_\sigma - \xi^\mu, \tag{2.12}$$

using the notation of appendix A for the mean curvature vector normal to the brane. Here, we have also included the freedom to perform arbitrary reparametrizations along the flow generated by a vector field ξ^μ; it is the same vector field that enters into the Ricci flow (2.4). The resulting equation coincides with the general form of the (unnormalized) mean curvature flow studied in mathematics. We will take this equation at face value and suppress all

JHEP06(2007)057

possible higher curvature terms[1] which may arise at higher orders in perturbation theory. Within this approximation, and from now on, the two terms "boundary renormalization group flow" and "mean curvature flow" will be used without distinction.

The dilaton Φ is introduced by generalizing the Dirichlet sigma model (2.2) to curved world-sheets, so that the two-dimensional action consists of the bulk term (2.5) plus boundary contributions,

$$S = S_{\rm bulk} + \frac{1}{2\pi\alpha'} \oint_{\partial\Sigma} d\tau \left(G_{\mu\nu}(X) V^\mu(X) \partial_n X^\nu + \alpha' \kappa \Phi(X) \right) , \tag{2.13}$$

thus also taking into proper account the coupling of the dilaton to the extrinsic curvature κ of the boundary. The quantum theory is renormalizable and the boundary flow is provided by equation (2.12) above with $\xi^\mu = -\partial^\mu \Phi$. However, it should be noted at this point that if the ambient space exibits isometries generated by a Killing vector field k^μ, the choice $\xi^\mu = -\partial^\mu \Phi + k^\mu$ will affect the mean curvature flow but not the Ricci flow. Recall that $\partial_{(\mu} k_{\nu)}$ vanishes identically and so $\beta(G_{\mu\nu})$ does not change. As for the dilaton, it can be consistently taken to satisfy the relation $k^\mu \partial_\mu \Phi = 0$ and $\beta(\Phi)$ also does not change. Thus, apart from the standard bulk flows, we obtain the following boundary flow

$$\frac{\partial f^\mu}{\partial t} = H^\sigma \hat{n}^\mu_\sigma + \partial^\mu \Phi - k^\mu \ . \tag{2.14}$$

Weyl invariance of the quantum Dirichlet sigma model leads to fixed points of the combined buck and boundary renormalization group equations satisfying the general relations

$$R_{\mu\nu} = -2 \nabla_\mu \nabla_\nu \Phi \, , \qquad H^\sigma \hat{n}^\mu_\sigma = k^\mu - \partial^\mu \Phi \, , \tag{2.15}$$

supplemented by the vanishing condition for the dilaton beta function, when Φ is non-trivial,

$$(\partial_\mu \Phi)(\partial^\mu \Phi) - \frac{1}{2} \nabla^2 \Phi - k^\mu \partial_\mu \Phi = \frac{26 - m}{6\alpha'} \ . \tag{2.16}$$

Fixed points of this type will be discussed later in section 6.

According to all this, Dirichlet sigma models provide a natural framework to realize and unite both Ricci and mean curvature flows, since one has bulk and boundary renormalization group equations defined with respect to the same deformation variable t. Simple fixed points correspond to backgrounds with Ricci flat metrics in which there are embedded branes as minimal submanifolds (of arbitrary codimension), so that their extrinsic curvature vanishes; these are the familiar D-branes. More general fixed points also arise in the presence of non-trivial dilaton field. In either case, the corresponding solutions are associated to two-dimensional conformal field theories defined on a disc with conformally invariant boundary conditions. Away from the fixed points one has deformations of branes in deforming metric backgrounds, in general, but there is also the simpler possibility to consider Dirichlet branes with non-conformal boundary conditions deforming in backgrounds

[1] Such terms have been computed systematically in some cases in ref. [37] and [38], in analogy to higher curvature correction terms computed for the Ricci flow, [2], on general grounds; we thank Arkady Tseytlin for bringing some of those references to our attention. Further results can also be found in the more recent work ref. [39].

JHEP06(2007)057

with fixed metric satisfying bulk conformal invariance. The simplest example of this kind arises in the two-dimensional quantum field theory of several free bosons, in which case $\mathcal{M} = R^m$, and impose non-conformal boundary conditions on $\partial\Sigma$ so that the branes will not be embedded as minimal submanifolds. Even in such simple cases there can be many interesting possibilities, as will be seen later; also the systematic construction of the corresponding boundary states in quantum field theory is far from being complete, up to this day.

2.2 Gradient flow description

It is well known fact that the mean curvature flow of branes can be formulated as gradient flow of their volume functional,

$$V[f] = \int_{\mathcal{N}} d^n y \ \sqrt{\det g}\,, \tag{2.17}$$

given in terms of the determinant of the induced metric g_{AB}. Indeed, simple calculation shows that the first variation of the volume with respect to the embedding variables f^μ yields

$$\delta V[f] = \int_{\mathcal{N}} d^n y \ \sqrt{\det g}\ G_{\mu\nu} H^\sigma \hat{n}^\mu_\sigma \delta f^\nu \ . \tag{2.18}$$

In the presence of dilaton one has to consider the effective volume functional

$$V[f,\Phi] = \int_{\mathcal{N}} d^n y \ e^{-\Phi} \ \sqrt{\det g}\,, \tag{2.19}$$

and derive the generalized mean curvature flow as gradient flow

$$\frac{\partial}{\partial t} f^\mu(y;t) = H^\sigma \hat{n}^\mu_\sigma + \partial^\mu \Phi = \mathcal{G}^{\mu\nu} \frac{\delta V[f,\Phi]}{\delta f^\nu(y)} \tag{2.20}$$

with

$$\mathcal{G}^{\mu\nu} = \frac{G^{\mu\nu}}{e^{-\Phi}\sqrt{\det g}} \tag{2.21}$$

which is positive definite. $V[f,\Phi]$ can be extended to the full Dirac-Born-Infeld action in the presence of fluxes, [24].

When an evolution equation arises as gradient flow of the general form

$$\frac{d\varphi^I}{dt} = -\mathcal{G}^{IJ} \frac{\delta S[\varphi]}{\delta \varphi^J}\,, \tag{2.22}$$

it is natural to investigate its dissipative character and try to associate with it monotonic functionals in time. $S[\varphi]$ itself evolves in time as

$$\frac{d}{dt} S[\varphi] = \frac{\partial S}{\partial \varphi^I} \frac{d\varphi^I}{dt} = -\mathcal{G}^{IJ} \frac{\partial S}{\partial \varphi^I} \frac{\partial S}{\partial \varphi^J} \tag{2.23}$$

and, therefore, it decreases along the flow when $\mathcal{G}$ is positive definite. The mean curvature flow is an example of this kind, and, naturally, the branes deform by lowering their total volume towards minimal submanifolds. Of course, there can be other functionals which are

JHEP06(2007)057

also decreasing monotonically in time and serve as entropy of the deforming data. Examples of this will be encountered in section 3 for the mean curvature flow defined in flat ambient spaces. In general, there is no straightforward procedure to construct entropy functionals for gradient flows, which may exist irrespective of the positivity of $\mathcal{G}$; see, however, [40], for some recent general results in this direction.

Similar considerations can be applied to the Ricci flow for comparison. The Ricci flow arises as gradient flow from the Einstein-Hilbert action

$$S_{\rm E}[G] = \int_{\mathcal{M}} d^m X \ \sqrt{\det G}\ R[G] \tag{2.24}$$

i.e.,

$$\frac{\partial}{\partial t} G_{\mu\nu}(X;t) = \mathcal{G}_{\mu\nu,\kappa\lambda} \frac{\delta S_{\rm E}[G]}{\delta G_{\kappa\lambda}(X)} = -R_{\mu\nu}\ . \tag{2.25}$$

In this case, the appropriate matrix $\mathcal{G}$ is provided by the DeWitt metric in superspace consisting of all target space metrics on $\mathcal{M}$,

$$\mathcal{G}_{\mu\nu,\kappa\lambda}\delta G^{\mu\nu}\delta G^{\kappa\lambda} = \frac{1}{4}\int_{\mathcal{M}} d^m X\ \sqrt{\det G}\left(\delta G_{\mu\nu}\delta G^{\mu\nu} - \frac{1}{2}(\delta G^{\mu}{}_{\mu})(\delta G^{\nu}{}_{\nu})\right). \tag{2.26}$$

In the presence of dilaton, the modified Ricci flow is also described as gradient flow using the Einstein-Hilbert-dilaton action

$$S_{\rm E}[G,\Phi] = \int_{\mathcal{M}} d^m X\ \sqrt{\det G}\ e^{-2\Phi}\left(R[G] + 4(\partial_\mu\Phi)(\partial^\mu\Phi) + 2\frac{26-m}{3\alpha'}\right). \tag{2.27}$$

More precisely, setting $\varphi^I = (G_{\mu\nu}, \Phi)$, one finds that the beta functions of the metric and dilaton fields take the form

$$\frac{d\varphi^I}{dt} = -\mathcal{G}^{IJ}\frac{\delta S[\varphi]}{\delta\varphi^J}\,, \qquad \frac{\delta S[\varphi]}{\delta\varphi^I} = -\mathcal{G}_{IJ}\frac{d\varphi^J}{dt} \tag{2.28}$$

with

$$\mathcal{G}^{IJ} = \frac{1}{e^{-2\Phi}\sqrt{\det G}}\begin{pmatrix} 4G_{\mu\lambda}G_{\nu\rho} & G_{\mu\nu} \\ G_{\lambda\rho} & \frac{1}{4}(m-2) \end{pmatrix} \tag{2.29}$$

and

$$\mathcal{G}_{IJ} = \frac{1}{2}e^{-2\Phi}\sqrt{\det G}\begin{pmatrix} \frac{1}{2}(G^{\mu\lambda}G^{\nu\rho} - \frac{1}{2}G^{\mu\nu}G^{\lambda\rho}) & G^{\mu\nu} \\ G^{\lambda\rho} & -4 \end{pmatrix}. \tag{2.30}$$

The latter expression generalizes the DeWitt metric to the metric-dilaton system so that (2.26) is replaced by

$$\mathcal{G}_{IJ}\delta\varphi^I\delta\varphi^J = \frac{1}{4}\int_{\mathcal{M}} d^m X\ \sqrt{\det G}\ e^{-2\Phi}\left(\delta G_{\mu\nu}\delta G^{\mu\nu} - \frac{1}{2}(\delta G^{\mu}{}_{\mu} - 4\delta\Phi)^2\right). \tag{2.31}$$

Remarkably, the Einstein-Hilbert-dilaton action is also the total time derivative of the effective volume of $\mathcal{M}$,

$$S_{\rm E}[G,\Phi] = \frac{d}{dt}\left(\int_{\mathcal{M}} d^m X\ e^{-2\Phi}\ \sqrt{\det G}\right). \tag{2.32}$$

JHEP06(2007)057

Note, however, that the DeWitt metric is not always positive definite for it is well known that the Weyl mode fluctuations of the metric on $\mathcal{M}$ have negative norm and they are naturally associated to "time-like" directions in superspace. By the same token, the extended DeWitt metric on the metric-dilaton superspace also exhibits "time-like" directions which now arise from a combination of the dilaton and the Weyl mode of the target space metric. Thus, unlike the case of mean curvature flow, $S_{\rm E}$ does not vary monotonically with time. However, there is a closely related functional introduced by Perelman, which serves as entropy for the Ricci flow on compact Riemannian manifolds. It can be thought as being inspired by string theory constructions combined with a special choice of reparametrizations along the flow, but the full details are beyond the scope of the present work. We only mention here that

$$\lambda[g] := \min_{\{\Phi\}} S_{\rm E}(G,\Phi) \qquad \text{with} \quad \int_{\mathcal{M}} d^m X \; e^{-2\Phi} \; \sqrt{\det G} = 1 \tag{2.33}$$

provides a monotonically increasing functional along the Ricci flow, [10], by removing the unwanted "time-like" directions of the DeWitt metric. Then, $\lambda[g]$ is interpreted as the lowest eigen-value of the operator $-\nabla^2 + R/4$, which is defined in terms of the metric at any given moment t, whereas the constraint on the effective volume of $\mathcal{M}$ provides the normalization of the corresponding eigen-function $\exp(-\Phi)$. In effect, $\lambda[g]$ is determined by applying the variational method of elementary quantum mechanics on $\mathcal{M}$. A simpler version of this construction appeared first in the physics literature, [41], and enters into the definition of the (monotonically decreasing) effective central charge along the Ricci flow; see also ref. [42] for more details and further generalizations, as well as ref. [43] for its extension to higher orders in α' and in connection with Zamolodchikov's c-function, [44]. Other important entropy functionals have also appeared in the literature, [10], but their physical interpretation is not yet as clear.

All properties and entropy functionals of the bulk flows are independent of the existence of embedded branes. On the other hand, the analysis of boundary flows depends crucially on the metric of the ambient space. Important entropy functionals for the mean curvature flow will be discussed later. It should be noted, nevertheless, that most results in mathematics are concerned with the mean curvature flow in flat Euclidean space or in curved Riemannian spaces with fixed metric, apart from some notable exceptions[2]. The physical origin of these flows suggests that they should be studied together in all generality and new entropy functionals should be found.

3. Mean curvature flow on the plane

The simplest framework for studying the boundary renormalization group flow of Dirichlet sigma models is provided by the two-dimensional quantum field theory of two free fields whose values at the boundary of the world-sheet are restricted to lie on a given curve. In this case the target space is R^2 and trivially satisfies conformal invariance for the bulk metric

[2]Some aspects of the combined system of Ricci and mean curvature flows have been considered by Hamilton, [45]; we thank Klaus Ecker for bringing this to our attention.

JHEP06(2007)057

beta function. Thus, the only interesting thing to consider are boundary effects, which in general are associated to deformations of the Dirichlet curve due to renormalization on the world-sheet. Since there is no dilaton or any other additional fields in this model, the boundary renormalization group flow is identical to the mean curvature flow of embedded curves in the plane,

$$\frac{\partial \vec{r}}{\partial t} = H\hat{n} - \vec{\xi}, \tag{3.1}$$

where $\vec{r}$ is their position vector and $\vec{\xi}$ includes the effect of reparametrizations along the flow; immersed curves can also be considered by allowing for self-intersections.

Although $\vec{\xi}$ will be left arbitrary in the mathematical presentation below, conformal invariance of the free field theory in the bulk requires that it can only be a Killing vector field on the plane so that the target space metric remains at its trivial fixed point; otherwise, one has to reabsorb it into the time evolution of the curve and eliminate it all together. Turning on a general $\vec{\xi}$ may lead to mathematical simplifications of the curve deformations; of course, the tangential part of the deformations can always be removed by appropriate diffeomorphisms. In either case, the mathematical structure of the equation is the same although the physical interpretation of its solutions differs. We will always insist on having conformal invariance for the bulk space theory and only allow for non-conformal boundary conditions.

3.1 Basic general elements

Let us first consider various forms of the mean curvature flow for embedded curves (open or closed) in the plane, which are convenient for later use and also help to set up the notation. The points of R^2 are parametrized by the position vector $\vec{r}$ with Cartesian coordinates (x, y) and any given curve will correspond to an orbit $\vec{r}(s) = (x(s), y(s))$ with respect to an affine parameter s. Alternatively, one may think of a curve as the graph of a function $y = \varphi(x)$ when x is identified with s. Such curves are not stationary but they evolve according to the mean curvature flow with respect to the deformation time t so that the corresponding trajectories are parametrized in Cartesian coordinates as $(x(s,t), y(s,t))$ or in equivalent graph form as $y = \varphi(x(t), t)$.

The tangent vector at each point of the curve is $\partial\vec{r}/\partial s$ and therefore the unit normal vector inward to the curve is

$$\hat{n} = \frac{1}{\sqrt{(\partial x/\partial s)^2 + (\partial y/\partial s)^2}} \left(-\frac{\partial y}{\partial s},\ \frac{\partial x}{\partial s}\right) = \frac{(-\varphi'(x),\ 1)}{\sqrt{1+\varphi'^2(x)}}\ . \tag{3.2}$$

Furthermore, since the induced metric (line element) on the curve is

$$dl^2 = \left(\left(\frac{\partial x}{\partial s}\right)^2 + \left(\frac{\partial y}{\partial s}\right)^2\right) ds^2\,, \tag{3.3}$$

JHEP06(2007)057

where l is the arc-length (or proper length) on the curve, it follows by definition of the mean curvature H that

$$H = \frac{1}{\left(\sqrt{(\partial x/\partial s)^2 + (\partial y/\partial s)^2}\right)^3}\left(\frac{\partial^2 y}{\partial s^2}\frac{\partial x}{\partial s} - \frac{\partial^2 x}{\partial s^2}\frac{\partial y}{\partial s}\right) = \frac{\varphi''(x)}{\left(\sqrt{1+\varphi'^2(x)}\right)^3}\,. \tag{3.4}$$

The arc-length of the curve can be used to cast the mean curvature flow in the form $\partial\vec{r}/\partial t = \partial^2\vec{r}/\partial l^2$, which resembles the heat equation, albeit is non-linear, but this is not very practical for finding explicit solutions. Instead, the mean curvature flow in R^2 assumes the following convenient form, also taking into account arbitrary reparametrizations generated by a vector field $\vec{\xi}$ along it,

$$\frac{\partial x}{\partial t} = -\xi^x - \frac{\varphi'\varphi''}{(1+\varphi'^2)^2}\,, \qquad \frac{\partial y}{\partial t} = -\xi^y + \frac{\varphi''}{(1+\varphi'^2)^2}\,. \tag{3.5}$$

Note at this point that since $y(t) = \varphi(x(t), t)$ we have

$$\frac{\partial y}{\partial t} = \frac{\partial \varphi}{\partial t} + \varphi'(x)\frac{\partial x}{\partial t}\,, \tag{3.6}$$

which in turn implies the following simple form of the mean curvature flow of graphs

$$\frac{\partial \varphi}{\partial t} = -\xi^y + \varphi'\xi^x + \frac{\varphi''}{1+\varphi'^2}\,. \tag{3.7}$$

The fixed points are characterized by the second order equation

$$\big(\arctan\varphi'(x)\big)' = \xi^y - \varphi'\xi^x \tag{3.8}$$

that also includes the effect of arbitrary reparametrizations in their classification.

Another convenient form of the mean curvature flow in R^2 follows by considering the mean curvature H as function of the slope of the curve,

$$\beta = \arctan\varphi'(x)\,, \tag{3.9}$$

which is the angle formed by the tangent at each point of the curve with the x-axis. In terms of this variable, the unit (inward) normal vector is $\hat{n} = (-\sin\beta, \cos\beta)$, whereas the unit tanget vector is $\hat{t} = \partial\vec{r}/\partial l = (\cos\beta, \sin\beta)$ at each point. Considering the projection of the position vector $\vec{r}$ onto the unit normal, $S(\beta) = -\vec{r}(\beta)\cdot\hat{n}$, it follows that the Cartesian coordinates of the curve can be expressed as functions of the slope,

$$x(\beta) = S'(\beta)\cos\beta + S(\beta)\sin\beta\,, \qquad y(\beta) = S'(\beta)\sin\beta - S(\beta)\cos\beta\,, \tag{3.10}$$

where prime denotes derivative with respect to β. Furthermore, we have the identity

$$S(\beta) + S''(\beta) = x'(\beta)\cos\beta + y'(\beta)\sin\beta = \frac{\partial\vec{r}}{\partial\beta}\cdot\hat{t} = \frac{1}{H(\beta)} \tag{3.11}$$

since $\partial l/\partial\beta = 1/H(\beta)$. Then, upon differentiation of equations (3.10), it turns out that $x'(\beta) = \cos\beta/H(\beta)$ and $y'(\beta) = \sin\beta/H(\beta)$. As a result, the curves are fully determined,

JHEP06(2007)057

up to translations, by specifying the mean curvature H as function of the slope β, according to the relations

$$x(\beta) = x_0 + \int_0^\beta \frac{\cos(\beta')}{H(\beta')} d\beta' \,, \qquad y(\beta) = y_0 + \int_0^\beta \frac{\sin(\beta')}{H(\beta')} d\beta' \,. \tag{3.12}$$

When the curves deform by the mean curvature flow, with $\vec{\xi} = 0$, the evolution for $S(\beta, t)$ satisfies the simple relation $\partial S/\partial t = -H$ that follows from its definition. Then, employing the identity (3.11), one easily finds that $H(\beta, t)$ satisfies the parabolic partial differential equation

$$\frac{\partial H}{\partial t} = H^2 \frac{\partial^2 H}{\partial \beta^2} + H^3 \,. \tag{3.13}$$

This form will be particularly useful for understanding the characteristic features of some special solutions listed in section 4. When reparametrizations generated by $\vec{\xi}$ are also included along the flow, one finds $\partial S/\partial t = -H + \vec{\xi} \cdot \hat{n}$ and the differential equation for the mean curvature generalizes to

$$\frac{\partial H}{\partial t} = H^2 \frac{\partial^2 H}{\partial \beta^2} + H^3 - H^2 \left(\frac{\partial^2}{\partial \beta^2} (\vec{\xi} \cdot \hat{n}) + \vec{\xi} \cdot \hat{n} \right) \,. \tag{3.14}$$

For locally convex closed curves with winding number n, there is a periodicity condition on both coordinates, $x(\beta + 2\pi n) = x(\beta)$ and $y(\beta + 2\pi n) = y(\beta)$, which implies that

$$\int_0^{2\pi n} \frac{e^{i\beta}}{H(\beta)} d\beta = 0 \,. \tag{3.15}$$

The extrinsic curvature of such curves satisfies the periodic condition $H(\beta + 2\pi n) = H(\beta)$, but there can be cases of closed curves, as will be seen later, where $H(\beta)$ has smaller period. Also note that solutions with periodic extrinsic curvature do not necessarily yield closed curves no matter how many times they are iterated. An elementary example of this kind corresponds to the choice $H(\beta) = 1 + \cos\beta$; it yields the curve $x(\beta) = \beta - \tan(\beta/2)$ and $y(\beta) = -\log(\cos^2(\beta/2))$ so that $x(\beta + 2\pi) = x(\beta) + 2\pi$ and $y(\beta + 2\pi) = y(\beta)$. Likewise, for $H(\beta) = 1 + \sin\beta$ one has $x(\beta + 2\pi) = x(\beta)$ and $y(\beta + 2\pi) = y(\beta) + 2\pi$.

Finally, we also include for completeness the form of the mean curvature flow on the plane using polar coordinates $x = r\cos\theta$ and $y = r\sin\theta$. In this case an arbitrary curve on the plane can be thought as graph $r = \rho(\theta)$ that evolves in time according to

$$\frac{\partial \rho}{\partial t} = -\frac{1}{\rho} \frac{\partial \beta}{\partial \theta} = -\frac{\rho^2 + 2\rho'^2 - \rho\rho''}{\rho(\rho^2 + \rho'^2)} \,. \tag{3.16}$$

Here, prime denotes the derivative with respect to θ and the evolution of $\rho(\theta(t), t)$ is computed using $\partial r(t)/\partial t = \partial \rho(\theta(t), t)/\partial t + \rho'(\theta) \partial \theta(t)/\partial t$. Arbitrary reparametrizations along the flow can also be included, if needed, in the system of polar coordinates.

3.2 Entropy functionals, curvature bounds and singularities

The mean curvature flow $\partial \vec{r}/\partial t = H\hat{n}$ tends to deform curves in the direction of their inward normal vector, as if there were tension forces depending on the magnitude of H at

JHEP06(2007)057

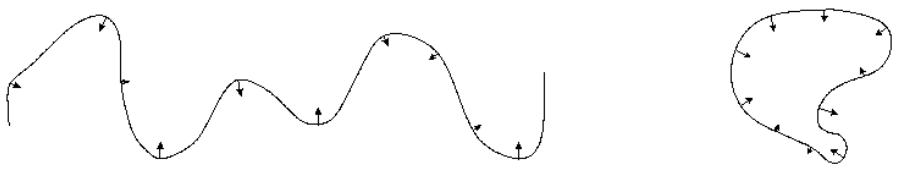

(a) (b)

Figure 1: Evolving open and closed curves on the plane.

each point. As a result, open lines tend to become straight, whereas closed curves tend to become round circles as depicted in figure 1.
The area A surrounded by closed curves γ also tends to decrease at constant pace as can be easily seen by computing

$$\frac{dA}{dt} = \int_\gamma \frac{\partial r}{\partial t} r d\theta = -\int_\gamma \frac{\partial \beta}{\partial \theta} d\theta = -\int_0^{2\pi} d\beta = -2\pi \ . \tag{3.17}$$

Thus, closed curves have the tendancy to shrink, as they become rounder and rounder, [46, 47], until they fully collapse to a point at some time T, which for all practical purposes can be taken to be zero.

Based on this observation one may consider rescaling the coordinates and redefining time as

$$\tilde{\vec{r}}(s,\tilde{t}) = \frac{1}{\sqrt{-2t}} \vec{r}(s,t)\,, \qquad \tilde{t} = -\frac{1}{2}\log(-2t)\,, \tag{3.18}$$

so that the evolution takes the equivalent form

$$\frac{\partial}{\partial \tilde{t}} \tilde{\vec{r}}(s,\tilde{t}) = \tilde{H}(s,\tilde{t})\hat{n} + \tilde{\vec{r}}(s,\tilde{t}) \tag{3.19}$$

in terms of the mean curvature $\tilde{H}$ of the rescaled curve in R^2; it so happens that $\tilde{H} = \sqrt{-2t}H$. The variant (3.19) is called *normalized* mean curvature flow, since, by construction, it preserves the area surrounded by the rescaled closed curves with respect to the new time variable $\tilde{t}$. As $-\infty < t \leq 0$, we see that $-\infty < \tilde{t} < \infty$ and so the normalized solutions exist for all time. The normalized flow can be alternatively viewed as special instance of the unnormalized flow (3.1) when reparametrizations are performed along it with $\vec{\xi} = -\vec{r}$ and the tilde is dropped for comparison. This will be quite useful later for understanding the structure of scaling solutions and the characterization of singularities that may form by the flow.

There are entropy functionals associated to the mean curvature flow. First, let us consider the backward heat kernel, defined on R^2 for all $t < 0$,

$$\mathcal{K}(\vec{r},t) = \frac{1}{\sqrt{2\pi(-2t)}} \exp\left(-\frac{r^2}{2(-2t)}\right), \tag{3.20}$$

JHEP06(2007)057

and integrate it over the curve by the induced arc-length that also varies with time. It follows that this is a monotonically decreasing functional, due to Huisken, [48], since

$$\frac{d}{dt}\int_C \mathcal{K}(\vec{r},t)dl = -\int_C \mathcal{K}(\vec{r},t)\left(H+\frac{1}{2t}S\right)^2 dl \leq 0 \tag{3.21}$$

by the unnormalized flow $\partial\vec{r}/\partial t = H\hat{n}$ which is applied to closed curves C. Since $S = -\vec{r}\cdot\hat{n}$, any closed curve that satisfies the special relation

$$(-2t)H\hat{n} + \vec{r} = 0 \tag{3.22}$$

keeps the entropy functional invariant. Configurations of this kind are self-similar solutions with factorized time dependence. The simplest example is provided by a uniformly shrinking round circle whose radius varies as $\sqrt{-2t}$ and H as $1/\sqrt{-2t}$.

Likewise, for the normalized mean curvature flow, we consider the Gaussian weight function

$$\tilde{\mathcal{K}}(\vec{\tilde{r}}) = \frac{1}{\sqrt{2\pi}}\exp\left(-\frac{\tilde{r}^2}{2}\right) \tag{3.23}$$

that depends implicitly upon $\tilde{t}$, and integrate it over the rescaled curve $\tilde{C}$ by the corresponding induced arc-length $\tilde{l}$. It follows again that this is a monotonically decreasing functional with respect to the rescaled time, [48], since

$$\frac{d}{d\tilde{t}}\int_{\tilde{C}} \tilde{\mathcal{K}}(\vec{\tilde{r}})d\tilde{l} = -\int_{\tilde{C}} \tilde{\mathcal{K}}(\vec{\tilde{r}})(\tilde{H}-\tilde{S})^2 d\tilde{l} \leq 0\ . \tag{3.24}$$

In this case the extrema of the entropy functional satisfy the normalized self-similar condition

$$\tilde{H}\hat{n} + \vec{\tilde{r}} = 0\,, \tag{3.25}$$

which is attained as $\tilde{t}\to\infty$. The round circle is a fixed point of the normalized flow. Other non-trivial fixed points also exist, and they are classified by the so called Abresch-Langer closed curves, as will be seen in the next section.

Next, we discuss certain bounds on H that are important for the classification of singularities formed by mean curvature flow. There is always a lower bound for the blow-up rate of the curvature which is derived by applying the maximum principle. Indeed, specializing equation (3.13) to the maximal value $H_{\max}(t)$ attained at each instant of time, we obtain the inequality

$$\frac{\partial}{\partial t}H_{\max} = H_{\max}^2\frac{\partial^2}{\partial\beta^2}H_{\max} + H_{\max}^3 \leq H_{\max}^3\ . \tag{3.26}$$

Closed convex curves have $H_{\max} > 0$ and they develop curvature singularities at some finite time, say $T = 0$. More generally, it follows

$$H_{\max}(t) \geq \frac{1}{\sqrt{-2t}}\,, \tag{3.27}$$

by integrating the inequality from t to 0, thus establishing a universal lower bound for all $t < 0$. The uniformly shrinking round circle saturates this curvature bound at all time.

JHEP06(2007)057

On the other hand, it is not at all guaranteed that there is an analogous upper bound for $H_{\max}(t)$ based on general grounds. Actually, the singularities of mean curvature flow are divided in two general categories. Their characterization is based on bounds of $|H|_{\max}(t)$, which is taken in absolute value in general. Type I singularities arise when an upper bound of the following form also exists,

$$\frac{C}{\sqrt{-2t}} \geq |H|_{\max}(t) \geq \frac{1}{\sqrt{-2t}}\,, \tag{3.28}$$

with appropriately chosen constant $C < \infty$. This is equivalently stated as

$$C \geq |\tilde{H}|_{\max}(\tilde{t}) \geq 1 \tag{3.29}$$

using the rescaled curvature $\tilde{H}$. In all other cases the singularities that are formed are called type II. All closed embedded curves in R^2 will eventually form type I singularities. Even if the curve is not convex at a given time it will become convex at later times and follow the evolution towards the singularity by becoming rounder and smaller, i.e., asymptote the uniformly contracting circle, [46, 47]. However, one can also imagine deformations of immersed curves, with self-intersections, whose curvature blows up at faster rate as they begin to develop cusps and yield type II singularities.

All closed planar curves satisfying the curvature bound (3.28) tend to self-similar solutions (3.22) in the vicinity of the singularity, [48] (but see also ref. [49] and [50]). The proof relies on the monotonic behavior of Huisken's functional whose extrema are the self-similar solutions. Thus, the classification of type I singularities reduces to the classification of self-similar solutions, which are completely known on the plane. The circle is the only embedded curve of this kind whereas the other solutions are special self-intersecting convex curves. In higher dimensions one may consider hypersurfaces that evolve by their mean curvature vector in flat space and generalize the constructions and results mentioned above. However, there is no systematic classification of the self-similar hypersurfaces that extremize the corresponding Huisken functional unless the hypersurface is compact with positive mean curvature. As a result, the general structure of type I singularities is less understood in higher dimensions.

Type II singularities arise when the curvature blows faster than $1/\sqrt{-2t}$ as $t \to 0^-$. In this case there is a sequence of times $t_n \to 0^-$ such that the curve obtained by appropriate magnification at each instance t_n, so that its maximal curvature becomes 1, will converge to a translating solution, [49] (but see also ref. [50]). The latter is a very special solution of the mean curvature flow that will be discussed later together with the scaling (self-similar) solutions on the plane. A typical example of this kind of singular behavior arises from the evolution of a cardioid. It is a convex closed curve with winding number 2 that self-intersects once and consists of two loops, the inner and outer, touching each other. It can be intuitively seen that the inner loop will contract faster and form a cusp before the outer loop has a chance to shrink to zero size. Then, as one zooms closer and closer to the diminishing inner loop, as it begins to form a cusp, the shape of a translating solution will emerge according to the general statement above. The basic idea is illustrated in figure 2 below focusing on the rescaled region of maximal curvature.

JHEP06(2007)057

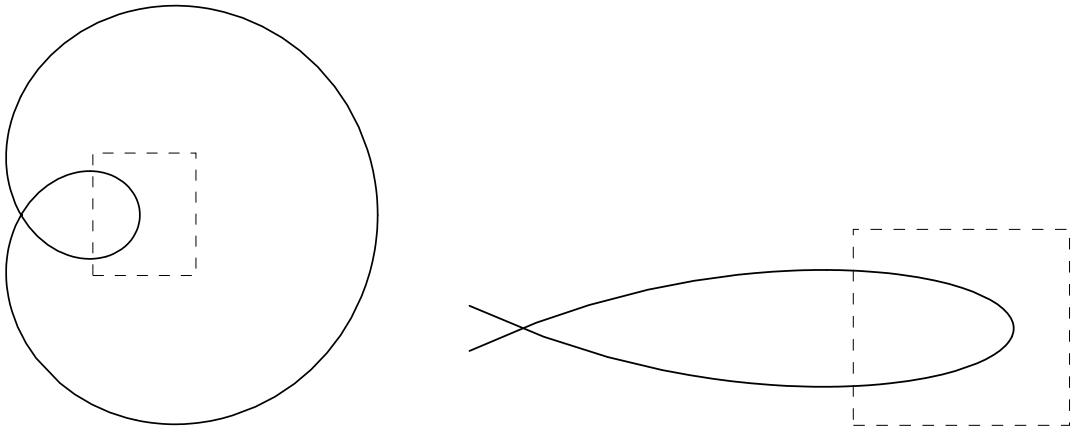

(a) (b)

Figure 2: A cardioid leading to cusp formation under the flow.

Similar results apply to the structure of type II singularities of evolving compact hypersurfaces of positive mean curvature in flat space.

For convex planar curves γ there is an additional entropy functional which is defined as follows,

$$\mathcal{E}(\gamma) = \frac{1}{2\pi}\int_\gamma ds\ H\ \log H = \frac{1}{2\pi}\int_0^{2\pi} d\beta\ \log H\ . \tag{3.30}$$

It can be easily seen following, for instance, [18] that

$$\frac{d^2\mathcal{E}}{d\tilde{t}^2} \geq 2\left(\left(\frac{d\mathcal{E}}{d\tilde{t}}\right)^2 + \frac{d\mathcal{E}}{d\tilde{t}}\right), \tag{3.31}$$

using the normalized variant of the flow that exists for all $\tilde{t} < \infty$. Note that if $d\mathcal{E}/d\tilde{t}$ were positive at some time, it would blow up at later times because $d^2\mathcal{E}/d\tilde{t}^2$ would also be positive. However, this is impossible for $\mathcal{E}$ exists for all values $\tilde{t}$. Thus, we conclude that

$$\frac{d\mathcal{E}}{d\tilde{t}} \leq 0 \tag{3.32}$$

for all $\tilde{t} < \infty$. The round circles extremize $\mathcal{E}$.

This functional is the mean curvature analogue of a similar expression

$$\mathcal{H} = \int d^2X\sqrt{\det G}\ R\ \log R \tag{3.33}$$

introduced for the Ricci flow on two dimensional surfaces, [51]. Using the normalized Ricci flow on compact surfaces with $R > 0$, which are analogous to convex planar curves, it follows that $\mathcal{H}$ decreases monotonically. Furthermore, the curvature remains bounded for all time, as

$$C \geq R \geq c > 0\,, \tag{3.34}$$

JHEP06(2007)057

with appropriately chosen constants c and $C < \infty$. These bounds are analogous to (3.29) for the normalized mean curvature flow. Note that the round spheres extremize $\mathcal{H}$.

Finally, another important result on the subject states that the number of self-intersections of immersed planar curves can not increase by the mean curvature flow in the forward time direction, [52].

It will be interesting to explore new methods for integrating the mean curvature flow on the plane, at least formally, and devise a Lax pair formulation for it, if it is at all appropriate, by developing analogies with the algebraic treatment of various intrinsic curvature flows on two dimensional surfaces, [53]. Until then, we can only rely on the general mathematical results concerning the qualitative behavior of the flow, as outlined above, and the construction of various explicit solutions that will follow next. Note at this end that there are other type of evolution equations for planar curves leading to known integrable systems, as explained in appendix B that is only included for comparison.

4. Special solutions on the plane

Several exact solutions of the mean curvature flow on R^2 are listed and comments are made relating their appearance in the physics and mathematics literature. Many details will be filled in for completeness and a number of new results will also be derived. We will speak in Euclidean terms calling a planar curve $D1$-brane, as opposed to the Lorentzian version of $D0$-branes having one-dimensional world-volume.

Although boundary interactions in quantum field theory provide the main framework for our work, as in ref. [26]–[31] where a few explicit solutions have been constructed, it should be noted that various running solutions were also constructed a long time ago in different physical context. They first appeared in the original work on the motion of grain boundaries in an annealing piece of metal, [14], and later in the magneto-hydrodynamic theory of resistive diffusion of force-free magnetic fields, [54], which is summarized in appendix C. Frequent references will be given to them at appropriate places in the text. In mathematics, some of these solutions are briefly discussed in the textbook [18] and references therein. However, not all of them have yet found their exact place in quantum field theory.

4.1 Trivial fixed points

The fixed points of the mean curvature flow (3.7) are simply described by $\partial\varphi/\partial t = 0$ and $\varphi''(x) = 0$ when no reparametrizations are taken into account ($\xi = 0$). Obviously, these are time invariant straight lines of the general form

$$y = \varphi(x) = ax + b \tag{4.1}$$

whose extrinsic curvature vanishes identically. They represent $D1$ branes on the plane, which are compatible with conformal invariance. $D0$ branes also arise as points with fixed position in the (x, y) plane; they can be thought as the end-point of shrinking closed planar curves.

JHEP06(2007)057

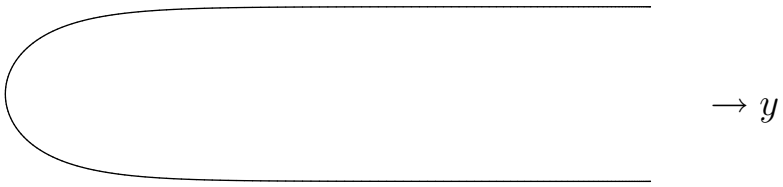

Figure 3: The hair-pin (or grim-reaper) curve on the plane.

4.2 Translating solution

The simplest static solution of equation (3.7), modulo reparametrizations, corresponds to the choice of a translational Killing vector field along the y-direction, $\xi = \partial/\partial y$ with components $\xi^x = 0$ and $\xi^y = 1$, up to a constant factor v. Then, it follows that the shape of the curve is given by the graph of the function

$$y = \varphi(x) = -\frac{1}{v}\,\mathrm{logcos}(vx + a) + b\,, \tag{4.2}$$

where a and b are integration constants. Setting them equal to zero amounts to placing the tip of the curve at the origin of the coordinates (x, y), in which case case it asymptotes the lines $x = \pm\pi/2v$.

The resulting curve is called *grim-reaper* in the mathematics literature or *hair-pin* in the physics literature, [27, 28], where it was encountered before. The same configuration was also found in the earlier works [14] and [54] (but see also ref. [20] among others). It is a translating solution along the y-direction for it can be alternatively viewed as moving linearly in time along the y-direction with constant spead v (in appropriate units), i.e., $\partial\varphi/\partial t = v$, so that

$$y = \varphi(x, t) = vt - \frac{1}{v}\,\mathrm{logcos}(vx)\ . \tag{4.3}$$

The graph of this configuration is given in figure 3 below.

A hair-pin facing in the opposite direction is obtained by setting $y \to -y$, in which case the corresponding time dependent configuration translates linearly in time towards the negative y-direction. Thus, the sign of v selects one of the two possible cases: the hair-pin or the anti-hair-pin. The slope of these curves is simply given by $\beta = vx$, in which case their mean curvature is

$$H(\beta) = v\mathrm{cos}\beta\ . \tag{4.4}$$

The solution satisfies the special condition $H''(\beta) + H(\beta) = 0$ that follows from equations (3.13) or (3.14) depending on how one views the evolution. Likewise, a translating solution along the x-axis, in either direction, arises by reversing the role of the x and y coordinates.

In all cases, the hair-pin solutions represent $D1$ branes supported by a linear dilaton Φ in the coordinate of the translating direction. For example, a hair-pin that moves with constant velocity v along the y-axis has $\xi^\mu = -\nabla^\mu\Phi$ with $\Phi = -vy$. In this respect, the translating solutions are examples of mean curvature solitons that do not affect the

JHEP06(2007)057

conformal field theory on the plane. Also, according to the variational method of section 2.2, in the presence of dilaton, such configurations represent geodesics on the plane equipped with the metric

$$ds^2 = e^{2vy}(dx^2 + dy^2) \ . \tag{4.5}$$

This is a Ricci flat metric as it relates to the Euclidean frame in polar coordinates by the change of variables

$$vr = e^{vy} \,, \qquad \theta = vx \,, \tag{4.6}$$

so that $ds^2 = dr^2 + r^2 d\theta^2$ with $1 \leq vr \leq \infty$ and $-\pi/2 \leq \theta \leq \pi/2$ for $v > 0$. This maps to a domain on the right half-plane plane, which is exterior to the disc $vr < 1$, and the hair-pin corresponds to the vertical straight line $vr\cos\theta = 1$ that is tangent to its boundary.

The hair-pin is a gradient soliton, which should be thought as the mean curvature analogue of the well known Ricci flow soliton associated to the intrinsic geometry of a two-dimensional cigar, [51]; the latter has the interpretation of a two-dimensional Euclidean black hole in conformal field theory, [55]. In appropriate context, the hair-pin serves as model for studying tachyon condensation in open string theory (see, for instance, [56] and references therein). When $v = 0$ the configuration becomes straight line, $y = 0$, as viewed from the origin of coordinates; alternatively, when this limit is considered from the viewpoint of an asymptotic "observer", situated at $y = \infty$, the hair-pin looks like a semi-circle with infinite radius.

Finally, we note the important property of this solution to exhibit just one point of maximal curvature situated at its tip. This is not accidental but consequence of a general theorem stating that any strictly convex solution of the mean curvature flow that exists for all time $-\infty < t < \infty$ and the mean curvature becomes maximum at only one point, must necessarily be a translating soliton, [57]. This is an important ingredient that goes into the study of type II singularities, which look like a hair-pin following a sequence of appropriate magnifications that keep the maximal curvature normalized to a fixed value, $v = 1$, through out the evolution.

4.3 Rotating solution

Using the rotational Killing vector field $\xi = \partial/\partial\theta = -y\partial/\partial x + x\partial/\partial y$ on the plane, up to an overall constant factor ω, other static solutions of (3.7) follow by integrating the differential equation

$$\big(\arctan\varphi'(x)\big)' = \omega\,\big(x + y\varphi'(x)\big) \,. \tag{4.7}$$

Then, for a graph $y = \varphi(x)$, one obtains

$$\arctan\varphi'(x) = \frac{\omega}{2}(x^2 + y^2) + c = \frac{\omega}{2}r^2 + c \tag{4.8}$$

in terms of the polar coordinate r. Setting the integration constant c equal to zero amounts to placing the curve at the origin of the coordinate system so that it starts tangentially to the x-axis. Further integration of the equation can not be performed in closed form, but this is no problem for drawing the shape of the resulting curve. Its slope at each point, as

JHEP06(2007)057

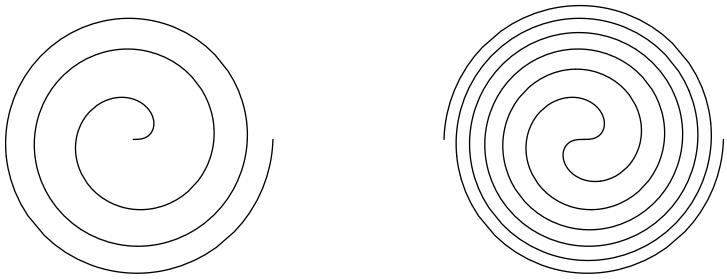

(a) (b)

Figure 4: Yin-Yang curve on the plane.

it reads from equation (4.8), is proportional to the distance-squared from the center, and, therefore, it follows the shape of an unbounded spiral as depicted in figure 4.

Thus, the integral curve of the differential equation (4.8) is the unique rotating solution on the plane, which is another example of a mean curvature soliton also known as Yin-Yang curve in the mathematics literature; in physics it has appeared much earlier in ref. [14]. Half of it is plotted in figure 4a, whereas the complete curve appears in figure 4b by also plotting its symmetrical part about the origin, i.e., its point of inflection. The turns of the spiral are separated by approximately $2\pi/\omega r$ for large r. An alternative (dynamical) description of the solution is provided by a revolving spiral with constant angular velocity ω about the origin, with simple time dependence

$$\arctan\varphi'(x(t),t) = \frac{\omega}{2}(x^2+y^2) + c = \frac{\omega}{2}r^2 + \omega t\,, \tag{4.9}$$

without making use of the compensating Killing vector field that stabilizes its rotation. If polar coordinates were used on the plane, the rotating solution (4.9) would be the graph of a linearly evolving function $r = \rho(\theta - \omega t)$; in this case, equation (3.16) simplifies a lot since $\partial/\partial t = -\omega\partial/\partial\theta$ when acting on ρ. In this frame, the mean curvature of the solution specializes to $H(\beta,t) = H(\beta - \omega t)$ and satisfies the non-liner equation in β

$$H^2(\beta)\big(H''(\beta) + H(\beta)\big) + \omega H'(\beta) = 0\,, \tag{4.10}$$

as follows from equations (3.13) or (3.14) depending on the view-point. It is a non-trivial task to find the solution in closed form.

The rotating solution represents an evolving infinitely long $D1$ brane with one point held fixed at the origin. Its existence, as static solution of equation (3.7), is attributed to the Killing vector field $\vec{\xi} = \omega(-y\partial/\partial x + x\partial/\partial y)$ having $\vec{\nabla}\times\vec{\xi} = 2\omega \neq 0$. As such, $\vec{\xi}$ can not be derived from a potential as gradient field, and, hence, there is no dilaton field associated to the static form of the solution that could account for its boundary conformal field theory description. Thus, unlike the grim-reaper, the Yin-Yang curve is not a gradient soliton. It corresponds to a boundary quantum state that does not satisfy conformal invariance, but it runs, via rotation, with the world-sheet energy scale. The sign of ω distinguishes the two different modes of rotation around the clock.

JHEP06(2007)057

4.4 Scaling solutions

Another type of static solutions of equation (3.7) follow by considering the vector field $\xi = r\partial/\partial r = x\partial/\partial x + y\partial/\partial y$, up to a constant factor c, which generates dilations of the plane. These are called scaling (or homothetic) solutions since they evolve by overall scaling when the time dependence is reinstated at the expense of suppressing the corresponding reparametrizations along the flow. As such, they satisfy the defining relation

$$\big(\arctan\varphi'(x)\big)' = c\,\big(\varphi(x) - x\varphi'(x)\big) \tag{4.11}$$

for $y = \varphi(x)$. Note, however, that the generator $\vec{\xi}$ of dilations is not a Killing vector field on the plane, although $\xi_\mu = -\nabla_\mu\Phi$ with

$$\Phi(x,y) = -\frac{c}{2}(x^2+y^2)\ . \tag{4.12}$$

If conformal invariance of the quantum field theory of the plane is to be maintained, the homothetic solutions will unavoidably arise as time dependent curves with factorized t-dependence so that

$$y = \varphi(x(t),t) = \sqrt{2ct}\ \varphi\left(\frac{x}{\sqrt{2ct}},1\right)\ . \tag{4.13}$$

The sign of c determines the basic features of time evolution. Note that in all cases ct should be strictly non-negative. Thus, for $c<0$, the scaling solutions are shrinking as t runs from $-\infty$ to some finite time that has been set equal to zero without loss of generality; the corresponding configurations have well defined ultra-violet limit and they fully collapse to a point at $t=0$. On the other hand, for $c>0$, the scaling solutions are expanding as t runs from 0 to ∞ and exhibit a well-defined infra-red limit.

Irrespective of the uses and interpretation of the scaling configurations, their x-dependence follows by seeking solutions of equation (4.11). Alternatively, the corresponding curves can be described using the parametric form of the mean curvature flow as

$$H\hat{n} = c\vec{r} \tag{4.14}$$

in terms of their position vector $\vec{r} = (x,y)$. As such, they may also be viewed as geodesics on the plane endowed with the metric

$$ds^2 = e^{c(x^2+y^2)}(dx^2+dy^2)\,, \tag{4.15}$$

which is not Ricci flat but it is induced by the potential (4.12) according to the variational method of section 2.2 in the presence of dilaton. These are the scaling solutions that characterize the extrema of Huisken's entropy functional. In the physics literature, they first arose in the early work [14] and later in magneto-hydrodynamic models for the solar flares, [54], where they were discussed in moderate detail.

Another equivalent description is obtained by considering the mean curvature flow in polar coordinates, as in equation (3.16), with factorized t-dependence $\rho(\theta(t),t) = R(\theta)\sqrt{2ct}$. Then, the slope of the curves depends only on θ, as $\beta(\theta)$, and satisfies the equation

$$\frac{d\beta}{d\theta} = -cR^2(\theta)\ . \tag{4.16}$$

JHEP06(2007)057

This formulation is advantageous for drawing the shape of the homothetic curves at fixed t. For this, let us assume without loss of generality that the curves are placed on the plane in a way so that $\beta(\pi/2) = 0$, meeting the y-axis perpendicularly at some point. Then, simple integration of equation (4.16) yields

$$\beta(\theta) = c \int_{\theta}^{\pi/2} R^2(\theta) d\theta \,, \tag{4.17}$$

stating that the slope of any such curve is proportional to the area subtended by the corresponding radius vector as it moves away from its vertical reference position. Clearly, the curves are placed symmetrically about the y-axis, since $\beta \to -\beta$ when $\theta \to \pi - \theta$.

Finally, note that the mean curvature of scaling solutions factorizes as $H(\beta, t) = H(\beta)/\sqrt{2ct}$, where their dependence on the slope follows from equation (3.13), which now reads as

$$\frac{d^2 H(\beta)}{d\beta^2} + H(\beta) + \frac{c}{H(\beta)} = 0 \,. \tag{4.18}$$

This last equation turns out to be particularly advantageous for understanding the structure of the homothetic solutions in detail as it provides an intuitive account for their classification depending on the sign of c. In the following, we study separately the self-shrinking and self-expanding solutions by stripping off their t-dependence and draw some characteristic figures that arise in each case.

(i) Self-shrinkers ($c < 0$): it is apparent from equation (4.18) that solutions with constant mean curvature $H(\beta)$ can only exist for $c < 0$. They represent circles with radius $R = 1/\sqrt{-c}$ for which $H = \sqrt{-c}$. In this case, equation (4.16) is trivially satisfied since $\beta = \theta + \pi/2$ at all points of a circle. When time dependence is reinstated, the circles evolve by uniform contraction, as $R(t) = \sqrt{2ct}$, until they collapse to a point; this special solution was studied in the context of boundary interactions in ref. [26], where it is referred to as circular brane model. Other solutions include rosette-like curves, which are symmetric about their maxima and minima, but they are not necessarily closed.

There is a special class of solutions, however, which are closed rosettes with winding number p and q petals called Abresch-Langer curves $\Gamma_{p,q}$, [58, 59]. Such curves are graphs of transcendental functions associated to any pair of relatively prime integers (p, q) so that

$$\frac{1}{2} < \frac{p}{q} < \frac{\sqrt{2}}{2} \,. \tag{4.19}$$

The simplest one has characteristic integers $(2, 3)$ and it is depicted in figure 5b next to the homothetically contracting round circle, whereas the next more complicated curve $(3, 5)$ is depicted in figure 5c. Other examples correspond to the values $(5, 8)$, $(7, 10)$, $(9, 14)$ $(12, 17)$ and so on.

The importance of these configurations stems from the fact that the mean curvature flow tends to evolve closed curves towards the scaling solutions with $c < 0$ provided that the maximum curvature remains bounded as $|H_{\max}(t)|\sqrt{2ct} \leq C < \infty$ (type I singularities). Thus, embedded closed curves have the tendency to become circular as they shrink,

JHEP06(2007)057

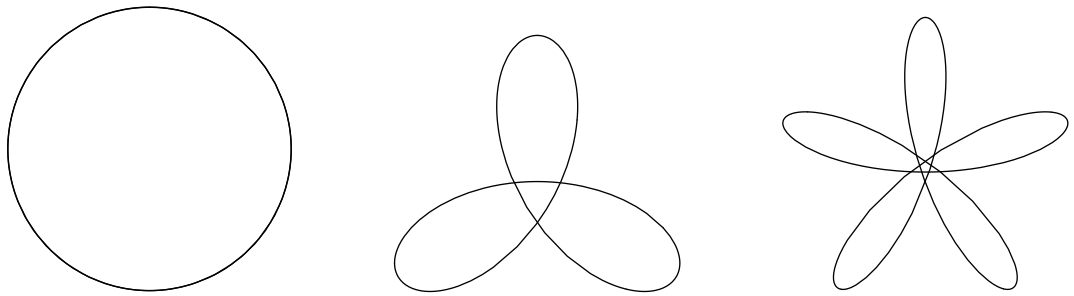

(a) (b) (c)

Figure 5: Closed curves representing scaling solutions on the plane.

whereas closed curves with self-intersections tend towards one of the special locally convex curves $\Gamma_{p,q}$. The corresponding scaling solutions may be alternatively viewed as describing the asymptotic limit of the normalized mean curvature flow in the type I case. Furthermore, it can be shown under appropriate technical condition, that any closed n-dimensional hypersurfaces in R^{n+1} with non-negative mean curvature also evolves towards scaling solutions, [48]. Such solutions obey $H\hat{n} = c\vec{r}$ in all dimensions, after extracting their factorized t-dependence, as before, and they fall into three different classes: S^n, $S^{n-m} \times R^m$ or $\Gamma_{p,q} \times R^{n-1}$ (see also ref. [18]). Thus, the classification of scaling solutions on the plane for $c < 0$ has more general value for the whole subject.

We illuminate the presentation with a brief description of the transcendental nature of the closed Abresch-Langer curves $\Gamma_{p,q}$, setting $c = -1$ without loss of generality. First, note that equation (4.18) has a first integral

$$\frac{1}{2}\left(\frac{dH}{d\beta}\right)^2 + V(H) = E\,, \tag{4.20}$$

with integration constant E and

$$V(H) = \frac{1}{2}\left(H^2 - \log H^2\right). \tag{4.21}$$

E can be viewed as the energy of a point particle that moves with respect to an effective time β in a potential well $V(H)$ having infinite height on both sides of the allowed range $0 \leq H < \infty$. Since the minimum of the effective potential is reached at $H = 1$, in which case $V(H) = 1/2$, bounded motion with respect to β becomes possible for all $E \geq 1/2$, as in figure 6.

Periodic solutions $H(\beta)$ with fixed E have primitive period

$$T(E) = 2\int_{H_-(E)}^{H_+(E)} \frac{dH}{\sqrt{2(E - V(H))}}\,, \tag{4.22}$$

where $H_\pm(E)$ are the roots of the equation $E = V(H)$ that correspond to the two turning points of the bounded motion. The primitive period determines the minimum effective

JHEP06(2007)057

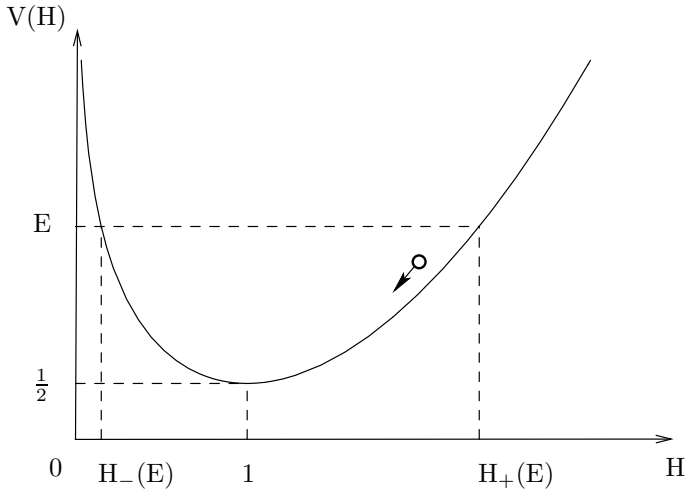

Figure 6: The effective potential for self-shrinkers.

time that takes H to return back to its original value. This, however, does not necessarily mean that the curve itself has the same period in β for it may require several such turns, say q, for $x(\beta)$ and $y(\beta)$ to return back to themselves. Also, in other cases, the resulting curves may never close back to themselves, thus leading to rosette-type open shapes that wind indefinitely on the plane.

Analysis of the problem shows that $T(E)$ varies monotonically with E and it decreases from $\sqrt{2}\pi$ to π as the energy ranges in $1/2 < E < \infty$. The upper bound of $T(E)$ is easily established by considering $H = 1 + \epsilon$ with small but non-vanishing ϵ. In this case equation (4.20) takes the harmonic oscillator form

$$\frac{1}{2}\left(\frac{d\epsilon}{d\beta}\right)^2 + \epsilon^2 = E - \frac{1}{2} \tag{4.23}$$

by expanding $V(H)$ to quadratic order. Then, $\epsilon(\beta)$ is given by the trigonometric functions $\sqrt{E-1/2}\,\sin(\sqrt{2}\beta)$ or $\sqrt{E-1/2}\,\cos(\sqrt{2}\beta)$ with $E - 1/2$ small but strictly positive constant. These are periodic functions with period $\sqrt{2}\pi$ that is insensitive to the value of E provided that E stays close to $1/2$. The lower bound of $T(E)$ can be established by asymptotic analysis that is rather involved and we refer the reader to the literature for the details, [58, 59].

According to this result, closed curves on the plane with $1/2 < E < \infty$ correspond to trajectories with primitive period

$$T(E) = 2\pi\frac{p}{q}\,, \tag{4.24}$$

where p and q are relatively prime integers subject to equation (4.19) above. This is a transcendental quantization condition for the parameter E showing that the emergence of closed rosettes on the plane is the exception rather than the rule. Other values of E result to rosette-type curves with infinite number of self-intersection points that never close back to themselves. Extending $H(\beta)$ periodically to $[0, 2\pi p]$ yields the Abresch-Langer curves $\Gamma_{p,q}$ with winding number p, as required, when the quantization condition (4.24) is fulfilled.

JHEP06(2007)057

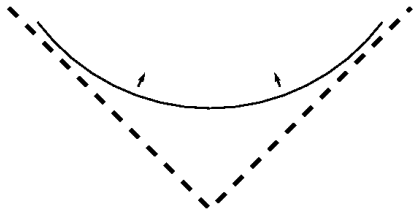

Figure 7: Scaling solution on the plane representing the decay of a wedge.

These curves have $2q$ critical points for their mean curvature reaches the minimal value $H = 1$ exactly twice within the primitive period $T(E)$. They also appear to have $q(p-1)$ self-intersection points in general. For other values of E the homothetic solutions are open and can be formally thought to arise as limiting cases $p \to \infty$ and $q \to \infty$ with infinite period.

Finally, note that $H(\beta)$ follows from equation (4.20) by expressing β as indefinite integral of $dH/\sqrt{2(E - V(H))}$, which obviously can not be written in terms of elementary functions. The dependence of the position vector of such curves upon β, as given by equation (3.12), turns out to be transcendental. It is also clear in this context that an elementary solution arises when the effective point particle sits still at the minimum of the potential $V(H)$ having $E = 1/2$. It corresponds to a round circle of unit radius so that its mean curvature is constant, $H = 1$, for all β, and describes the only simple closed curve that shrinks by scaling in t. In that case the period of the curve is 2π and suffers discontinuous jump from the lower bound of $T(E)$ when $E > 1/2$.

(ii) Self-expanders ($c > 0$): this case allows only for hyperbola-like curves whose slope increases monotonically as one varies clockwise the polar coordinate θ. These curves are necessarily open with asymptotic lines placed symmetrically about the y-axis, as shown in figure 7. The need for asymptotic lines follows by inspection of the integral equation (4.17), for, otherwise, the area subtended by the radius vector of the corresponding curve, as measured from the tip of the asymptotic wedge, will become unlimited in contradiction with the finite change of their slope. The curves can be thought as representing an intermediate stage for the decay of a wedge to straight line.

The details of the solution can be investigated from the point of view of equation (4.18), setting $c = 1$ without loss of generality. As before, it has a first integral of the form (4.20), with integration constant E, but with effective potential

$$V(H) = \frac{1}{2}\left(H^2 + \log H^2\right) \tag{4.25}$$

that differs from the $c < 0$ case by a relative sign. As a result, $V(H)$ is not bounded from below, for it is a monotonically increasing function ranging from $-\infty$ to ∞ when $0 \leq H < \infty$. E can take any arbitrary real value in this case, and, clearly, $V(H)$ can not

JHEP06(2007)057

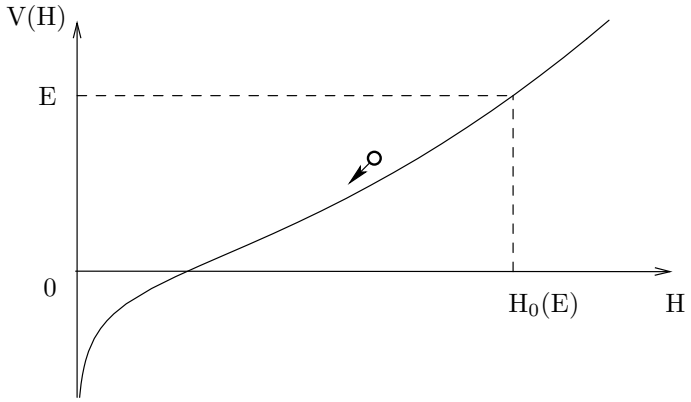

Figure 8: The effective potential for self-expanders.

support bounded motion with finite period; the corresponding scaling solution of the mean curvature flow is an open curve. For any given E, $H(\beta)$ follows, as before, by expressing β as indefinite integral of $dH/\sqrt{2(E-V(H))}$, which in turn determines the form of the solution implicitly via transcendental functions.

The mechanical analogue also helps to provide an intuitive explanation for the presence of asymptotic lines and illustrate how scaling solutions can emerge from a wedge. $H(\beta)$ is the classical trajectory of a particle that rolls down the potential (4.25) having fixed energy E with respect to the effective time β, as shown in figure 8.

The effective time that takes such a particle to go down the drain, when it starts with zero velocity, is

$$\Delta\beta(E) = \int_0^{H_0(E)} \frac{dH}{\sqrt{2(E-V(H))}}\,, \tag{4.26}$$

where $H_0(E)$ is the (single) root of the equation $E = V(H)$ that specifies its position at some initial time β_0. Thus, as one transverses the corresponding curve on the plane, the slope changes by an overall finite amount $\Delta\beta(E)$ that depends on E. The curve tends asymptotically to a straight line, with $H = 0$, which represents the universal attractor point of the potential. Actually, this effective particle motion traces only half of the corresponding curve on the plane, which can always be arranged to meet perpendicularly the y-axis by choosing $\beta_0 = 0$; the mean curvature of the curve at the starting point is $H_0(E)$, whereas the slope of the right asymptotic line is $\Delta\beta(E)$. The other half of the curve, together with the left asymptotic line, are placed symmetrically about the y-axis and can be obtained by simply reversing the direction of effective time. Then, tracing the complete curve from one asymptotic limit to the other amounts to shooting a particle up from the bottom of the potential and let it fall back to it after reaching a maximum height $H_0(E)$ that depends on its energy. The two asymptotic lines meet at a point of the y-axis forming a wedge with opening angle $\pi - 2\Delta\beta(E)$; this angle varies monotonically from π to 0 as E ranges from $-\infty$ to ∞.

Particles with very low energy stay deep inside the throat of the potential, having $H \simeq 0$ everywhere, and they correspond to straight lines; in this case the wedge is wide

JHEP06(2007)057

open to 180^0 and the curve is lying horizontally on it. On the other hand, highly energetic particles have $H_0(E) \to \infty$ and the two sides of the wedge tend to collapse against each other. The same thing happens to the curve that folds up on the wedge, having infinite curvature at the vertex and practically zero everywhere else. For intermediate energies the typical scaling solution is a hyperbola-like curve with finite curvature everywhere. When the t-dependence is reinstated into the solutions, the coordinates x and y scale in the same way, as $1/\sqrt{t}$, without affecting the angle of the asymptotic wedge $y \sim |x|$. The curves themselves appear as straight lines when one zooms closer and closer to them, whereas it becomes increasingly difficult to distinguish them from the surrounding asymptotic wedge when they are looked up from larger and larger distances away.

Therefore, in this context, the scaling solution can be thought as the mean curvature analogue of the fundamental solution to the heat equation, whose initial configuration at $t = 0$ is a delta function. It is known as Brakke's wedge in mathematics, [16, 19], but it also arose earlier in physics in ref. [14] and [54]. The initial curvature singularity is fully dissipated after infinitely long time by flowing to the infra-red region. Clearly, it serves as model for studying tachyon condensation for intersecting branes and can be further used in connection with other works[3] on the subject (see, for instance, [60] and references therein). An analogous solution that describes the decay of a cone to the plane also exists for the Ricci flow, [61] (but see also [53]); it serves as model for studying tachyon condensation in closed string theory. Here, however, it is not possible to obtain the solution in closed form.

4.5 Paper-clip model

A genuine running solution of the mean curvature flow (3.7), with $\xi = 0$, corresponds to the time dependent curve $y = \varphi(x(t), t)$,

$$e^{v^2 t}\cosh(vy) = \cos(vx) \ . \tag{4.27}$$

with t running from $-\infty$ to some finite value T that has been chosen to be zero for convenience. The parameter v is free to take any arbitrary value. An equivalent form of the curve is

$$y_\pm = \frac{1}{v}\log\left(\cos(vx) \pm \sqrt{\cos^2(vx) - e^{2v^2 t}}\right) - vt \tag{4.28}$$

with two branches that are simply related to each other by $y \to -y$ or equivalently by $v \to -v$. The variable x assumes values within the interval $-\pi/2v$ to $\pi/2v$, but the precise range depends non-linearly on time t.

The complete curve is closed since the two branches are glued symmetrically about the $y = 0$ axis. For $v = 0$, the configuration reduces to a round circle that evolves by scaling of its radius, i.e., $x^2 + y^2 = -2t$, as can be seen by expanding $\cos(vx)$ and $\cosh(vy)$ up to second order in their arguments. As such, it is common to the circular homothetic solution discussed earlier. For $v \neq 0$, however, the solution represents a convex curve in R^2 having oval (or paper-clip) shape at any given time t, as depicted in figure 9; hence the name paper-clip model.

[3]We thank Vassilis Niarchos for a discussion on this subject.

JHEP06(2007)057

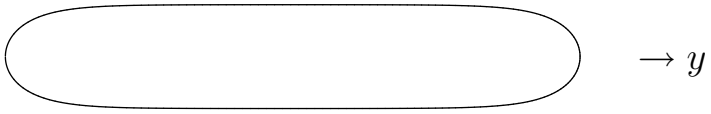

Figure 9: The paper-clip curve on the plane.

This solution arose independently in the physics and mathematics literature. It appeared as model for boundary interactions in ref. [27, 28], but it was also investigated much earlier in connection to magneto-hydrodynamics, [54]. It has the special property that its extrinsic curvature H, when viewed as function of the slope β and the time t, satisfies the special ansatz

$$H^2(\beta, t) = a(\beta) + b(t) \ . \tag{4.29}$$

Substituting into equation (3.13) one finds the following system,

$$\left(\frac{da}{d\beta}\right)^2 + 4a^2 = 4c^2 \,, \qquad \frac{db}{dt} - 2b^2 = -2c^2 \,, \tag{4.30}$$

where c is a constant. The relevant solution in this class has

$$a(\beta) = \frac{v^2}{2}\cos(2\beta) \,, \qquad b(t) = \frac{v^2}{2}\coth(-v^2 t) \tag{4.31}$$

for $c = v^2/2$ and gives rise to the following dependence of the position vector upon β,

$$x(\beta) = \frac{1}{v}\,\arcsin\left(\sqrt{1 - e^{2v^2 t}}\,\sin\beta\right) , \qquad y(\beta) = -\frac{1}{v}\,\mathrm{arcsinh}\left(\sqrt{e^{-2v^2 t} - 1}\,\cos\beta\right) , \tag{4.32}$$

up to translations, according to equation (3.12). Then, it is straightforward to verify that this coincides with the paper-clip curve (4.27) after eliminating the dependence on β.

The corresponding arc-length, as measured from the tip of the paper-clip, follows by integrating $dl = d\beta/H$ and equals to the incomplete elliptic integral of the first kind

$$l(\beta) = \frac{k}{v}\int_0^\beta \frac{d\beta'}{\sqrt{1 - k^2 \sin^2\beta'}} = \frac{k}{v} F(\beta; k) \tag{4.33}$$

in terms of the slope β, with modulus $k = \sqrt{1 - e^{2v^2 t}}$; k varies from 1 to 0 as t runs from $-\infty$ to 0. Thus, in general, we have the relation

$$\sin\beta = \mathrm{sn}(vl/k; k) \tag{4.34}$$

in terms of the corresponding sine-amplitude Jacobi elliptic function.

Clearly, when $v \to 0$ one obtains the characteristic limit $H^2 = -1/2t$ of a circular curve for all t. Also, when $v \neq 0$, the ultra-violet limit $t \to -\infty$ of the paper-clip becomes asymptotic to the curve

$$y = \frac{1}{v}\log\left(2\cos(vx)\right) - vt \,, \tag{4.35}$$

JHEP06(2007)057

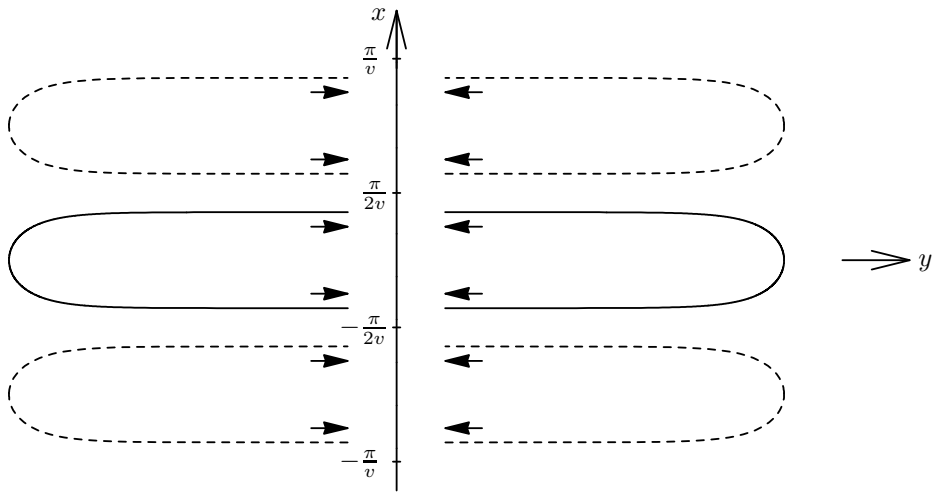

Figure 10: Schematic gluing of hair-pins to form a paper-clip.

as viewed from the tip of the configuration associated to the y_+ branch. This is the hair-pin solution up to an irrelevant constant shift in t. In the ultra-violet region, the mean curvature of the paper-clip tends to the limit $H^2 = v^2\cos^2\beta$ with $\beta \simeq vx$ up to exponentially small corrections in time. A hair-pin facing in the opposite direction is also obtained in the ultra-violet region by viewing the curve from the other tip associated to the y_- branch.

More generally, as t runs from $-\infty$ to 0, the paper-clip evolves by shrinking until it fully collapses to the point $x = 0 = y$ at $t = 0$ and becomes extinct. Note that its size in the x-direction varies as $2v^{-1}\text{arccos}(\exp(v^2 t))$, and deminishes from π/v at $t = -\infty$ to zero at $t = 0$. Likewise, its size in the y-direction varies as $2v^{-1}\text{arccosh}(\exp(-v^2 t))$, which also diminishes from infinite to zero length. Thus, as time goes on, the configuration becomes rounder and rounder by shrinking until it crunches to a point. Only when $v = 0$ the two characteristic lengths of the configuration are equal and diminish evenly by preserving the circular shape of the corresponding solution. According to this, the paper-clip provides the mean curvature analogue of the sausage model encountered in the Ricci flow on S^2, [41].

When the configuration is viewed from its "center of mass", and not from its tips, it looks as a "two-body" problem: two hair-pins with opposite orientation are glued together in their asymptotic region, $y = 0$, and move against each other until their tips merge. Their bound state is pictured schematically in figure 10 by putting together two periodic arrays of hair-pin and anti-hair-pin curves. The paper-clip is depicted by solid lines, whereas the dotted lines denote periodic repetition of the same configuration.

Note that a similar interpretation holds for the sausage model as a "two-body" problem for Ricci solitons that merge together, [41, 53]. The metric of the sausage model can also be expressed in terms of the sine-amplitude Jacobi elliptic function, when written in proper coordinates, which is analogous to the elliptic dependence of the arc-length induced on the paper-clip curve.

JHEP06(2007)057

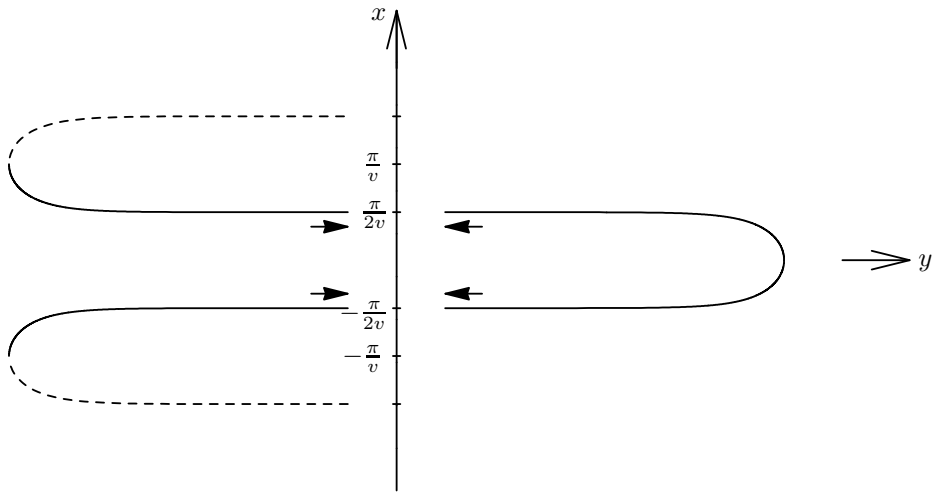

Figure 11: Schematic gluing of hair-pins to form an oxlip.

4.6 Oxlip model

An open variant of the paper-clip model is obtained by considering the following curve on the plane,

$$e^{v^2 t}\sinh(vy) = \cos(vx)\,, \tag{4.36}$$

for $v \neq 0$. In this case, x ranges from $-\pi/v$ to π/v, irrespective of t, and y can be either positive or negative. An equivalent description is given by the graph of the function

$$y = \frac{1}{v}\log\left(\cos(vx) + \sqrt{\cos^2(vx) + e^{2v^2 t}}\right) - vt\ . \tag{4.37}$$

For $-\pi/2v \leq x \leq \pi/2v$ the variable y is positive, assuming that $v > 0$, whereas for $-\pi/v \leq x \leq -\pi/2v$ and $\pi/2v \leq x \leq \pi/v$ the y coordinate is negative. The points $(x = \pm\pi/2v, y = 0)$ are inert under the flow, since these are the points of inflection where the extrinsic curvature vanishes.

This particular solution appears to be new and it is quite interesting in many respects. When compared to the usual paper-clip model, the curve is formed by gluing together two periodic arrays of hair-pins facing in the opposite direction but with a relative shift in x equal to π/v, as in figure 11. Thus, it is a again a bound state problem of hair-pin and anti-hair-pin curves but of slightly different kind. The oxlip curve is depicted by the solid line, extending from $-\pi/v$ to π/v, whereas the dotted lines denote periodic repetition of the same configuration.

The remarkable feature of this solution is that the mean curvature flow exists for all time, as t ranges from $-\infty$ to ∞. In the ultra-violet limit, $t \to -\infty$, one readily gets an infinitely long hair-pin configuration as seen from its tip situated infinitely far away from the gluing region $y = 0$. On the other hand, in the infra-red limit $t \to \infty$, the configuration tends towards the special curve $y = 0$ with $-\pi/v \leq x \leq \pi/v$, which is a segment of a straight line. Thus, it appears that the hair-pin on the right is decaying while its two

JHEP06(2007)057

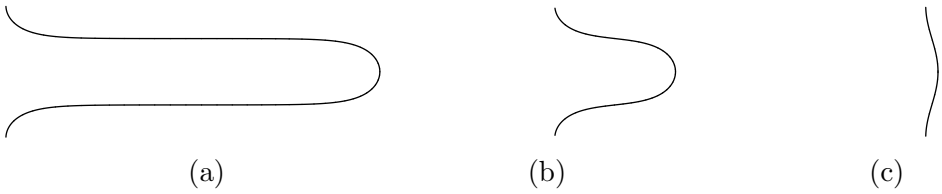

Figure 12: Transition of a hair-pin to a line segment.

sides are getting squeezed against each other. Throughout the process, the two ends of the hair-pin stay firm at $(x = \pm\pi/2v, y = 0)$. The two half hair-pins on the left undergo similar decay until a line segment is finally formed in the infra-red limit. Three consecutive steps of the flow are depicted in figure 12. The same picture arises for $v < 0$, but with opposite orientation for the constituent hair-pins.

This solution satisfies the special ansatz $H^2(\beta, t) = a(\beta) + b(t)$ for the mean curvature with

$$a(\beta) = \frac{v^2}{2}\cos(2\beta)\,, \qquad b(t) = \frac{v^2}{2}\tanh(-v^2 t)\ . \tag{4.38}$$

It is similar to the form of the paper-clip model, but $b(t)$ is now given by the hyperbolic tangent rather than cotangent function; as a result, $b(t)$ never blows up and the solution exists for all time. Then, $x(\beta)$ and $y(\beta)$ can be calculated as for the paper-clip curve, and the same applies to the arc-length $l(\beta)$ which is also expressed in terms of the incomplete elliptic integral of the first kind. The only difference is the choice of modulus, which here is $\tilde{k} = \sqrt{1 + e^{2v^2 t}}$, and varies from 1 to ∞ as t ranges from $-\infty$ to ∞. It relates to the modulus k of the paper-clip curve by the transformation $\tilde{k} = \sqrt{2 - k^2}$ in the common time interval $(-\infty, 0]$. Standard identities among Jacobi elliptic functions show that the slope of the decaying hair-pin at different points of the curve is expressed in terms of its arc-length at any given instance of time by

$$\sin\beta = \frac{1}{\tilde{k}}\mathrm{sn}(vl; \frac{1}{\tilde{k}}) \tag{4.39}$$

with $0 \leq 1/\tilde{k} \leq 1$. Clearly, the slope β vanishes everywhere in the infra-red limit where $1/\tilde{k} = 0$.

Next, we will find, among other things, that the mean curvature flows for the paper-clip and oxlip models are naturally related to certain instability modes of the hair-pin configuration as one begins to move away from the ultra-violet region.

5. Modes of instability and transitions on the plane

In this section we perform a general analysis regarding the linearized (in)stability of special solutions that move by translations, rotations or scaling on the plane. In all cases, we work with the parabolic equation for the mean curvature and obtain an eigen-value problem of the form

$$\mathcal{L}h(\beta) = \lambda h(\beta) \tag{5.1}$$

JHEP06(2007)057

governing small fluctuations about a given solution,

$$H(\beta,t) = H_0(\beta) + h(\beta)\exp(\lambda t)\ . \tag{5.2}$$

$H_0(\beta)$ denotes the mean curvature of the unperturbed curve in a reference frame that all time dependence has been accounted by the appropriate choice of vector field ξ^μ. The operator $\mathcal{L}$ is linear of second order, thus leading to an effective quantum mechanics problem in one dimension parametrized by the slope β. The form of the corresponding potential depends on $H_0(\beta)$ and will be determined in all three cases. General conclusions about its spectrum will be drawn in each case separately.

In general, eigen-states with positive λ account for instabilities since the perturbations grow larger as time goes on. On the other hand, perturbations with negative λ tend to dissipate exponentially fast and the configuration settles quickly back to its initial form, thus leading to stability. Usually, we refer to them as relevant and irrelevant deformations, respectively. Finally, if zero modes are present, they will only act on the parameter space of the given solution without affecting its time dependence. Our primary aim here is to identify potential instabilities about some given reference curves, which arise as fixed points of the mean curvature flow modulo translations, rotations or dilations, and associate transitions towards more stable configurations.

5.1 Translating solution

In this case, small fluctuations of the hair-pin take the form

$$H(\beta,t) = v\cos\beta + h(\beta)e^{\lambda t}\,, \tag{5.3}$$

measuring its response against possible squeezing modes. Then, in the linearized approximation, equation (3.14) for the mean curvature becomes

$$v^2\cos^2\beta\left(\frac{d^2h}{d\beta^2}+h\right) = \lambda h \tag{5.4}$$

since $\vec{\xi}\cdot\hat{n} = v\cos\beta$ and $(d^2/d\beta^2+1)(\vec{\xi}\cdot\hat{n}) = 0$. It turns out that the spectrum of λ can be fully determined by simple transformation to an exactly solvable problem.

For this, consider the change of variables

$$z = \log\left(\tan\left(\frac{\beta}{2}+\frac{\pi}{4}\right)\right), \qquad \Psi(z) = h(\beta)\sqrt{\cosh z} \tag{5.5}$$

that transform the fluctuation equation (5.4) into the following Schrödinger problem

$$-\frac{d^2\Psi}{dz^2} + \frac{1}{4}\left(1-\frac{3}{\cosh^2 z}\right)\Psi = -\frac{\lambda}{v^2}\Psi \tag{5.6}$$

with $-\infty < z < \infty$ as $-\pi/2 \le \beta \le \pi/2$. The variable z is obtained by integrating $dz = d\beta/\cos\beta = v d\beta/H(\beta)$ for the hair-pin curve and as such it coincides with its arc-length l (multiplied by v) as measured from the tip; a useful relation here is $\cosh z = 1/\cos\beta$.

JHEP06(2007)057

Thus, we arrive at an eigen-value problem for a particle moving on the real line under the influence of a symmetric Rosen-Morse potential $U(z) = W^2(z) - W'(z)$ with superpotential

$$W(z) = \frac{1}{2}\tanh z \tag{5.7}$$

and energy $E = -\lambda/v^2$.

This problem has been exactly solved in the literature, [62], in the context of supersymmetric quantum mechanics, and it was found that it admits only one normalizable eigen-state,

$$\Psi_0(z) = \frac{1}{\sqrt{\cosh z}}\,, \tag{5.8}$$

whose energy is zero. The ground state, which corresponds to $h_0(\beta) = \cos\beta$ under the change of variables (5.5), does not induce a decay of the initial configuration but only amounts to shifting v by constant, as can be readily seen from equation (5.3); it is the expected behavior for a zero mode acting on the moduli v of the underlying hair-pin curve. There is also a continuum of scattering eigen-states with energies $E \geq 1/4$, which, however, have $\lambda < 0$ and correspond to stability modes of the problem as one flows away from the ultra-violet regime. According to this, the hair-pin (4.3) looks absolutely stable and acts as infra-red attractor for all hair-pin-like shapes that deviate from it by the appropriate perturbations. It is the expected behavior for a solitonic solution.

There is an additional infinite set of discrete eigen-states in the Rosen-Morse potential with $E < 0$, and hence $\lambda > 0$, which may serve as instability modes of the hair-pin configuration. The existence of negative energy states in a problem of supersymmetric quantum mechanics looks strange at first sight, but it only implies that the corresponding Hamiltonian operator is not self-adjoint in the space of the corresponding wave functions, thus violating the lower energy bound. The reason is that such states are not normalizable, since they blow up at the two ends of the hair-pin as $z \to \pm\infty$, and should be disregarded on normal grounds. This is indeed the case for the stability analysis of a single hair-pin, but as it turns out negative energy states play an interesting role in understanding the linearized evolution of bound state problems of hair-pins, such as the paper-clip in section 4.5 and its open variant in section 4.6. It will be seen later that gluing two hair-pins with the opposite orientation amounts to canceling the divergent perturbations in their asymptotic region, thus giving rise to regular solutions.

More precisely, it can be easily verified that that the Schrödinger problem (5.6) has eigen-states

$$\Psi_n(z) = i^{n+1}\sqrt{\cosh z}\; P_n^1(i\sinh z) \tag{5.9}$$

with quantized energies $E_n = -n(n+1)$ for all $n = 1, 2, 3, \cdots$. Here, $P_n^1(x)$ denote, up to normalization, the associated Legendre functions of x

$$P_n^1(x) = \sqrt{1-x^2}\;\frac{d^{n+1}}{dx^{n+1}}[(1-x^2)^n]\;. \tag{5.10}$$

Despite appearances, all states $\Psi_n(z)$ are real. Then, λ assumes discrete values $\lambda_n = v^2 n(n+1)$, which are non-negative, and the corresponding modes are associated to instabilities of the hair-pin configuration. The ground state of the Rosen-Morse potential,

JHEP06(2007)057

$\Psi_0(z) = 1/\sqrt{\cosh z}$, may also be appended to these formulae by extending their validity to $n = 0$.

The first non-normalizable state in this series has $n = 1$ with $\lambda_1 = 2v^2$ and $\Psi_1(z) = (\cosh z)^{3/2}$, which corresponds to $h_1(\beta) = 1/\cos\beta$, up to normalization. A simple calculation shows that this is precisely the perturbation driving the evolution of the paper-clip at the linearized level, as seen from one of its tips close to the ultra-violet region. Indeed, by expanding the mean curvature $H(\beta, t)$ of the paper-clip model one finds

$$H(\beta,t) = \frac{v}{\sqrt{2}}\sqrt{\cos(2\beta) - \coth(v^2 t)} = v\cos\beta + \frac{v}{2\cos\beta}e^{2v^2 t} + \mathcal{O}(e^{4v^2 t}) \ . \tag{5.11}$$

This is a valid expansion as long as $t \to -\infty$ and β parametrizes small deviations away from the tip of one of the two constituent hair-pins so that $1/\cos\beta$ remains bounded. It has precisely the form

$$H(\beta,t) \simeq H_0(\beta) + h_1(\beta)\exp(\lambda_1 t)\,, \tag{5.12}$$

as noted above. Similar conclusions are drawn by expanding around the other tip of the curve. Likewise, for the oxlip model one finds

$$H(\beta,t) = \frac{v}{\sqrt{2}}\sqrt{\cos(2\beta) - \tanh(v^2 t)} = v\cos\beta - \frac{v}{2\cos\beta}e^{2v^2 t} + \mathcal{O}(e^{4v^2 t}) \tag{5.13}$$

which is valid in the same domain of parameters and corresponds to the same linearized perturbation (5.12).

This identification puts the negative energy states on firm basis and makes them physically relevant for the bound state problems under consideration. Of course, it is important to realize that the gluing conditions, which stick together the open ends of the constituent hair-pins, miraculously cancel the divergences of $h_1(\beta)$ on each component when $\beta \to \pm\pi/2$. The free ends of a hair-pin and an anti-hair-pin effectively attract each other, but this is a non-linear effect that can not be seen by expanding far away from their overlap. Only the exact solution, in either case, reveals the correct value of the extrinsic curvature at the connection points. Higher excited states $n \geq 2$ may also be used to describe potential decay channels for bound state problems of the hair-pin curves, since λ_n is strictly positive, but their form is more complicated; for instance, for $n = 2$, $\Psi_2(z) = (\cosh z)^{3/2}\sinh z$, which corresponds to $h_2(\beta) = \sin\beta/\cos^2\beta$ with $\lambda_2 = 6v^2$ and so on. To the best of our knowledge, there is no exact description of the corresponding trajectories at the non-linear level, as in the case of the paper-clip and oxlip models. It is an interesting problem that deserves further investigation while searching for exact solutions of the mean curvature flow.

Finally, we note for completeness that all positive energy states in the Rosen-Morse potential (5.6) can be obtained from the discrete set of negative modes (5.9) by appropriate continuation. More precisely, using the standard description of the associated Legendre functions in terms of hypergeometric functions, and replacing n by $ik - 1/2$ in their arguments, so that $E = -n(n+1)$ becomes $E = k^2 + 1/4$, we obtain solutions with continuous spectrum $E \geq 1/4$ for all real values of k. If time were flowing in the opposite direction these would have been the instability modes of the problem.

JHEP06(2007)057

5.2 Scaling solutions

Next, we investigate the existence of instability modes for perturbations of the scaling solutions. Naturally, there are two different cases here depending on the sign of the scaling parameter c. In either case it is appropriate to look at the linearized problem in terms of equation (3.14) for $H(\beta,t) = H_0(\beta) + h(\beta)\exp(\lambda t)$ with $\vec{\xi}\cdot\hat{n} = -c(x(\beta)\sin\beta - y(\beta)\cos\beta) = -cS(\beta)$, in which case $(d^2/d\beta^2+1)(\vec{\xi}\cdot\hat{n}) = -c(S''(\beta)+S(\beta)) = -c/H(\beta)$.

(i) Self-shrinkers ($c<0$): for self-shrinking solutions the small fluctuation operator $\mathcal{L}$ reads

$$\mathcal{L}_{c<0} = H_0^2(\beta)\frac{d^2}{d\beta^2} + H_0^2(\beta) + 1 \tag{5.14}$$

setting $c=-1$ without loss of generality. Focusing on closed curves, as we do in the sequel, amounts to solving the eigen-value problem $\mathcal{L}h(\beta) = \lambda h(\beta)$ on the space of periodic functions $h(\beta+T) = h(\beta)$ with period $T = 2\pi p$ given in terms of the winding number p; note, however, that the periodicity on $h(\beta)$ is necessary but not sufficient condition to ensure closure of the resulting curve via equation (3.12) for $x(\beta)$ and $y(\beta)$, and it should be checked separately. Since the operator (5.14) is self-adjoint on the space of square-integrable functions $L^2(S^1, d\mu)$ with measure $d\mu = d\beta/H_0^2(\beta)$, it follows from the general theory, [63], that its spectrum is discrete

$$\lambda_0 > \lambda_1 \geq \lambda_2 > \lambda_3 \geq \lambda_4 > \cdots \tag{5.15}$$

accumulating at $-\infty$. The corresponding eigen-functions $h_n(\beta)$ are orthonormal and although they can not be explicitly computed, due to the transcendental form of $H_0(\beta)$, they are bound to have a fixed number of nodes depending on n; in particular, h_0 has no nodes, whereas h_{2n-1} and h_{2n} with $n>1$ have exactly $2n$ zeros in S^1 within a period $2\pi p$.

One easily sees in the present case that $H_0(\beta)$ is an eigen-function of the operator (5.14) with eigen-value 2, which is necessarily the largest, i.e., $\lambda_0 = 2$, since $h_0(\beta) = H_0(\beta) \geq 1$ vanishes nowhere. Thus, there is at least one potential mode of instability modulo the question of keeping the deformed curve closed. There are additional modes of instability for the linearized perturbations of the Abresch-Langer curves $\Gamma_{p,q}$ with winding number p and q petals, which depend on $q>1$. For this note that $H_0'(\beta)$ is also an eigen-function of the operator (5.14) but with zero eigen-value. Since it has $2q$ zeros, equal to the number of times $H_0(\beta)$ reaches its minimum value 1 within a period $2\pi p$, it follows from above that $H_0'(\beta)$ should be identified with either eigen-function h_{2q-1} or h_{2q}. Actually, it turns out that $h_{2q-1}(\beta) = H_0'(\beta)$ and zero is a simple eigen-value. The effect of the zero mode on the Abresch-Langer curves is to rotate them on the plane since $H_0(\beta+\epsilon) = H_0(\beta) + \epsilon H_0'(\beta)$ to lowest order in ϵ. Thus, in general, there are $2q-1$ discrete modes of instability $h_0, h_1, \cdots, h_{2q-2}$ for all $\Gamma_{p,q}$ curves; among these there are two eigen-functions, $\cos\beta$ and $\sin\beta$, which both have $\lambda = 1$. All other modes have negative eigen-values leading to exponentially damped perturbations in time. It turns out that the total number of instability modes that also preserve the closure of the curves is $2q-3$; further details can be found in ref. [59].

JHEP06(2007)057

There is a more systematic way to examine the spectrum of small fluctuations using the arc-length $l = z$, for $dz = d\beta/H(\beta)$, and the variable $\Psi(z) = h(\beta)/\sqrt{H_0(\beta)}$, as for the translating solution. The effective quantum mechanics problem now reads

$$\left(-\frac{d^2}{dz^2} + U(z)\right)\Psi(z) = (2-\lambda)\Psi(z)\,, \tag{5.16}$$

where $U(z) = W^2(z) + W'(z)$ with corresponding super-potential

$$W(z) = \frac{1}{2H_0(z)}\frac{dH_0(z)}{dz} = \frac{dH_0(\beta)}{2d\beta}\ . \tag{5.17}$$

The variable z ranges over a finite distance, equal to the total length of the $\Gamma_{p,q}$ curves, along which H_0 remains positive ranging from $H_-(E)$ to $H_+(E)$. Thus, z can be regarded as periodic variable. Also, $W(z)$ never becomes singular in this domain; it is equal to (one-half) the velocity of a particle moving in the potential well (4.21). Thus, according to supersymmetric quantum mechanics, the energy spectrum is strictly positive, so that $\lambda \leq 2$, supporting an infinite but discrete set of periodic solutions as discussed above. Of course, one may also have bands with continuum spectrum when more general Bloch-wave solutions are allowed to occur; these generalizations, however, do not yield periodic perturbations of the Abresch-Langer curves breaking their closure.

The special case $q = 1$ is a round circle with $H_0(\beta) = 1$ everywhere and its perturbations can be studied separately by solving the eigen-value problem $(d^2/d\beta^2+2)h(\beta) = \lambda h(\beta)$ on S^1 with period $2\pi p$. The periodic solutions are simply $\cos(n\beta/p)$ and $\sin(n\beta/p)$ with integer n. In either case, the eigen-values are $\lambda = 2 - (n/p)^2$, which are positive only for those n satisfying the inequality $n^2 < 2p^2$. Clearly, there can be no zero mode for $1/\sqrt{2}$ is an irrational number; the absence of zero modes is also consistent with the fact that the position of the circle on the plane does not change by rotation, unlike the case of Abresch-Langer curves. For winding number $p = 1$, there are no unstable modes that preserve the closure of the curve. Indeed, although $\cos\beta$ and $\sin\beta$ have $\lambda = 1$ and can be potential modes of instability, they are ruled out because they do not yield periodic $x(\beta)$ and $y(\beta)$, respectively (see the remark towards the end of section 2.1). Thus, there is a unique simple homothetic closed curve on the plane which is absolutely stable against all perturbations; this is also consistent with the fact that a circle with winding number $p = 1$ always attracts locally convex simple closed curves under the flow, [46, 47]. For circles with higher winding number $p > 1$, it follows from above that the number of potentially unstable modes equals to the number of integers n, positive or negative, that satisfy the inequality $|p/n| > 1/\sqrt{2}$. All these modes preserve the closure of the curve apart from two, $\cos\beta$ and $\sin\beta$, which have $\lambda = 1$ for all p.

Thus, as time goes on, one can envisage transitions from a circular configuration with winding number p towards an Abresch-Langer curve $\Gamma_{p,q}$ with $1/2 < p/q < 1/\sqrt{2}$ followed by a transition towards a singular closed curved with q cusps, where the mean curvature blows up. The various stages of deformation are shown schematically in figure 13 for the simplest case $(p, q) = (2, 3)$, as in ref. [58].

In this case, turning on an instability mode, say $h(\beta) = \sin(\beta/2)$, for a circle with $p = 2$, which is pictured as two $p = 1$ copies sitting on top of each other, amounts to

JHEP06(2007)057

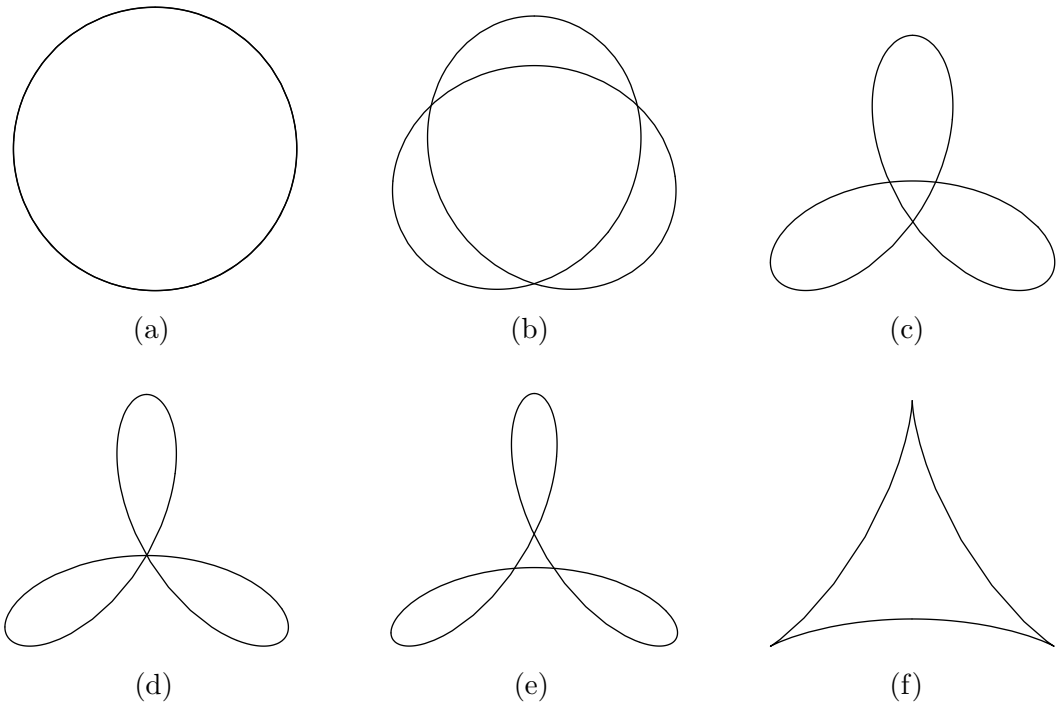

Figure 13: Transition from a double-folded circle to a singular curve.

enlarging the mean curvature of the first copy (covered by $0 \leq \beta \leq 2\pi$) and decrease that of the second copy (covered $2\pi \leq \beta \leq 4\pi$). It is easy to imagine that such uneven deformation, which keeps the curvature unchanged at the points $\beta = 0,\ 2\pi$ and 4π is pictured schematically by the closed curve figure 13b. Subsequent evolution towards the Abresch-Langer curve $\Gamma_{2,3}$, as shown in figure 13c, is then due to non-linear effects. The instability modes of $\Gamma_{2,3}$ are capable to deform it further towards the configurations shown in figure 13d and figure 13e until the singular curve shown in figure 13f is reached. None of the intermediate configurations correspond to scaling solutions apart from (a) and (c). Unfortunately, such transitions are not available in closed form; it is also an interesting problem for future work.

The stability modes of the Abresch-Langer curves can be formally viewed as instability modes of the backward mean curvature flow. Thus, one may also envisage transitions from $\Gamma_{p,q}$ to a circle with winding number p, as given schematically in the figure above by flowing continuously from figure 13c to figure 13b and finally to figure 13a. In this case, the periodic functions $\cos(q\beta/p)$ and $\sin(q\beta/p)$ with $p/q < 1/\sqrt{2}$ are stability modes of the circle with winding number p showing that the configuration figure 13a can act as attractor for the corresponding flow. It also explains from a more intuitive point of view the upper bound on p/q that defines the initial scaling solution $\Gamma_{p,q}$ provide that such transitions (among others) are indeed possible. In this respect, it can be shown that the mean curvature flow with initial data $\vec{r}_0 = \vec{r}_{p,q} + \epsilon\hat{n}$, given in terms of the position vector of any Abresch-Langer curve $\Gamma_{p,q}$ with $|\epsilon|$ small, tends asymptotically to an p-fold circle when $\epsilon > 0$ and to a

JHEP06(2007)057

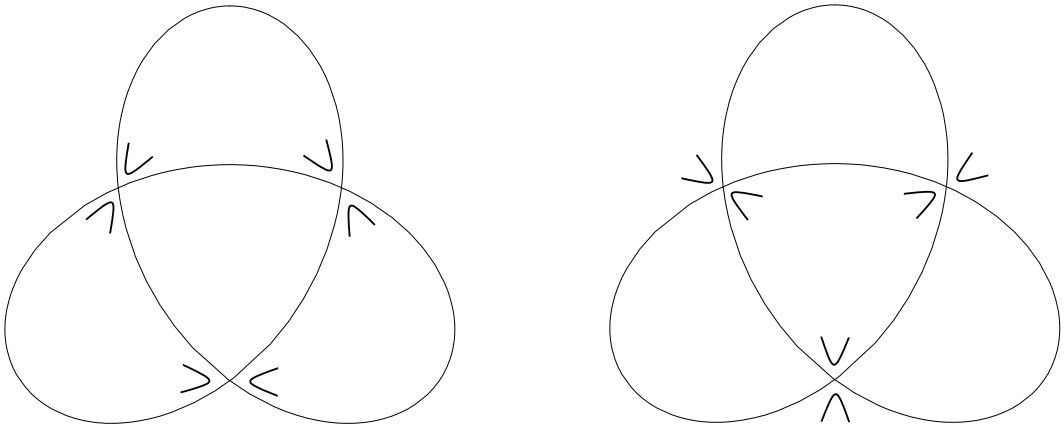

(a) (b)

Figure 14: Cutting rules familiar from knot theory.

singular closed curve with q cusps when $\epsilon < 0$, [64].

There are additional transitions one may envisage. One possibility is to have a decay channel for the singular curve figure 13f, which can be roughly thought as bound state of three wedges held together by appropriate gluing conditions, to a diminishing simple circle. Although there is no explicit solution of this kind, one may imagine that each corner will decay to a smooth curve coming out of the wedge and all three local solutions can be patched together to form a smooth closed curve that will eventually shrink to a point. Combining this transition with the one depicted in figure 13, we arrive at the reasonable conclusion that a configuration can change its winding number, e.g., from $p = 2$ to $p = 1$, when it passes through a singular shape. Another possibility based on the physical idea of tachyon condensation is that any curve with self-intersections, like the Abresch-Langer curves, will cut itself and follow the decay channel of two intersecting lines in the vicinity of each self-intersection point[4]. Recombination of the outgoing curves from each local wedge will result into a collection of circular branes that eventually shrink to points. This procedure resembles the construction of knot invariants out of planar closed curves, using appropriate cutting rules at the self-intersection points; see, for instance, [65] and references therein. These are depicted in figure 14 below.

It may very well be that such formal connection holds the key for the systematic construction of the corresponding boundary states in quantum field theory. We plan to return to this problem elsewhere.

(ii) Self-expanders ($c > 0$): finally, we consider the case of self-expanding solutions for which the small fluctuation operator $\mathcal{L}$ reads

$$\mathcal{L}_{c>0} = H_0^2(\beta)\frac{d^2}{d\beta^2} + H_0^2(\beta) - 1\,, \tag{5.18}$$

[4]We thank Boris Pioline for a discussion on this point.

JHEP06(2007)057

setting $c = 1$ for convenience. Note that the spectrum of $\mathcal{L}_{c>0}$ follows by subtracting two units from the spectrum of $\mathcal{L}_{c<0}$, although the form of the eigen-functions $h(\beta)$ is different for $H_0(\beta)$ is not the same. Also, in this case, the reference curves are open and one should impose a different set of boundary conditions on the corresponding eigen-functions. Here, $H_0(\beta)$ is an eigen-function with $\lambda = -2$, whereas $H_0'(\beta)$ is still an eigen-function with $\lambda = 0$. This zero mode, as before, describes the freedom to rotate the curve on the plane and orient it differently with respect to the y-axis; the same rotation applies to its asymptotic lines. There are also two obvious modes with $\lambda = -1$ corresponding to the eigen-functions $\cos\beta$ and $\sin\beta$.

In general we would like to solve the eigen-value problem (5.18) with a prescribed set of boundary conditions. Here, β ranges in the interval $[\pi - \Delta\beta(E),\ \Delta\beta(E)]$ whose end points are given in terms of the slope (4.26) of the asymptotic lines to the scaling solution. If the perturbed curve is to remain asymptotic to the wedge, one has to consider solutions $h(\beta)$ that vanish at the end points of this interval. This is a well-defined bound state problem having discrete spectrum $\lambda \leq -2$ that accumalates to $-\infty$. The proof relies on the observation that $H_0(\beta)$, which is an eigen-state of the operator (5.18) with the above boundary conditions, vanishes nowhere else but at the end points of the interval; as such, it serves as the ground state of the problem. All higher excited states will have $\lambda < -2$ and exhibit additional zeros at various intermediate points of the interval. The conclusion is that all perturbations of this kind correspond to stability modes.

Instability modes may only arise if one alters the boundary conditions. Note that perturbations which can grow infinite large at the end points of the interval, while they remain bounded in all intermediate points, are capable to produce solutions with $\lambda > -2$. For example, the zero mode $H_0'(\beta)$ is a monotonically decreasing function starting from ∞ at $\beta = \pi - \Delta\beta(E)$ and ending to $-\infty$ at $\beta = \Delta\beta(E)$; it has only one zero at $\beta = 0$ around which the perturbation stays small. It is easy to anticipate the existence of excited eigen-states with the same blow up behavior at the end points of the interval that exhibit more zeros at intermediate points. Although it is not possible to construct them explicitly, they are bound to have $\lambda > 0$ and lead to instabilities of the scaling solution. These positive modes are similar in nature to the instability modes of the hair-pin configuration that also blow up at the end points of the β-interval. It will be interesting to examine them further and associate various decay channels towards some more stable configurations in "bound state" problems with curvature singularities, e.g., configurations of closed curves with cusps.

A more systematic description is also provided here by supersymmetric quantum mechanics using the arc-length $l = z$ that ranges from $-\infty$ to ∞ as one traces the curve from its far left to its far right asymptotic lines. Letting $\Psi(z) = h(\beta)/\sqrt{H_0(\beta)}$, as before, the corresponding linearized equation becomes

$$\left(-\frac{d^2}{dz^2} + U(z)\right)\Psi(z) = -(2+\lambda)\Psi(z)\,, \tag{5.19}$$

where $U(z) = W^2(z) + W'(z)$ with super-potential given by the same functional form (5.17). This super-potential equals to (one-half) the velocity of a particle in the unbounded poten-

JHEP06(2007)057

tial well (4.25) and can take any real value. Under usual boundary conditions at $z \to \pm\infty$ the spectrum is non-negative leading to $\lambda \leq -2$ by supersymmetry.

5.3 Rotating solution

Next, we consider small fluctuations around the static Yin-Yang curve with curvature $H_0(\beta)$, satisfying the defining relation (4.10), and substitute into equation (3.14). Note that in this case $\vec{\xi} \cdot \hat{n} = \omega(x(\beta)\cos\beta + y(\beta)\sin\beta) = \omega S'(\beta)$ and so simple calculation yields $(d^2/d\beta^2 + 1)(\vec{\xi} \cdot \hat{n}) = \omega(S''(\beta) + S(\beta))' = -\omega H'(\beta)/H^2(\beta)$. Then, the corresponding linearized problem reads $\mathcal{L}h(\beta) = \lambda h(\beta)$ with

$$\mathcal{L} = H_0^2(\beta)\frac{d^2}{d\beta^2} + \omega\frac{d}{d\beta} + H_0^2(\beta) - 2\omega\frac{H_0'(\beta)}{H_0(\beta)} \,. \tag{5.20}$$

Clearly, $H_0'(\beta)$ is a zero mode that corresponds to the freedom to perform rigid rotation of the Yin-Yang curve on the plane.

In order to examine the spectrum of the operator $\mathcal{L}$ it is convenient, once again, to introduce the arc-length parameter $l = z$ and change variable to

$$h(\beta) = \Psi(z)\sqrt{H_0(z)}\exp\left(-\frac{\omega}{2}\int_0^z \frac{dz'}{H_0(z')}\right) \,. \tag{5.21}$$

This results into an effective Schrödinger problem for a particle in the state $\Psi(z)$ with energy $E = -\lambda$ moving in the following potential

$$U(z) = W^2(z) - W'(z) - H^2(z)\,, \tag{5.22}$$

where

$$W(z) = \frac{1}{2}\left(\frac{1}{H(z)}\frac{dH(z)}{dz} + \frac{\omega}{H(z)}\right) = \frac{1}{2}\left(\frac{dH(\beta)}{d\beta} + \frac{\omega}{H(\beta)}\right). \tag{5.23}$$

The effective coordinate z ranges from $-\infty$ to ∞, as one traces the complete Yin-Yang curve from one end to the other, with $z = 0$ corresponding to the point of inflection located at its center. The curvature remains bounded everywhere and tends to zero far away from the center of the spiral.

If the term $H^2(z)$ were not present, the potential $U(z)$ would support a zero energy state as well as higher energy states by supersymmetric quantum mechanics. Note, however, that $H^2(z)$ is a positive definite term that vanishes asymptotically as $z \to \pm\infty$ and lowers the potential everywhere. Thus, the energy spectrum of $U(z)$ is also lower having at least one negative energy state that arises by shifting the energy of the "would be supersymmetric" ground state. It also supports a zero energy state, as noted above, which arises by shifting the energy of some otherwise excited supersymmetric state; furthermore, it supports other positive energy states. Although it is difficult to determine the exact form of the shifted energy eigen-states, it is clear that the presence of negative modes, which have $\lambda > 0$, will lead to instabilities of the Yin-Yang curve.

JHEP06(2007)057

6. Mean curvature flow on two-dimensional surfaces

In this section we extend the previous discussion to two-dimensional curved spaces, so that the mean curvature flow is naturally combined with the Ricci flow. We will present examples of curves embedded in conformal backgrounds, such as the Ricci soliton, as well as examples of deforming curves embedded in spaces with deforming metrics. Among them there are mini-superspace models that capture the competition of shrinking curves on shrinking backgrounds. Closed curves may fully collapse before the metric reaches a singularity or they may collapse simultaneously to a point.

6.1 General aspects

Let us consider a general two-dimensional ambient space $\mathcal{M}$ whose metric is expressed in conformally flat form

$$ds^2_{\mathcal{M}} = \frac{1}{\Omega}\left(dx^2 + dy^2\right). \tag{6.1}$$

The conformal factor Ω depends on the coordinates x and y and it may also depend on the renormalization group time t when the background deforms under the Ricci flow. In this space we consider embedded curves $(x(s), y(s))$ whose induced line element is

$$dl^2 = \frac{1}{\Omega}\left(\left(\frac{\partial x}{\partial s}\right)^2 + \left(\frac{\partial y}{\partial s}\right)^2\right) ds^2 \ . \tag{6.2}$$

According to the definitions given in appendix A, the unit normal vector to each point of these curves is

$$\hat{n} = \frac{\sqrt{\Omega}}{\sqrt{1+\varphi'^2(x)}}(-\varphi'(x),\ 1)\,, \tag{6.3}$$

and the mean curvature is

$$H = \frac{\sqrt{\Omega}\ \varphi''(x)}{\left(\sqrt{1+\varphi'^2(x)}\right)^3} + \frac{1}{2\sqrt{\Omega}\sqrt{1+\varphi'^2(x)}}\left(\partial_y\Omega - \varphi'(x)\partial_x\Omega\right)\ , \tag{6.4}$$

which generalize the corresponding expressions for planar curves used in section 3. The notation $y = \varphi(x)$ is used here, as before, to express the embedded curves in graph form.

The mean curvature flow in $\mathcal{M}$ is formulated, as usual, by computing the deformations of the coordinate functions $x(s,t)$ and $y(s,t)$ driven by the mean curvature vector. The result is better described by the deformation of graphs $y = \varphi(x(t),t)$, which turn out to satisfy equation

$$\frac{\partial\varphi}{\partial t} = \frac{\Omega\ \varphi''(x)}{1+\varphi'^2(x)} + \frac{1}{2}\left(\partial_y\Omega - \varphi'(x)\partial_x\Omega\right) - k^y + \varphi'(x)k^x\ . \tag{6.5}$$

Here, we have properly included the effect of reparametrizations generated by a Killing vector field k (if it is at all present) along the flow. This equation should be combined with the Ricci flow of the target space metric, which reads in terms of Ω

$$\frac{\partial\Omega^{-1}}{\partial t} = \frac{1}{2}(\partial_x^2 + \partial_y^2)\log(\Omega^{-1}) \tag{6.6}$$

JHEP06(2007)057

when there is no dilaton present in the model. Thus, the combined system of Ricci and mean curvature flows for embedded curves in arbitrary two-dimensional Riemannian spaces are described by equations (6.5) and (6.6) for the two unknown functions Ω and φ, which in general depend on t.

In the presence of a dilaton field Φ, the conformal factor should satisfy the following constraints

$$\partial_x(\Omega\partial_y\Phi) + \partial_y(\Omega\partial_x\Phi) = 0\,, \qquad \partial_x(\Omega\partial_x\Phi) = \partial_y(\Omega\partial_y\Phi)\,, \tag{6.7}$$

for, otherwise, the different components of the Ricci flow equations for the metric are not compatible. In view of the applications that will be considered later, let us assume that both Φ and Ω are independent of the coordinate x so that the model exhibits an isometry with Killing vector field $\partial/\partial x$. Then, the constraints above are automatically satisfied provided that $\Omega\partial_y\Phi$ is independent of y. This term is actually constant, and not function of t, for otherwise the y-derivative of the dilaton flow will be incompatible with the Ricci flow. This constant is of order $1/\alpha'$ and may be chosen so that

$$\Omega\partial_y\Phi = \frac{4}{\alpha'} \tag{6.8}$$

when the dilaton field is non-trivial; otherwise it is zero. The normalization ensures that fixed points of the Ricci flow are also fixed points of the dilaton flow accounting for the balance between the field dependent and central terms of $\beta(\Phi)$ in two dimensions. Thus, the two fields Φ and Ω are taken to satisfy equation (6.8) for all t, and, from now on, we set for convenience $\alpha' = 4$.

According to this, the Ricci flow for $\Omega(y,t)$ is given by the evolution

$$\frac{\partial}{\partial t}\Omega^{-1} = \frac{1}{2}\partial_y^2\log(\Omega^{-1}) - \partial_y(\Omega^{-1})\,, \tag{6.9}$$

whereas the dilaton $\Phi(y,t)$ follows by integration of equation (6.8). Also, the equation for the mean curvature flow, expressed in terms of the graph $\varphi(x(t),t)$ for embedded curves, takes the following form

$$\frac{\partial\varphi}{\partial t} = \frac{\Omega\ \varphi''(x)}{1+\varphi'^2(x)} + \frac{1}{2}\partial_y\Omega + 1 + k^x\varphi'(x) - k^y \tag{6.10}$$

accounting also for the dilaton and the effect of reparametrizations generated by the Killing vector field (k^x, k^y) along the flow.

It is convenient sometimes, when the ambient space is surface of revolution, to use proper coordinates (r,θ) so that the metric takes the form

$$ds^2_{\mathcal{M}} = A^2(t)\left(dr^2 + f^2(r,t)d\theta^2\right) \tag{6.11}$$

with scale factor $A(t)$ and profile function $f(r,t)$. These coordinates are best suited for drawing the surface and the curves embedded in it. The corresponding Killing vector field is $(k^r, k^\theta) = (0,\omega)$ and it is associated to arbitrary angular velocity ω. Assuming that the dilaton is independent of θ, the Ricci flow equations become

$$\frac{\partial A^2}{\partial t} = \frac{f''}{f} - 2\Phi''\,, \qquad \frac{\partial f}{\partial t} = \frac{1}{A^2}(f\Phi'' - f'\Phi')\,, \tag{6.12}$$

JHEP06(2007)057

where prime denotes the derivative with respect to the radial coordinate. The dilaton flow accompanying them is

$$\frac{\partial\Phi}{\partial t} = \frac{1}{2A^2}\left(\Phi'' + \frac{f'}{f}\Phi' - 2\Phi'^2\right) + 1\,, \tag{6.13}$$

setting, once again, $\alpha' = 4$. Also, the mean curvature flow for deforming curves can be formulated in this frame by considering $r = \rho(\theta(t), t)$. Explicit calculation shows that it takes the following form

$$\frac{\partial\rho}{\partial t} = \frac{1}{A^2\left(f^2(\rho) + (\partial\rho/\partial\theta)^2\right)}\left(\frac{\partial^2\rho}{\partial\theta^2} - \frac{f'(\rho)}{f(\rho)}\left(f^2(\rho) + 2\left(\frac{\partial\rho}{\partial\theta}\right)^2\right)\right) + \frac{1}{A^2}\Phi'(\rho) + \omega\frac{\partial\rho}{\partial\theta}\,, \tag{6.14}$$

adding also the contribution of the dilaton and the effect of possible reparametrizations generated by uniform rotation along the flow.

Rotating solitons exist on all surfaces of revolution, thus generalizing the planar Yin-Yang curve. They correspond to fixed points of equation (6.14), with $\omega \neq 0$, satisfying the ordinary non-linear differential equation for $\rho(\theta)$,

$$\frac{d}{d\theta}\arctan\left(\frac{1}{f(\rho)}\frac{d\rho}{d\theta}\right) + f(\rho)\Phi'(\rho) - f'(\rho) + \omega A^2 f(\rho)\frac{d\rho}{d\theta} = 0\ . \tag{6.15}$$

This equation can not be easily solved in closed form. Even in the simplest case of planar rotating solitons, for which equation (6.15) can be integrated once, the solution is only given implicitly. On curved surfaces, the background fields undergo continuous deformations by Ricci flow, and, therefore, rotating solitons correspond to curves solving equation (6.15) at each given instance of time. Some non-trivial examples will be studied later.

Another class of special solutions arise on all surfaces of revolution when ρ is independent of the angular variable θ. They correspond to circular curves that can roll on the surface while remaining symmetric about the principal axis. In this case, ρ only depends on t and satisfies the equation

$$\frac{d\rho}{dt} = \frac{1}{A^2}\left(\Phi'(\rho) - \frac{f'(\rho)}{f(\rho)}\right). \tag{6.16}$$

The solutions generalize the uniformly contracting circular planar curves to curved backgrounds. However, their time evolution depends on the geometry of the surface. We will also see examples of this later.

6.2 Branes on constant curvature surfaces

Trivial dilaton in proper coordinates implies that the profile function $f(r)$ is independent of t, so that all time dependence is fully encoded into the scale factor $A(t)$. In this case, $f''(r)/f(r)$ is constant that can be normalized to -1, $+1$ or 0 without loss of generality. These are precisely constant curvature metrics on $\mathcal{M}$ with positive, negative or zero curvature, respectively, for which $A^2(t)$ turns out to be $-t$, t or 1, up to normalization. Here, we will examine some simple solutions of the mean curvature flow on the sphere with

JHEP06(2007)057

$f(r) = \sin r$ and on the one-sheeted hyperboloid with $f(r) = \cosh r$. In the former case, r is an angular variable ranging from 0 to π as one moves from one pole of the sphere to the other, whereas in the latter r ranges over the entire real line.

The simplest running solutions correspond to circular curves satisfying equation (6.16). On the sphere one gets the solution

$$|\cos\rho(t)| = -\frac{t_0}{t}\,, \tag{6.17}$$

where t_0 is a non-negative integration constant. Thus, as time flows from $-\infty$ to 0 the background is a uniformly contracting sphere. The circular brane appears to come from the equator and slip off the side, on either hemisphere, until it fully collapses to a point at $t = -t_0$ before the big crunch. There is also the special solution $\rho = \pi/2$, which corresponds to $t_0 = 0$ and represents a great circle that follows the collapse of the sphere all the way to a point. The corresponding solution on the hyperboloid reads

$$|\sinh\rho(t)| = \frac{t_0}{t}\,, \tag{6.18}$$

where the integration constant t_0 is again non-negative. In this case, as time flows from 0 to ∞, the background evolves uniformly by lowering its curvature. The circular brane appears to come from the asymptotic region of the hyperboloid, which corresponds to $\rho \to \pm\infty$, and stabilizes to a circle at $\rho = 0$ in the infra-red limit. As before, there is also the special solution $\rho = 0$ for $t_0 = 0$ that does not roll at all on either side.

Another interesting problem is the construction of rotating solutions on constant curvature spaces. The problem has already been investigated, to some extend, in ref. [66] under the unnatural condition that the metric does not Ricci flow. These results, however, can be easily generalized to uniformly varying backgrounds without much effort. One way is to rescale the metric and redefine time so that constant curvature metrics appear as fixed points of the normalized Ricci flow. The mean curvature flow should be modified accordingly when expressed in the new variables. Another way is to use equation (6.15) for rotating solitons, as it stands, and define an effective angular velocity,

$$\omega_{\text{eff}} = \omega A^2\ . \tag{6.19}$$

Then, the shape of the resulting curves is identical to those drawn in ref. [66] at any given instance of time. As time flows, ω_{eff} changes; on the sphere it diminishes from ∞ to 0, whereas on the hyperboloid it increases from 0 to ∞. Following the analysis of ref. [66], we give a schematic representation of the rotating solitons at some intermediate time.

On the sphere, the curve oscillates around the equator and keeps coming closer to it as it winds. In the process it also keeps crossing itself. This behavior is best seen by the numerical plot $r(\theta)$ shown in figure 15 below.

On the hyperboloid, the curve resembles the shape of the planar Yin-Yang curve, which is now stretched on from $-\infty$ to ∞ along the symmetry axis. The corresponding solution is depicted in figure 16 below.

JHEP06(2007)057

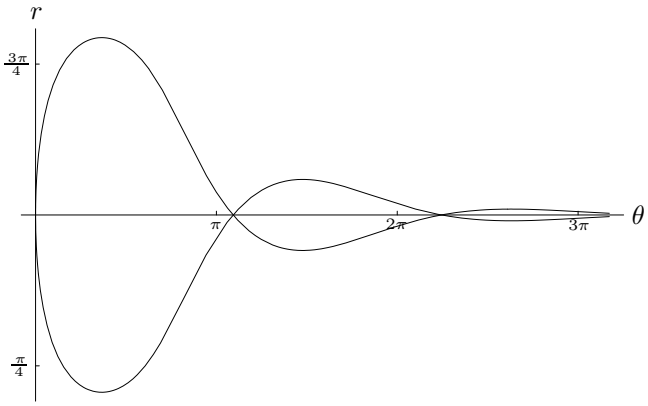

Figure 15: The graph of a rotating soliton on the sphere.

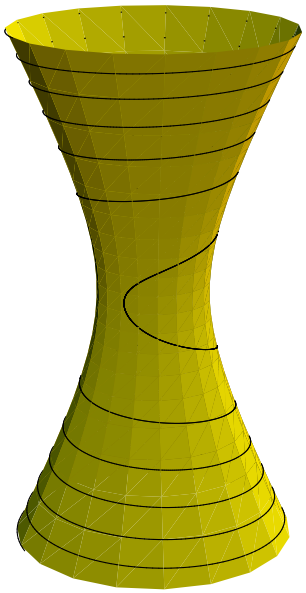

Figure 16: A rotating soliton on the one-sheeted hyperboloid.

6.3 Branes on Ricci solitons

The simplest static example of curved ambient space is provided by the following choice of metric and dilaton fields, in conformally flat frame,

$$\Omega(y) = 1 + e^{2y}\,, \qquad \Phi(y) = -\frac{1}{2}\log\left(1 + e^{-2y}\right)\ . \tag{6.20}$$

The coordinate y takes all values from $-\infty$ to ∞, whereas x is an angular variable ranging from 0 to 2π; in this frame, the space is conformally equivalent to the cylinder[5]. The

[5]An alternative description exists by changing frame to $X \pm iY = \exp(-y \pm ix)$ that maps the cylinder to the plane. Then, the metric is conformally equivalent to the plane with metric $ds^2 = (dX^2 + dY^2)/(1 + X^2 + Y^2)$, whereas the dilaton is $-2\Phi = \log(1 + X^2 + Y^2)$.

JHEP06(2007)057

configuration corresponds to the well known Ricci soliton associated to non-trivial fixed point of the Ricci flow in the presence of dilaton, [51] (but see also [8]). In the physics literature it serves as model for string propagation on a two-dimensional Euclidean black hole background, [55]. The mean curvature flow will be studied in this space using equation (6.10) in the system of conformally flat coordinates. Since $\partial_y \Omega = 2\Omega - 2$, the mean curvature flow simplifies to

$$\frac{\partial \varphi}{\partial t} = \Omega \left(\frac{\varphi''(x)}{1+\varphi'^2(x)} + 1 \right) + k^x \varphi'(x) - k^y \ . \tag{6.21}$$

This background exhibits a rotational isometry generated by $\partial/\partial x$, so that $k^x = \omega$ and $k^y = 0$ with angular velocity ω of either sign. Clearly, there is no other isometry.

The fixed points of the mean curvature flow correspond to curves described by the equation

$$\frac{\varphi''(x)}{1+\varphi'^2(x)} + 1 = 0 \, , \tag{6.22}$$

without taking into account reparametrizations generated by the Killing vector field k. It is identical to the hair-pin equation on the plane, with parameter $v = -1$, and the general solution is

$$e^{y-y_0} = \cos(x - x_0) \, , \tag{6.23}$$

allowing also for the possibility to shift the coordinates by constant (x_0, y_0). Thus, we recover the standard D1-brane on the Ricci soliton that exists by itself, without need for reparametrizations, thanks to the special form of the supporting dilaton field. This coincidence makes the hair-pin a rather special configuration with infinitely many symmetries inherited by the Euclidean black hole geometry.

The same solution can be alternatively described using proper coordinates (r, θ) in target space. In this frame, the Ricci soliton corresponds to the choice of profile and dilaton functions

$$f(r) = \tanh r \, , \qquad \Phi(r) = -\log(\cosh r) \, , \tag{6.24}$$

whereas the overall scale factor A is a constant set equal to 1. Then, the hair-pin on the Ricci soliton is the curve $r = \rho(\theta)$,

$$\frac{\sinh \rho_0}{\sinh \rho} = \cos(\theta - \theta_0) \, , \tag{6.25}$$

which provides the static solution of equation (6.14) with $\omega = 0$. Of course, the two descriptions are related to each other by the coordinate transformation

$$\sinh \rho = e^{-y} \, , \qquad \theta = x \ . \tag{6.26}$$

The tip of the cigar corresponds to $y = \infty$ and its asymptotic region to $y = -\infty$.

The parameters ρ_0 and θ_0 are integration constants, but, clearly, $\rho \geq \rho_0$ for the solution to make sense. Thus, ρ_0 determines the position of the tip of the hair-pin relative to the tip of the cigar, which is located at $\rho = 0$. By the same token, $y \leq y_0$. The other parameter, $\theta_0 = x_0$, measures the rotation angle of the cigar relative to a given position about its axis

JHEP06(2007)057

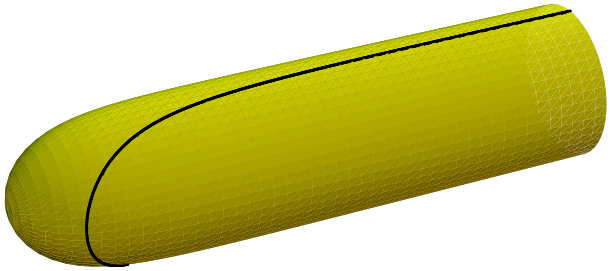

Figure 17: A hair-pin curve supported by the cigar background.

and can be set equal to zero for all practical purposes. In the asymptotic region, $\rho \to \infty$, the cigar looks like a cylinder and the hair-pin reduces to a pair of diametrically opposite parallel lines placed on it, since $\theta - \theta_0 \to \pm\pi/2$. As ρ decreases, these two lines bend towards each other and meet smoothly at $\rho = \rho_0$. When $\rho_0 = 0$, the curve passes through the origin and its two legs are diametrically opposite for all ρ. The solution represents an open curve sitting still on the surface of a semi-infinite long cigar, as shown in figure 17 below.

We will see later that this particular configuration can be used as component for constructing the analogue of a paper-clip on axially symmetric evolving backgrounds with spherical topology.

Rotating solutions on the two-dimensional black hole geometry correspond to generalized fixed points of the mean curvature flow with $\omega \neq 0$. Explicit calculation shows that the resulting equation can be integrated once, as on the plane, leading to

$$\arctan\varphi'(x) + x - \frac{\omega}{2}\log\left(1 + e^{-2y}\right) = 0 \ . \tag{6.27}$$

The same analysis can be performed in proper coordinates, where the rotating soliton satisfies the equation

$$\arctan\left(\coth\rho\frac{d\rho}{d\theta}\right) + \omega\log(\cosh\rho) = \theta - \theta_0 \ . \tag{6.28}$$

To compare this curve to the planar Yin-Yang spiral, it is necessary to use a common frame. Thinking of the plane as being conformally equivalent to a cylinder (x, y) with periodic variable x and metric $ds^2 = (dx^2 + dy^2)/e^{2y}$, the planar Yin-Yang curve satisfies the equation

$$\arctan\varphi'(x) + x - \frac{\omega}{2}e^{-2y} = 0 \ . \tag{6.29}$$

The two equations match on the side $y \to \infty$, in which case the rotating soliton becomes independent of ω and approximates the hair-pin curve $\arctan\varphi'(x) + x = 0$, i.e., $\exp(y - y_0) = \cos x$. Note that the tip of the hair-pin should be placed very far away, i.e., $y_0 \to \infty$, for otherwise the approximation would have not been valid. According to this, the rotating solution on the cigar starts from its tip, as expected by symmetry.

JHEP06(2007)057

The identification of the two curves is also valid relatively close to infinity, since $\log(1+e^{-2y}) \simeq e^{-2y}$, but it breaks down to order $\mathcal{O}(e^{-4y})$. Thus, close to the tip of the cigar, the equation becomes approximately

$$\varphi'(x) = -\tan x + \frac{\omega}{2}\frac{e^{-2y}}{\cos^2 x}\,, \tag{6.30}$$

dropping all terms of order $\mathcal{O}(e^{-4y})$, and it is solved by $y = \varphi(x)$,

$$e^{2y} = e^{2y_0}\cos^2 x + \frac{\omega}{3}(\tan x + \sin 2x)\ . \tag{6.31}$$

Setting $\delta y = y - y_0$ and expanding the trigonometric functions around the tip, where $x = 0$, we obtain to first order

$$\delta y = \frac{\omega}{2} e^{-2y_0}\delta x\ . \tag{6.32}$$

This shows the tendency of the curve to twist as it moves away from the tip.

On the other hand, close to the asymptotic region of the cigar, $y \to -\infty$, the rotating soliton is described approximately by equation

$$\varphi'(x) = \tan(\omega y - x)\ . \tag{6.33}$$

It is solved exactly by the following expression

$$y + \omega x = \log\left(\sin(\omega y - x) - \frac{1}{\omega}\cos(\omega y - x)\right) \tag{6.34}$$

up to an irrelevant integration constant. Then, it becomes clear that the asymptotic dependence of the curve $y = \varphi(x)$ is

$$\omega y - x = \arctan\frac{1}{\omega}\ (\mathrm{mod}\ \pi)\,, \qquad \text{as}\ \ y \to -\infty\ . \tag{6.35}$$

For, otherwise, the right-hand side of equation (6.34) can not match the infinity appearing on the left-hand side. This assertion can also be verified by direct substitution of (6.35) into equation (6.33). When $\omega = 0$, the asymptotic relation (6.35) reproduces the well known asymptotic description of the hair-pin as two parallel lines with $x = \pi/2\ (\mathrm{mod}\pi)$. When $\omega \neq 0$, the hair-pin ends up in a double helix whose components are π/ω apart from each other. The sign of ω determines the handedness of the helix.

The corresponding curve is centered at the tip of the cigar and winds around the asymptotic cylinder as shown in figure 18. The structure of the curve is more complicated in the middle region and thorough numerical analysis is required to draw its shape. Certainly, it is quite different from the planar Yin-Yang curve.

Finally, we consider running solutions on the cigar that represent circular branes placed perpendicularly to the axis of symmetry. In this case ρ depends solely on t and simple integration of equation (6.16) yields

$$\cosh\rho = e^{t_0 - t} \tag{6.36}$$

when $A = 1$. These curves originate from the asymptotic region of the cigar at $t = -\infty$ and move towards the tip until they fully collapse to the point $\rho = 0$ at some finite time $t = t_0$.

JHEP06(2007)057

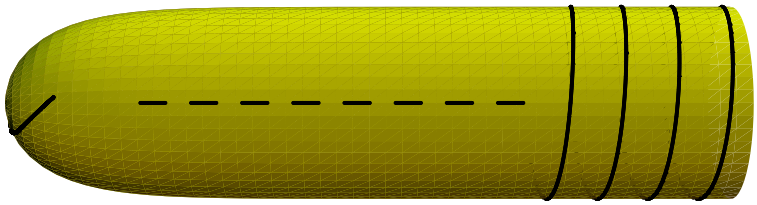

Figure 18: The end-point structure of a rotating soliton on the cigar.

They can be thought as analogue of the uniformly shrinking circles on the plane, although the radial dependence on t is different now. It is natural to expect that all closed curves winding around the cigar will contract to a point at its tip irrespective of initial conditions. It should be analogous to the well known fact on the plane that all closed curves shrink to a point at finite time.

6.4 Branes on a sausage

The sausage model was introduced in the physics literature more than a decade ago, [41], and describes axially symmetric deformations of the sphere by Ricci flow. It is defined by the following ansatz

$$\Omega(y,t) = a(t) + b(t)\cosh 2y \tag{6.37}$$

in a system of conformally flat coordinates (x, y), whereas $\Phi(y) = 0$. The coordinate y can take all values on the real line and x is taken to be periodic ranging from 0 to 2π. This ansatz yields a consistent truncation of the Ricci flow to a simpler system of ordinary differential equations for the two moduli $a(t)$ and $b(t)$,

$$\frac{da}{dt} = 2b^2\,, \qquad \frac{db}{dt} = 2ab\,, \tag{6.38}$$

which can be easily solved as

$$a(t) = \gamma\coth(-2\gamma t)\,, \qquad b(t) = \frac{\gamma}{\sinh(-2\gamma t)}\,. \tag{6.39}$$

The integration constant γ is assumed to be non-negative and determines the ultra-violet limit of the configuration. Indeed, as $t \to -\infty$, Ω tends to a constant value, γ, and the space looks like an infinitely long cylinder of radius $1/\sqrt{\gamma}$. Then, as t increases, the configuration looks like a sausage that evolves by becoming shorter and rounder until it fully collapses to a point at some finite time $t = 0$. When $\gamma = 0$, the trajectory corresponds to a uniformly contracting round sphere of radius $\sqrt{-t}$.

On this two-parameter space we will examine the mean curvature flow for embedded curves, $y = \varphi(x(t), t)$,

$$\frac{\partial\varphi}{\partial t} = \frac{\gamma}{\sinh(-2\gamma t)}\left((\cosh(-2\gamma t) + \cosh 2y)\frac{\varphi''(x)}{1+\varphi'^2(x)} + \sinh 2y\right) \tag{6.40}$$

and construct special solutions that generalize the paper-clip and the oxlip planar curves to the sausage. They provide explicit realizations of the curve shortening problem on a

JHEP06(2007)057

Figure 19: The paper-clip as composition of two hair-pin curves on cigars.

deforming background and, in this respect, there are two natural scale parameters at work. There is the time at which the background is fully collapsed to a point, taken here to occur at $t = 0$, and the time at which the closed curves collapse to a point, denoted by t_0 in the sequel. Clearly, $t_0 \leq 0$ and in most cases one expects, based on intuition, that the curve will become singular before the background. The paper-clip and other examples that will be considered later have $t_0 < 0$, but for the oxlip model we find $t_0 = 0$. The solutions simplify considerably when $\gamma = 0$, in which case they describe deforming curves on a uniformly contracting sphere.

It can be easily verified that equation (6.40) admits the following simple solution

$$\frac{\kappa \cosh y}{\sinh(-\gamma t)} = \cos(x - x_0)\,, \tag{6.41}$$

where κ is a positive integration constant and x_0 represents the freedom to rotate the sausage by an arbitrary angle about its axis of symmetry. This solution describes a closed curve on the sausage that can be thought as superposition of two hair-pin solutions. As such, it provides the analogue of the paper-clip curve on the sausage. One way to see this is by rewriting the sausage model metric as

$$ds^2_{\mathcal{M}} = \frac{1}{\gamma}\left(\frac{1}{1+e^{2y+2\gamma t}} - \frac{1}{1+e^{2y-2\gamma t}}\right)(dx^2 + dy^2)\ . \tag{6.42}$$

It represents the bound state of two cigars glued together in their asymptotic region that begin eating each other as time flows. The corresponding dilaton fields also come with opposite signs and cancel each other, up to spatially independent terms. Then, the closed curve (6.41) can be interpreted as two hair-pins placed appropriately against each other on the constituents cigars. The decomposition of the curve on very long sausages reads, in particular,

$$\kappa\left(e^{y+\gamma t} + e^{-y+\gamma t}\right) = \cos(x - x_0) + \mathcal{O}(e^{2\gamma t})\ . \tag{6.43}$$

The gluing of the individual components is performed in a certain way, as depicted schematically in figure 19 below. Another type of gluing condition will be considered later that is reminiscent of the oxlip planar curve.

The picture becomes more clear in proper coordinates, which are best suited for drawing pictures. Introducing the change of variables

$$\mathrm{sn}(r;k) = \tanh y\,, \qquad \theta = x\,, \qquad k = \tanh(-\gamma t)\,, \tag{6.44}$$

the sausage model metric assumes the following form

$$ds^2_{\mathcal{M}} = \frac{k}{\gamma}\left(dr^2 + \mathrm{sn}^2(r;k)d\theta^2\right) \tag{6.45}$$

JHEP06(2007)057

written in terms of the Jacobi elliptic function $\mathrm{sn}(r;k)$ with modulus k. One tip of the sausage is located at $r = 0$ and the other at $r = 2K(k)$ given in terms of the complete elliptic integral of the first kind. There is also a dilaton field

$$\Phi'(r) = rk'^2 - E(r,k) \tag{6.46}$$

whose form is determined by consistency of the Ricci flow in proper coordinates. Here, $E(r,k)$ denotes the incomplete elliptic integral of the second kind; $\Phi(r,t)$ can be expressed in terms of Jacobi's theta function by simple integration.

The ultra-violet limit of the ambient space corresponds to $k = 1$, in which case the length of the sausage becomes infinite, whereas $k = 0$ corresponds to $t = 0$ and the configuration fully collapses to a point. In the ultra-violet limit, the sausage looks like a cylinder from its middle point $y = 0$. In proper coordinates, however, one sees an infinitely long sausage from one of its tips and the structure looks identical to the two-dimensional cigar,

$$ds^2_{\mathcal{M}} \simeq \frac{1}{\gamma}(dr^2 + \tanh^2 r d\theta^2)\,, \tag{6.47}$$

since $\mathrm{sn}(r;1) = \tanh r$. The radius of the circle in the asymptotic region $r \to \infty$ is $1/\sqrt{\gamma}$, as required. The picture is alike from the other tip, since $\mathrm{sn}^2(r+2K(k);k) = \mathrm{sn}^2(r;k)$. Thus, the interpretation of the sausage as bound state of two Euclidean black holes becomes rather precise.

The paper-clip on the sausage takes the following form in proper coordinates,

$$\frac{\kappa}{k}\frac{\mathrm{dn}(r;k)}{\mathrm{sn}(r;k)} = \cos(\theta - \theta_0) \tag{6.48}$$

using Jacobi elliptic functions. In the ultra-violet limit $k = 1$ one has

$$\frac{\mathrm{dn}(r;1)}{\mathrm{sn}(r;1)} = \frac{1}{\sinh r}\,, \tag{6.49}$$

and so one recovers the hair-pin curve (6.25) on one of the two constituent cigars with parameter $\kappa = \sinh r_0$. From the other tip of the sausage one sees a second hair-pin placed symmetrically with respect to its center, as in a mirror; on the second hair-pin one makes the identification $\kappa = -\sinh r_0$ because the function $\mathrm{dn}(r;k)/\mathrm{sn}(r;k)$ flips sign when its argument is shifted by $2K(k)$. Then, the two pieces are glued together in the central region. The open ends of each hair-pin, which are diametrically opposite in the ultra-violet limit, are joined smoothly to form an infinitely long paper-clip on an infinitely long sausage. As time goes on, the curve tends to slip off the side until it collapses to a point before the sausage shrinks to zero size. The collapse of the curve occurs at time t_0

$$\sinh(-\gamma t_0) = \kappa\,, \qquad \text{i.e.,} \quad k = \frac{1}{\sqrt{1+1/\kappa^2}}\,. \tag{6.50}$$

The parameters γ and κ are, in general, independent. figure 20 below depicts the evolution pattern of the paper-clip on a sausage with $\gamma \neq 0$. The limiting case of a paper-clip on the uniformly contracting sphere appears to be singular because $\gamma = 0$. It can only

JHEP06(2007)057

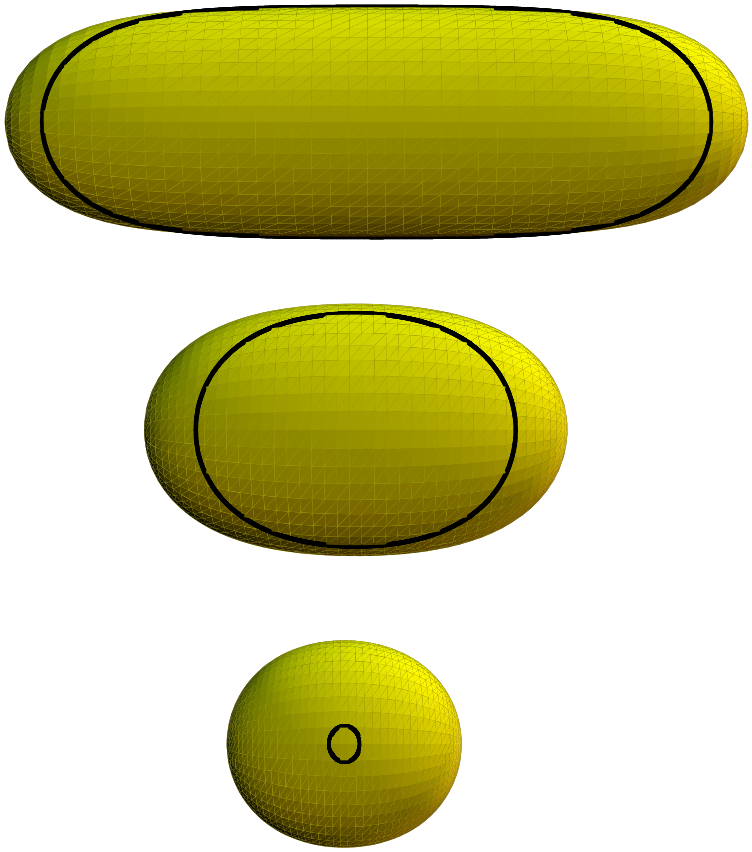

Figure 20: Schematic evolution of a paper-clip on the sausage.

be accommodated by considering a correlated limit of parameters so that κ/γ remains fixed to a constant.

An interesting variant of the solution above is provided by the following curve on the sausage,

$$\kappa \frac{\sinh y}{\cosh(-\gamma t)} = \cos(x - x_0) \ . \tag{6.51}$$

As can be easily checked, it satisfies the mean curvature flow (6.40). When expressed in proper coordinates it takes the form

$$\kappa \frac{\mathrm{cn}(r;k)}{\mathrm{sn}(r;k)} = \cos(\theta - \theta_0) \ . \tag{6.52}$$

In the ultra-violet limit, the curve looks similar to the one considered before, because $\mathrm{cn}(r;1) = \mathrm{dn}(r;1)$. However, the picture is slightly different from the other tip of the sausage because both functions $\mathrm{sn}(r;k)$ and $\mathrm{cn}(r;k)$ flip sign when their argument is shifted by $2K(k)$. As a result, the relative orientation of the two hair-pins changes and one gets $\kappa = \sinh\rho_0$ on both sides. Thus, the solution represents a closed curve on the sausage, which is formed by putting together two hair-pins on the constituent cigars, as before, but this time the gluing prescription is different. In particular, one of the two cigars should

JHEP06(2007)057

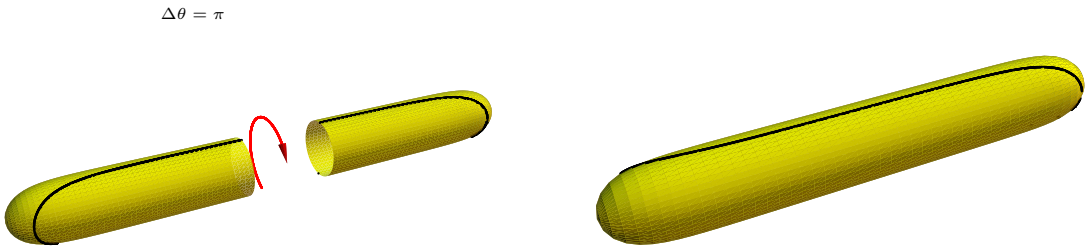

Figure 21: Cross-joining two hair-pin curves on cigars.

be rotated by an angle π before gluing it to the other. This operation does not alter the metric of the ambient space, but affects the curves embedded in it. This is also clearly seen by comparing equation (6.51) on very long sausages,

$$\kappa \left(e^{y+\gamma t} - e^{-y+\gamma t}\right) = \cos(x - x_0) + \mathcal{O}(e^{2\gamma t}) \,, \tag{6.53}$$

to the analogous expression (6.43) for the paper-clip curve. The flip of the relative sign is attributed to the rotation of the second component. The resulting configuration, before and after the twist, is depicted in figure 21 below.

This solution provides the analogue of the oxlip curve on the sausage. The analogy is revealed by comparing equation (6.51) in conformally flat frame to the oxlip solution on the plane. They both share the characteristic $\sinh y$ dependence as opposed to the $\cosh y$ dependence of the paper-clip curves. The oxlip solution exists for all time as long as the ambient space is regular. Thus, on the plane, it exists for infinitely long time, whereas on the sausage it shrinks together with the space until they become singular simultaneously at $t = 0$. This behavior is easily understood on intuitive grounds: the curve goes around the two tips of the sausage on opposite sides and cannot slip off to one side. As time goes on, the curve has the tendency to become shorter by moving evenly towards the center of the sausage, which also gets shorter and rounder, until the big crunch. The topology of the ambient space affects only the shape of the oxlip curve, which is closed on the sausage and open on the plane.

7. Mean curvature flow in three dimensions

In this section we consider the mean curvature flow of two-dimensional surfaces embedded in three dimensions. We will only examine the case of flat ambient space, R^3, which already poses a non-trivial problem. Branes in curved ambient spaces are much more difficult to study since the mean curvature flow should be combined with the Ricci flow, which is very complex problem. We will avoid such unnecessary complications and also ignore the effect of fluxes that can be turned on in three (and higher) dimensional spaces. The role of fluxes in the boundary renormalization group equations of sigma models is fully captured by the Dirac-Born-Infeld that will be further studied elsewhere.

JHEP06(2007)057

7.1 General aspects of evolving branes in R^3

The mean curvature flow of surfaces in R^3 is obtained by considering the general embedding equation

$$X = X(s,u;t)\,, \qquad Y = Y(s,u;t)\,, \qquad Z = Z(s,u;t) \tag{7.1}$$

associated to two parameters s and u and the renormalization group time t. It is convenient, where appropriate, to think of the surface as graph of a function $Z = \varphi(X(t), Y(t); t)$ that evolves in time.

Using the formulae given in appendix A, it turns out that the mean curvature of the surface is

$$H = \frac{\left(1+(\partial_Y\varphi)^2\right)\partial_X^2\varphi + \left(1+(\partial_X\varphi)^2\right)\partial_Y^2\varphi - 2(\partial_X\varphi)(\partial_Y\varphi)(\partial_X\partial_Y\varphi)}{\left(\sqrt{1+(\partial_X\varphi)^2+(\partial_Y\varphi)^2}\right)^3}\,, \tag{7.2}$$

whereas the inward unit normal vector is

$$\hat{n} = \frac{1}{\sqrt{1+(\partial_X\varphi)^2+(\partial_Y\varphi)^2}}\,(-\partial_X\varphi,\ -\partial_Y\varphi,\ 1)\,. \tag{7.3}$$

Then, the mean curvature flow takes the form

$$\begin{aligned}\frac{\partial\varphi}{\partial t} = {} & \frac{\left(1+(\partial_Y\varphi)^2\right)\partial_X^2\varphi + \left(1+(\partial_X\varphi)^2\right)\partial_Y^2\varphi - 2(\partial_X\varphi)(\partial_Y\varphi)(\partial_X\partial_Y\varphi)}{1+(\partial_X\varphi)^2+(\partial_Y\varphi)^2} \\ & +\xi^X\partial_X\varphi + \xi^Y\partial_Y\varphi - \xi^Z\end{aligned} \tag{7.4}$$

by also adding the effect of arbitrary reparametrizations generated by a vector field (ξ^X, ξ^Y, ξ^Z), if appropriate.

The induced metric on the two-dimensional surface evolves according to the equations

$$\frac{\partial}{\partial t}g_{AB} = -2HK_{AB}\,, \qquad \frac{\partial}{\partial t}g^{AB} = 2HK^{AB}\,, \tag{7.5}$$

so that

$$\frac{\partial}{\partial t}\sqrt{\det g} = -H^2\sqrt{\det g}\,. \tag{7.6}$$

Also, the second fundamental form of the surface follows the evolution

$$\frac{\partial}{\partial t}K_{AB} = g^{CD}\nabla_C\nabla_D K_{AB} - 2H(K^2)_{AB} + (\mathrm{Tr}K^2)K_{AB}\,, \tag{7.7}$$

where $(K^2)_{AB} = g^{CD}K_{AC}K_{BD}$ and $\mathrm{Tr}K^2 = g^{AB}g^{CD}K_{AC}K_{BD} = H^2 - R$ is expressed in terms of the Ricci curvature of the surface by the Gauss-Codazzi relations. Then, the extrinsic mean curvature satisfies the parabolic equation

$$\frac{\partial H}{\partial t} = g^{AB}\nabla_A\nabla_B H + (\mathrm{Tr}K^2)H \tag{7.8}$$

generalizing equation (3.13) to two-dimensional branes.

Clearly, the structure of these equations is much more complicated than those for the evolution of planar curves. Although several general results have been obtained in the literature so far, the level of our current understanding is by no means complete. Some aspects will be discussed here while considering the dimensional reduction of the mean curvature flow in R^3 for special classes of surfaces.

JHEP06(2007)057

7.2 Dimensional reduction of the curvature flow

We present two general classes of surfaces, associated to particular ansatz for their embedding functions, which allow for consistent reduction of the problem to an effective curve shortening problem on the plane. They correspond to cylindrical surfaces and surfaces of revolution as brane models. Specific solutions of different topologies will also be discussed in the sequel. It should be mentioned, however, that there are other examples of surfaces, like the class of ruled surfaces, which do not admit consistent truncation of the mean curvature flow away from fixed points (in that case the helicoid).

(i) Cylindrical surfaces: the simplest possibility arises for surfaces with embedding equations

$$X = x(s;t)\,, \qquad Y = y(s;t)\,, \qquad Z = u\,, \tag{7.9}$$

where $(x(s), y(s))$ is the parametric form of a planar curve $\mathcal{C}$ that evolves in time and u is the second parameter on the surface. These are cylindrical surfaces of the form $R \times \mathcal{C}$ and it is entirely obvious that their mean curvature flow in R^3 is equivalent to the mean curvature flow of the curve $\mathcal{C}$ on the plane perpendicular to the Z-axis. As such, they provide a trivial dimensional reduction of the mean curvature flow to lower dimensions. Other ansatz may also reduce the problem to lower dimension, as deformations of planar curves, but the effective dynamics differs from the ordinary mean curvature flow in R^2, as will be seen shortly.

Any solution of the mean curvature flow on the plane is elevated to a deforming cylindrical brane in R^3, and vice-versa. Thus, for example, all self-shrinking solutions of this type are classified by the cylinder $R \times S^1$ and the self-intersecting surfaces $R \times \Gamma_{p,q}$ given in terms of the Abresch-Langer curves $\Gamma_{p,q}$. Also, the self-expanding solution, associated to the decay of a wedge on the plane, is elevated to an open surface going out of the intersection of two planes in R^3, meeting on the Z-axis. In the context of quantum field theory one has D2-branes in the conformal field theory of three free bosons but the third boson essentially acts as spectator in the boundary flow equations.

(ii) Surfaces of revolution: next, we consider surfaces of revolution in R^3 described in all generality by the embedding equation

$$X = y(s;t)\,\cos\theta\,, \qquad Y = y(s;t)\,\sin\theta\,, \qquad Z = x(s;t)\ . \tag{7.10}$$

They are formed by rigid rotation of a planar curve $(x(s), y(s))$ around the Z-axis by an angle θ that ranges from 0 to 2π. The time evolution is encoded into the revolving planar curve and the mean curvature flow in R^3 is consistently reduced to planar deformations of a certain kind.

The reduced flow is derived by first computing the tangent vectors to the surface,

$$\vec{e}_s = \left(\left(\frac{\partial y}{\partial s}\right)\cos\theta,\ \left(\frac{\partial y}{\partial s}\right)\sin\theta,\ \frac{\partial x}{\partial s}\right), \qquad \vec{e}_\theta = (-y\,\sin\theta,\ y\,\cos\theta,\ 0)\,, \tag{7.11}$$

which give rise to the induced metric with components

$$g_{ss} = \left(\frac{\partial x}{\partial s}\right)^2 + \left(\frac{\partial y}{\partial s}\right)^2, \qquad g_{\theta\theta} = y^2, \qquad g_{s\theta} = 0\ . \tag{7.12}$$

JHEP06(2007)057

The normal vector inward to the brane is

$$\hat{n} = \frac{1}{\sqrt{1+\varphi'^2(x)}} \left(\cos\theta,\ \sin\theta, -\varphi'(x)\right) \tag{7.13}$$

using the notation $y = \varphi(x)$ for the graph of the underlying planar curve. Then, the mean curvature of the surface turns out to be

$$H = g^{AB} \left(\nabla_A \vec{e}_B\right) \cdot \hat{n} = \frac{1}{\sqrt{1+\varphi'^2(x)}} \left(\frac{\varphi''(x)}{1+\varphi'^2(x)} - \frac{1}{\varphi(x)} \right). \tag{7.14}$$

The mean curvature flow in R^3 is dimensionally reduced to the following deformation on the plane

$$\frac{\partial \varphi}{\partial t} = \frac{\varphi''(x)}{1+\varphi'^2(x)} - \frac{1}{\varphi(x)}\,, \tag{7.15}$$

which clearly differs from the usual mean curvature flow in R^2 by the extra term $1/\varphi(x)$. This difference is attributed to the extrinsic curvature of the S^1 direction following the revolution around the Z-axis. Reparametrizations generated by a vector field $\vec{\xi}$ can also be added along the flow, as usual. Note, however, that there is no simple variant of equation (3.13) satisfied by the curvature of the underlying planar curve that could be used further, as in sections 3 and 4.

Static solutions are characterized by the equation $\varphi(x)\varphi''(x) = 1 + \varphi'^2(x)$ and they correspond to minimal surfaces of revolution in R^3. In particular, one obtains

$$\varphi(x) = \cosh x\,, \tag{7.16}$$

which is the graph of the *catenary* curve on the plane. The solution is equivalently described in terms of Liouville equation

$$f''(x) + e^{f(x)} = 0 \tag{7.17}$$

using the relation

$$e^{f(x)} = \frac{2}{\varphi^2(x)} = \frac{2}{\cosh^2 x}\ . \tag{7.18}$$

Then, according to the embedding equations in R^3, the complete surface is described by the algebraic equation

$$X^2 + Y^2 = \cosh^2 Z \tag{7.19}$$

so that the two principal curvatures cancel each other at all points. The catenoid surface approximates the one-sheeted hyperboloid $X^2 + Y^2 - Z^2 = 1$ only for small Z; it yields the well known shape of soap bubbles extended between two parallel circular boundaries. Another minimal surface in R^3 is the plane, but it appears in a somewhat singular way in the present formalism, as surface of revolution of the planar line $x = 0$ around the Z-axis perpendicular to it.

Self-similar solutions provide the simplest examples of immersed surfaces that evolve by overall time scaling so that the functions (7.10) have common factorized dependence by $\sqrt{2ct}$. Their position vector $\vec{r} = (X, Y, Z)$ satisfies by definition the special relation

$$H\hat{n} = c\vec{r}\ . \tag{7.20}$$

JHEP06(2007)057

For surfaces of revolution it yields the effective planar curve equation for $y = \varphi(x)$

$$c(y - x\varphi'(x)) = \frac{\varphi''(x)}{1 + \varphi'^2(x)} - \frac{1}{\varphi(x)}\,, \tag{7.21}$$

since $(x(s;t), y(s;t))$ also evolves by overall scaling. Here, we only discuss examples of self-shrinkers with $c < 0$ so that t runs from $-\infty$ to 0 and the whole surface shrinks to the origin by dilations. We will examine solutions with cylindrical, spherical and toroidal topology and refer briefly to some of their consequences.

In all cases, these surfaces correspond to stationary points of Huisken's functional

$$\int_{\mathcal{N}} e^{cr^2(s)/2}\,\sqrt{\det g}\;ds d\theta = \int_{\mathcal{N}} e^{c(x^2(s)+y^2(s))/2}\;y(s)\,\sqrt{(\partial x/\partial s)^2 + (\partial y/\partial s)^2}\;ds d\theta \tag{7.22}$$

for the normalized mean curvature flow in R^3. Integration over θ is performed trivially and one is left with an integral over s representing the length of a planar curve with appropriate metric. In this context, self-similar solutions are effectively described by geodesics in the upper half-plane (x, y), with $y > 0$, that comes equipped with the metric

$$ds^2 = y^2 e^{c(x^2+y^2)}(dx^2 + dy^2)\;. \tag{7.23}$$

If the factor y^2 were missing the answer would be the same as for the geodesic interpretation of scaling solutions on the plane found in section 4.4. The presence of this additional factor accounts for the extra term $1/\varphi(x)$ in equation (7.15), differentiating the dimensionally reduced equation from the ordinary planar mean curvature flow.

The first example is provided by self-shrinking cylinders of radius $a\sqrt{2ct}$ with $a = 1/\sqrt{-c}$, which are common to the classes (i) and (ii). In the present context, they correspond to solutions of equation (7.21) with $\varphi(x) = a$. Next, there is the example of self-shrinking spheres of radius $a\sqrt{2ct}$ with $a = \sqrt{-2/c}$. They correspond to solutions of equation (7.21) with $\varphi(x) = \sqrt{a^2 - x^2}$, which represents a semi-circle in (x, y) plane. Comparison between the two solutions shows that spheres shrink faster that cylinders of equal initial radius. This is also expected on intuitive grounds since spheres are more curved than cylinders of equal radii. Finally, there are self-shrinking doughnuts in R^3 whose existence was first established in ref. [67]; for a discussion see also ref. [18]. They correspond to simple closed geodesic in the upper half-plane equipped with the metric (7.23), which is symmetric with respect to reflection in the y-axis. The proof relies on the so called shooting method and proceeds in several steps that are omitted here. Unfortunately, there is no closed formula that describes the corresponding planar curve that accounts for such solution. Certainly, it can not be a round circle for this does not provide solution to the reduced flow (7.21).

The classification of self-similar solutions in R^3 and the formation of singularities under the flow are not fully explored in all generality. Apart from the obvious scaling solutions $R \times S^1$, $R \times \Gamma_{p,q}$, the round S^2 and the self-shrinking doughnut there can be many more surfaces of various topologies that may also admit self-intersections. The general situation is well understood only for surfaces of positive mean curvature, since the sphere is the only compact surface of this kind that evolves by scaling, [48]. There are other important

JHEP06(2007)057

differences with the mean curvature flow in R^2 that complicate things further. Closed curves embedded in the plane always shrink to a point irrespective of their initial shape. Even if the curve is not convex at some initial time, it will become convex at later times, [47], and then approach the homothetic collapse of the round circle towards a point, [46]. This property does not generalize to higher dimensions as singularities can arise before the surface has the chance to become convex.

The existence of self-similar shrinking doughnuts can be employed to provide a qualitative proof of this behavior, [67]. For it suffices to consider a dumbbell in R^3 consisting of two large approximately round spheres connected with a thin long cylinder as initial configuration. By considering a small self-similar shrinking doughnut that encircles the neck of the surface, one easily sees that the doughnut, and hence the neck of the dumbbell, will become singular well before the two spherical regions have a chance to collapse.

Similar constructions and arguments apply to hypersurfaces of codimension 1 embedded in all higher dimensional flat spaces. Much less is known about the general features of evolving hypersurfaces in flat space when their codimension is bigger than 1 and/or when the ambient space is curved.

8. Conclusions

The quantum field theory of two-dimensional sigma models provides a natural framework for the realization of both intrinsic and extrinsic curvature flows. These theories have all the necessary geometric ingredients to define the flows. Classically, the target space fields as well as the embedding equations for branes are fixed once and for all, but, in the quantum theory, they are regarded as generalized couplings that depend on the energy scale. Thus, the renormalization group equations of the sigma models induce flows that can be computed perturbatively. The first order corrections in α' expansion are given by the curvature (intrinsic or extrinsic) and the resulting equations combine into a coupled system of Ricci and mean curvature flows. There can be additional fields, such as anti-symmetric tensor, dilaton and gauge fields, whose beta functions combine with the others into a larger system of flows. The deformations of the bulk couplings form a closed system, which is independent of the existence of branes and can be studied separately. On the other hand, the deformations of the boundary couplings depend on the background in which branes are embedded. The resulting picture puts the boundary renormalization group equations on firm mathematical base, as for the bulk equations. It also suggests generalizations of the combined Ricci and mean curvature flows in the presence of fluxes, via the Dirac-Born-Infeld action, which demand further attention.

Fixed point configurations are reached when the quantum field theory is conformal. It is possible, however, to have non-conformal boundary conditions for branes that deform in a conformally invariant background. Then, in this context, ordinary D-branes are characterized by conformally invariant boundary conditions in a conformal field theory. We have examined several interesting examples of either kind in two- and three-dimensional ambient spaces using appropriate mini-superspace reductions of the more general problem. Even in the simplest case of the conformal quantum field theory of two free bosons, represented

JHEP06(2007)057

by the plane, the possibilities for brane evolution are enormous and there is no systematic way to solve the associated curve shortening problem in all generality. It will be useful to develop new algebraic techniques, as for the Ricci flow in two dimensions, which will enable to cast the mean curvature flow into zero curvature form. In the same spirit, it will be interesting to investigate all integrable perturbations of a given fixed point solution, such as the hair-pin, and associate renormalization group trajectories to new infra-red fixed points, in analogy with the integrable perturbations of bulk conformal field theories.

The construction of entropy functionals and their physical interpretation in terms of the underlying quantum field theory of Dirichlet sigma models are other directions of future research. In principle, one should be able to generalize Huisken's functional, mentioned in section 3, to branes deforming in curved ambient spaces with or without fluxes. Even the simplest cases corresponding to the target space of exact conformal field theories, such as the two-dimensional Euclidean black hole or S^3 stabilized by fluxes, have not been considered to this day. It is also natural to expect that the critical points of such generalized entropy functionals will help to characterize the singularities of collapsing branes in curved spaces, in analogy with the self-shrinking solutions in flat space. When the branes deform in running backgrounds the problem becomes even more interesting for there can be branes that become singular before or simultaneously with the metric. None of these possibilities have been analyzed before in the mathematics literature and the corresponding entropy functionals are yet to be found. It should also be noted in this context that the g-function of boundary flows, [68, 69], is still awaiting its proper mathematical place in the framework of mean curvature flows, as for the c-function of bulk flows expressed by Perelman's entropy of Ricci flows, [43].

The boundary state formalism of Dirichlet sigma models should be developed further in order to provide exact characterization of the fixed points as well as the running solutions of the flow from the world-sheet view-point. In this context, it will be interesting to consider the effect of instantons on the mean curvature flow, as for the Ricci flow, and investigate the emergence of non-trivial infra-red fixed points. A simple example of this kind is the $O(3)$ sigma model with $\theta = \pi$ topological term in which there can be embedded closed curves that normally deform to a point. The θ-term yields the Gaussian model of a free boson as infra-red limit of the bulk theory, which is compactified on a circle of self-dual radius, and the branes ought to flow to D-branes on this circle (see, for instance, [70] for their complete classification). Another class of models is provided by the planar Abresch-Langer curves, which, in the presence of the appropriate θ-term, may give rise to some kind of minimal (p, q) exact boundary states in the quantum field theory of two free bosons. Other interesting applications arise in the context of tachyon condensation in string theory and in the Kondo effect (for a recent discussion see, for instance, [71]), where boundary renormalization group equations play pivotal role. All these questions are currently under investigation and further results will be reported elsewhere.

Acknowledgments

This work was supported in part by the European Research and Training Network "Con-

JHEP06(2007)057

stituents, Fundamental Forces and Symmetries of the Universe" under contract number MRTN-CT-2004-005104, the INTAS programme "Strings, Branes and Higher Spin Fields" under contract number 03-51-6346, and the ΕΠΑΝ programme of the General Secretariat for Research and Technology of Greece under contract number B.545. C.S. also acknowledges partial support from the programme "Particle Physics Phenomenology, NCSR-D". I.B. is particularly thankful to the participants of the Workshop on Geometric and Renormalization Group Flows, held in Golm, Germany, for many useful discussions and to Gerhard Huisken for his interest in this work and encouragement.

A. Embedding equations in Riemannian geometry

In this appendix we review the main parts from the theory of embedding hypersurfaces in Riemannian geometry. The presentation is kept quite general so that it can accommodate branes of Dirichlet models with arbitrary codimension defined in general ambient target spaces. A more complete account can be found in the textbooks; see, for example, the classic reference [72].

Consider a Riemannian manifold M of dimension m with local coordinate system X^μ and metric $G_{\mu\nu}(X)$ so that its line element is

$$ds^2_{\mathcal{M}} = G_{\mu\nu}(X) dX^\mu dX^\nu \ ; \qquad \mu, \nu = 1, 2, \cdots, m \ . \tag{A.1}$$

Also consider a submanifold $\mathcal{N}$ of $\mathcal{M}$ with dimension $n < m$ and local coordinates y^A that describes an embedded hypersurface with defining relations $X^\mu = f^\mu(y^A)$. The line element in $\mathcal{N}$ is given by the corresponding metric $g_{AB}(y)$,

$$ds^2_{\mathcal{N}} = g_{AB}(y) dy^A dy^B \ ; \qquad A, B = 1, 2, \cdots, n \, , \tag{A.2}$$

which, of course, is obtained by restricting the line element of the ambient space to $\mathcal{N}$. Thus, $g_{AB}(y)$ is the induced metric on $\mathcal{N}$ equal to

$$g_{AB}(y) = G_{\mu\nu} f^\mu_{,A} f^\nu_{,B} \ . \tag{A.3}$$

The tangent vectors to the hypersurface are given in terms of the derivatives of the embedding functions, $\partial f^\mu / \partial y^A = f^\mu_{,A}$, and they are n of them labeled by the index A. Since f^μ are scalars with respect to covariant differentiation on $\mathcal{N}$, we have equivalently $D_A f^\mu = f^\mu_{,A}$. The (unit) normal vectors to the hypersurface will be denoted by $\hat{n}^\mu_\sigma$, thus being labeled with the index $\sigma = n+1, n+2, \cdots, m$, and they are chosen to satisfy the orthonormalization conditions

$$G_{\mu\nu} \hat{n}^\mu_\sigma \hat{n}^\nu_\tau = \delta_{\sigma\tau} \ . \tag{A.4}$$

By definition they are orthogonal to the tangent vectors to the hypersurface, i.e.,

$$G_{\mu\nu} f^\mu_{,A} \hat{n}^\nu_\sigma = 0 \, , \tag{A.5}$$

and all together they satisfy the following completeness relation in $\mathcal{M}$,

$$g^{AB} f^\mu_{,A} f^\nu_{,B} + \hat{n}^\mu_\sigma \hat{n}^\nu_\tau \delta^{\sigma\tau} = G^{\mu\nu} \ . \tag{A.6}$$

JHEP06(2007)057

Apart from the induced metric g_{AB} there is also the second fundamental (quadratic) form on $\mathcal{N}$, which is a collection of symmetric tensors defined as

$$K^{\sigma}_{AB} = G_{\mu\nu}\hat{n}^{\mu}_{\sigma}\left(D_A D_B f^{\nu} + \Gamma^{\nu}_{\rho\lambda} f^{\rho}_{,A} f^{\lambda}_{,B}\right) \tag{A.7}$$

and labeled by the number of transverse directions to the hypersurface. The eigen-values of the matrix representing the second fundamental form provide the principal curvatures of the hypersurface at each point. The (extrinsic) mean curvature of $\mathcal{N}$ in $\mathcal{M}$ is defined by taking the trace of the second fundamental form,

$$H^{\sigma} = g^{AB} K^{\sigma}_{AB}\,, \tag{A.8}$$

whereas the *mean curvature vector* associated to each point of the hypersurface is defined to be $H^{\sigma}\hat{n}^{\mu}_{\sigma}$. When the codimension of the hypersurface is bigger than one there is also the so called third fundamental form on $\mathcal{N}$, which is defined as

$$T^{\sigma\tau}_{A} = G_{\mu\nu}\hat{n}^{\mu}_{\sigma}\left(\hat{n}^{\nu}_{\tau,A} + \Gamma^{\nu}_{\rho\lambda}\hat{n}^{\rho}_{\tau} f^{\lambda}_{,A}\right) \tag{A.9}$$

and it is anti-symmetric under the interchange of its two labels σ and τ.

According to these definitions, the equations for the derivatives of the tangent and unit normal vector fields on $\mathcal{N}$ take the form

$$D_A D_B f^{\mu} = K^{\sigma}_{AB}\hat{n}^{\mu}_{\sigma} - \Gamma^{\mu}_{\rho\lambda} f^{\rho}_{,A} f^{\lambda}_{,B}\,, \tag{A.10}$$

and

$$\hat{n}^{\mu}_{\sigma,A} = K^{\sigma}_{AB} g^{BC} f^{\mu}_{,C} - \Gamma^{\mu}_{\rho\lambda} f^{\rho}_{,A}\hat{n}^{\lambda}_{\sigma} - T^{\sigma\tau}_{A}\hat{n}^{\mu}_{\tau}\,, \tag{A.11}$$

thus extending the Serret-Frenet relations for embedded curves in R^3 to general situations. They are called embedding equations since the hypersurface is completely specified by the set of these vectors.

Finally, there are compatibility conditions for the existence of solutions to the embedding equations, when a given system of tangent and unit vectors is prescribed, which take the following form:

$$R_{ABCD} = R_{\mu\nu\rho\lambda} f^{\mu}_{,A} f^{\nu}_{,B} f^{\rho}_{,C} f^{\lambda}_{,D} + K^{\sigma}_{C[A} K^{\sigma}_{B]D}\,, \tag{A.12}$$

$$D_{[C} K^{\sigma}_{B]A} = R_{\mu\nu\rho\lambda} f^{\mu}_{,A} f^{\rho}_{,B} f^{\lambda}_{,C}\hat{n}^{\nu}_{\sigma} + T^{\tau\sigma}_{[C} K^{\tau}_{B]A}\,, \tag{A.13}$$

$$D_{[B} T^{\sigma\tau}_{A]} + T^{\rho\sigma}_{[B} T^{\rho\tau}_{A]} + g^{CD} K^{\sigma}_{C[B} K^{\tau}_{A]D} + R_{\mu\nu\rho\lambda} f^{\mu}_{,A} f^{\nu}_{,B}\hat{n}^{\rho}_{\sigma}\hat{n}^{\lambda}_{\tau} = 0\,. \tag{A.14}$$

Summation is implicitly assumed over all repeated indices. The first two conditions are known as Gauss-Codazzi equations, whereas the last one is known as Ricci equation. They all relate the various fundamental forms with the Riemann curvature tensor on $\mathcal{N}$ and $\mathcal{M}$. In general, there are more unknown functions than relations in the embedding equations, but their number is reduced by performing local transformations in the normal space to the hypersurface, which rotate the components of the second and third fundamental forms.

JHEP06(2007)057

B. Deforming curves and integrability

The mean curvature flow on the plane is special case of more general dynamics of curves that deform as

$$\frac{\partial \vec{r}}{\partial t} = U\hat{n} + W\hat{t}\ . \tag{B.1}$$

The unit normal and tangent vectors provide the orthonormal base to decompose vectors at each point of the curve and the coefficient functions U and W are taken to be local functionals of $S = -\vec{r}\cdot\hat{n}$ or functionals of the extrinsic curvature H and their derivatives. It is always convenient to think of the extrinsic curvature as function of the slope β, in which case $H(\beta)$ is related to $S(\beta)$ by equation (3.11). Then, the mean curvature flow, in its simplest form, $\partial\vec{r}/\partial t = H\hat{n}$, corresponds to the choice $U = H$ and $W = 0$, whereas the normalized mean curvature flow $\partial\vec{r}/\partial t = H\hat{n}+\vec{r}$ corresponds to $U = H(\beta)-S(\beta)$ and $W = S'(\beta)$, since $\vec{r} = (\vec{r}\cdot\hat{t})\hat{t}+(\vec{r}\cdot\hat{n})\hat{n} = S'(\beta)\hat{t}-S(\beta)\hat{n}$. Under the general circumstances (B.1), the evolution for the extrinsic curvature becomes, [73],

$$\frac{\partial H}{\partial t} = H^2\left(U''(\beta)+U\right) + HH'(\beta)\left(W''(\beta)+W\right)\ , \tag{B.2}$$

substituting for equation (3.13) or (3.14) when $U(\beta)$ and $W(\beta)$ are arbitrary.

Neither variant of the mean curvature flow preserves the length of the curve. If we are prepared to study generalized evolution equations (B.1) that keep invariant the length of the curves, not only globally but also locally, then we are led to consider coefficient functions that satisfy the special relation

$$W'(\beta) = U(\beta)\ . \tag{B.3}$$

In this case, the derivatives with respect to the arc-length l and time t commute. Furthermore, if U is of the general form $HV'(\beta) = dV(l)/dl$ for some local functional V, the evolutions so defined will also preserve the total area surrounded by such closed curves. The physical picture is to consider inextensible strings, open or closed, that deform on the plane by those general rules. It is quite remarkable that there is an infinite hierarchy of flows, other than the mean curvature flow, which satisfy the constraints mentioned above and yield integrable equations for $H(\beta)$, which in turn can determine the curve by equation (3.12). This puts our investigation in a wider framework and points out that, unlike other cases, the mean curvature flow does not seem to reduce to some known integrable system.

Elaborating more on this point, note that the choice $W(\beta) = H^2(\beta)/2$ and $U(\beta) = HH'(\beta)$, which is consistent with the relation (B.3), amounts to having a third order differential equation for $H(\beta)$, as follows from the general evolution (B.2) above, that is equivalent to the modified Korteweg-de Vries (mKdV) equation. This is best seen in terms of the arc-length l of the curve, rather than β, since the corresponding equation for the extrinsic curvature takes the standard mKdV form [73]

$$\frac{\partial H}{\partial t} = H'''(l) + \frac{3}{2}H^2H'(l)\,, \tag{B.4}$$

JHEP06(2007)057

where prime denotes here the derivative with respect to l. In this context, W is naturally identified with the first conserved quantity of the mKdV equation. More generally, one can show that choosing W as any one of the higher conserved quatities of the mKdV equation (B.4), and U according to the relation (B.3), amounts to reducing the general evolution (B.2) for the curvature into integrable equations that coincide with the other members of mKdV hierarchy.

Finally, we note for completeness that several other type of integrable systems have been obtained in the literature by considering evolutions of curves in two or higher dimensional spaces, which may also be curved, via general evolutions of the form (B.1). None of these, however, can accommodate the mean curvature flow in two or higher dimensional ambient spaces.

C. Resistive diffusion of magnetic fields

In this appendix we review the emergence of the mean curvature flow for planar curves via dimensional reduction of the magneto-hydrodynamic equations for time dependent force-free magnetic fields in R^3, following ref. [54].

Consider the resistive diffusion of a magnetic field $\vec{B}(\vec{x},t)$ in a medium (plasma), which is free to move with velocity $\vec{v}(\vec{x},t)$ to accommodate the changing magnetic configuration in real time. The basic magneto-hydrodynamic equation controlling the process is

$$\frac{\partial \vec{B}}{\partial t} + \eta \vec{\nabla} \times (\vec{\nabla} \times \vec{B}) = \vec{\nabla} \times (\vec{v} \times \vec{B}) \,, \tag{C.1}$$

where η is the constant resistivity of the medium. It provides a good approximation to the real world in the limit of vanishing gas pressure when the magnetic field obeys the force-free condition $(\vec{\nabla} \times \vec{B}) \times \vec{B} = 0$. Thus, one is led to consider magnetic fields of the form

$$\vec{\nabla} \times \vec{B} = a\vec{B} \,, \tag{C.2}$$

where $a(\vec{x},t)$ is a scalar function satisfying the special relation

$$(\vec{B} \cdot \vec{\nabla})a = 0 \tag{C.3}$$

so that the source free Maxwell equation $\vec{\nabla} \cdot \vec{B} = 0$ is obeyed. The case of constant a in a static medium is trivial and corresponds to an exponentially decaying field satisfying the linear equation $\partial \vec{B}/\partial t + \eta a^2 \vec{B} = 0$. In the following we will be concerned with magnetic fields with non-constant a.

The relations (C.1), (C.2) and (C.3) form, in general, a non-linear coupled system of seven equations for seven unknown $(\vec{B}, \vec{v}, a)$ that fully determine the resistive diffusion of a force-free magnetic field in passive medium. Here we consider their reduction to one spatial direction, say z, by assuming that the magnetic field takes the special form

$$\vec{B}(z,t) = (B_0 \cos\beta(z,t),\ B_0 \sin\beta(z,t),\ 0) \,, \tag{C.4}$$

JHEP06(2007)057

where B_0 is constant that can be set equal to 1, whereas the velocity in the medium is taken to be

$$\vec{v} = (0,\ 0,\ v_z(z,t))\,. \tag{C.5}$$

Then, the magneto-hydrodynamic equations reduce to the following simpler system for the unknown functions β and v_z,

$$\eta\left(\frac{\partial\beta}{\partial z}\right)^2 + \frac{\partial v_z}{\partial z} = 0\,, \tag{C.6}$$

$$\frac{\partial\beta}{\partial t} - \eta\frac{\partial^2\beta}{\partial z^2} + v_z\frac{\partial\beta}{\partial z} = 0\,, \tag{C.7}$$

whereas the function a, which is also considered as function of z and t, is determined by

$$a(z,t) = -\frac{\partial\beta}{\partial z}\ . \tag{C.8}$$

Thus, one is only left to determine β and v_z.

Considering $v_z(z,t)$ as function of $\beta(z,t)$ and t, and defining the quantity

$$H(\beta,t) = \frac{\partial v_z(\beta,t)}{\partial\beta}\,, \tag{C.9}$$

it follows that the system of equations (C.6) and (C.7) take the equivalent form

$$\eta\frac{\partial\beta}{\partial z} + H(\beta,t) = 0\,, \tag{C.10}$$

$$\eta\frac{\partial H}{\partial t} = H^2\left(\frac{\partial^2 H}{\partial\beta^2} + H\right). \tag{C.11}$$

According to the ansatz (C.4), the magnetic field $\vec{B}(\vec{x},t)$ is uniform on the $z=$ constant planes and changes direction as one moves across these planes. Close inspection with the mean curvature flow of planar curves shows that $-z/\eta$ represents the arc-length of a virtual curve, as measured from the origin of coordinates, $z=0$, β is the slope and $H(\beta)$ the extrinsic curvature at each point of the curve. The magnetic field on the $z=$ constant planes, $B_0(\cos\beta,\ \sin\beta)$, provides the tangent vector to such curves at different points and the function $a(z)$ equals to H/η. Finally, the velocity of the medium, $v_z(z)$, is nothing else but the (Euler-Bernoulli) elastic energy of the curve segment of length z/η, assuming that the velocity vanishes at $z=0$. Then, in this context, the evolution equation (C.11) coincides with equation (3.13) for the extrinsic curvature of the deforming virtual curve with respect to the rescaled time t/η. Any solution of the mean curvature flow gives rise to a process for the resistive diffusion of force-free magnetic fields in R^3.

A typical initial value problem for these equations is defined by the following conditions

$$\beta(z,0) = -\beta(-z,0)\,, \qquad \frac{\partial\beta(z,0)}{\partial z} > 0 \tag{C.12}$$

for $t=0$, as $-\infty < z < \infty$, together with the boundary conditions

$$\beta(\pm\infty,t) = \pm\beta_0 \tag{C.13}$$

JHEP06(2007)057

for all $t \geq 0$, having finite β_0 independent of t; the initial and boundary conditions for $v_z(z,t)$ follow from equation (C.6). The direction of $\vec{B}$ is held fixed at $z = \pm\infty$ for all time by the above boundary conditions, experiencing an overall rotation by $2\beta_0$ from one end to the other. An interesting question that arises in this context, and has applications in modeling the eruption of solar flares, is to determine the conditions under which $H(\beta, t)$ becomes infinite at some time. According to the analysis of ref. [54], a modest criterion is provided by comparing $2\beta_0$ to π. If $2\beta_0 < \pi$, $\vec{B}(z,t)$ will evolve toward a uniform field irrespective of the initial value $\beta(z,0)$. If $2\beta_0 > \pi$, $\vec{B}(z,t)$ will develop infinite field gradient after some time, irrespective of the initial value $\beta(z,0)$, thus leading to infinite H by equation (C.10). The marginal case $2\beta_0 = \pi$ includes the steady state solution

$$\vec{B}(z) = (\pm B_0 \ \mathrm{sech}(Az),\ B_0 \ \tanh(Az),\ 0)\,, \tag{C.14}$$

$$v_z(z) = -\eta A \ \tanh(Az)\,, \qquad a(z) = \mp A \ \mathrm{sech}(Az) \tag{C.15}$$

that corresponds to the translating soliton of the mean curvature flow on the plane.

It is quite interesting, in many respects, that apart from the translating soliton other simple solutions of these equations were constructed in ref. [54], including the paper-clip model (in modern language). Scaling solutions (self-shrinkers and expanders) were also investigated there to some extend. There is appropriate mention to them in the main text of our paper.

References

[1] A.M. Polyakov, *Interaction of Goldstone particles in two dimensions. Applications to ferromagnets and massive Yang-Mills fields*, *Phys. Lett.* **B 59** (1975) 79; *Gauge fields and strings*, *Contemporary Concepts in Physics*, vol. 3, Harwood Academic Publishers, Chur (1987).

[2] D. Friedan, *Nonlinear models in two + epsilon dimensions*, *Phys. Rev. Lett.* **45** (1980) 1057; *Nonlinear models in two + epsilon dimensions*, *Ann. Phys. (NY)* **163** (1985) 318.

[3] D.J. Gross and F. Wilczek, *Ultraviolet behavior of non-abelian gauge theories*, *Phys. Rev. Lett.* **30** (1973) 1343;
H.D. Politzer, *Reliable perturbative results for strong interactions?*, *Phys. Rev. Lett.* **30** (1973) 1346.

[4] E.S. Fradkin and A.A. Tseytlin, *Effective field theory from quantized strings*, *Phys. Lett.* **B 158** (1985) 316.

[5] C.G. Callan Jr., E.J. Martinec, M.J. Perry and D. Friedan, *Strings in background fields*, *Nucl. Phys.* **B 262** (1985) 593.

[6] C.G. Callan Jr., I.R. Klebanov and M.J. Perry, *String theory effective actions*, *Nucl. Phys.* **B 278** (1986) 78.

[7] R. Hamilton, *Three-manifolds with positive Ricci curvature*, *J. Diff. Geom.* **17** (1982) 255.

[8] B. Chow and D. Knopf, *The Ricci flow: an introduction*, *Mathematical Surveys and Monographs*, vol. 110, American Mathematical Society, Providence (2004).

JHEP06(2007)057

[9] H.-D. Cao, B. Chow, S.-C. Chu and S.-T. Yau eds, *Collected papers on Ricci flow*, Series in Geometry and Topology, vol. 37, International Press, Somerville (2003).

[10] G. Perelman, *The entropy formula for the Ricci flow and its geometric applications*, preprint, `math.DG/0211159`; *Ricci flow with surgery on three-manifolds*, `math.DG/0303109`; *Finite extinction time for the solutions to the Ricci flow on certain three-manifolds*, `math.DG/0307245`.

[11] J. Morgan, *Recent progress on the Poincaré conjecture and the classification of 3-manifolds*, *Bull. Amer. Math. Soc.* **42** (2005) 57.

[12] H. Levine, S.B. Libby and A.M.M. Pruisken, *Electron delocalization by a magnetic field in two-dimensions*, *Phys. Rev. Lett.* **51** (1983) 1915;
D.E. Khmel'nitskii, *Quantization of Hall conductivity*, *Sov. Phys. JETP* **38** (1983) 552;
V.G. Knizhnik and A. Morozov, *Renormalization of topological charge*, *Sov. Phys. JETP* **39** (1984) 240.

[13] I. Affleck and F.D.M. Haldane, *Critical theory of quantum spin chains*, *Phys. Rev.* **B 36** (1987) 5291;
R. Shankar and N. Read, *The $\theta = \pi$ nonlinear sigma model is massless*, *Nucl. Phys.* **B 336** (1990) 457.

[14] W.W. Mullins, *Two-dimensional motion of idealized grain boundaries*, *J. Appl. Phys.* **27** (1956) 900.

[15] W.W. Mullins, *Theory of thermal grooving*, *J. Appl. Phys.* **28** (1957) 333.

[16] K. Brakke, *The motion of a surface by its mean curvature*, Princeton University Press, Princeton, New Jersey (1978).

[17] K.-S. Chou and X.-P. Zhu, *The curve shortening problem*, Chapman and Hall/CRC, Boca Raton (2001).

[18] X.-P. Zhu, *Lectures on mean curvature flows*, Studies in Advanced Mathematics, vol. 32, International Press, Somerville (2002).

[19] K. Ecker, *Regularity theory for mean curvature flow*, Progress in Nonlinear Differential Equations and Their Applications, vol. 57, Birkhäuser, Boston (2004).

[20] T. Ohta, D. Jasnow and K. Kawasaki, *Universal scaling in the motion of random interfaces*, *Phys. Rev. Lett.* **49** (1982) 1223;
R. Brower, D. Kessler, J. Koplik and H. Levine, *Geometrical models of interface evolution*, *Phys. Rev. A* **29** (1984) 1335.

[21] S.A. Langer, R.E. Goldstein and D.P. Jackson, *Dynamics of labyrinthine pattern formation in magnetic fluids*, *Phys. Rev. A* **46** (1992) 4894.

[22] S. Smith, M. Broucke and B. Francis, *Curve shortening and the rendezvous problem for mobile autonomous robots*, arXiv preprint cs.RO/0605070.

[23] G. Huisken and T. Ilmanen, *The inverse mean curvature flow and the Riemannian Penrose inequality*, *J. Diff. Geom.* **59** (2001) 353;
H. Bray, *Proof of the Riemannian Penrose inequality using the positive mass theorem*, *J. Diff. Geom.* **59** (2001) 177.

[24] R.G. Leigh, *Dirac-Born-Infeld action from Dirichlet σ-model*, *Mod. Phys. Lett.* **A 4** (1989) 2767.

JHEP06(2007)057

[25] I. Bakas, *Renormalization group equations and geometric flows*, hep-th/0702034.

[26] S.L. Lukyanov and A.B. Zamolodchikov, *Integrable circular brane model and Coulomb charging at large conduction*, *J. Stat. Mech.* **0405** (2004) P003 [hep-th/0306188].

[27] S.L. Lukyanov, E.S. Vitchev and A.B. Zamolodchikov, *Integrable model of boundary interaction: the paperclip*, *Nucl. Phys.* **B 683** (2004) 423 [hep-th/0312168].

[28] S.L. Lukyanov, A.M. Tsvelik and A.B. Zamolodchikov, *Paperclip at $\theta = \pi$*, *Nucl. Phys.* **B 719** (2005) 103 [hep-th/0501155].

[29] S.L. Lukyanov and A.B. Zamolodchikov, *Dual form of the paperclip model*, *Nucl. Phys.* **B 744** (2006) 295 [hep-th/0510145].

[30] V.A. Fateev and S.L. Lukyanov, *Boundary RG flow associated with the AKNS soliton hierarchy*, *J. Phys.* **A 39** (2006) 12889 [hep-th/0510271].

[31] S.L. Lukyanov, *Notes on parafermionic QFT's with boundary interaction*, hep-th/0606155.

[32] J.L. Cardy, *Boundary conditions, fusion rules and the Verlinde formula*, *Nucl. Phys.* **B 324** (1989) 581;
N. Ishibashi, *The boundary and crosscap states in conformal field theories*, *Mod. Phys. Lett.* **A 4** (1989) 251.

[33] E.S. Fradkin and A.A. Tseytlin, *Nonlinear electrodynamics from quantized strings*, *Phys. Lett.* **B 163** (1985) 123;
A.A. Tseytlin, *Vector field effective action in the open superstring theory*, *Nucl. Phys.* **B 276** (1986) 391.

[34] A. Abouelsaood, C.G. Callan Jr., C.R. Nappi and S.A. Yost, *Open strings in background gauge fields*, *Nucl. Phys.* **B 280** (1987) 599.

[35] C.G. Callan Jr., C. Lovelace, C.R. Nappi and S.A. Yost, *String loop corrections to beta functions*, *Nucl. Phys.* **B 288** (1987) 525.

[36] G. Curci and G. Paffuti, *Consistency between the string background field equation of motion and the vanishing of the conformal anomaly*, *Nucl. Phys.* **B 286** (1987) 399.

[37] N. Wyllard, *Derivative corrections to D-brane actions with constant background fields*, *Nucl. Phys.* **B 598** (2001) 247 [hep-th/0008125]; *Derivative corrections to the D-brane Born-Infeld action: non-geodesic embeddings and the Seiberg-Witten map*, *JHEP* **08** (2001) 027 [hep-th/0107185].

[38] V.S. Rychkov, *Wilson loops, D-branes and reparametrization path-integrals*, *JHEP* **12** (2002) 068 [hep-th/0204250].

[39] A. Barabanschikov, *Boundary sigma-model and corrections to D-brane actions*, *Phys. Rev.* **D 67** (2003) 106001 [hep-th/0301012].

[40] K. Ecker, D. Knopf, L. Ni and P. Topping, *Local monotonicity and mean value formulas for evolving Riemannian manifolds*, math.DG/0608470.

[41] V.A. Fateev, E. Onofri and A.B. Zamolodchikov, *Integrable deformations of $O(3)$ sigma model. The sausage model*, *Nucl. Phys.* **B 406** (1993) 521.

[42] T. Oliynyk, V. Suneeta and E. Woolgar, *A gradient flow for worldsheet nonlinear sigma models*, *Nucl. Phys.* **B 739** (2006) 441 [hep-th/0510239].

JHEP06(2007)057

[43] A.A. Tseytlin, *On sigma model RG flow, 'central charge' action and Perelman's entropy*, *Phys. Rev.* **D 75** (2007) 064024 [hep-th/0612296].

[44] A.B. Zamolodchikov, *Irreversibility of the flux of the renormalization group in a 2-D field theory*, *JETP Lett.* **43** (1986) 730.

[45] R. Hamilton, *The formation of singularities in the Ricci flow*, *Surveys in Diff. Geom.* **2** (1995) 7.

[46] M. Gage and R. Hamilton, *The heat equation shrinking convex plane curves*, *J. Diff. Geom.* **23** (1986) 69.

[47] M. Grayson, *The heat equation shrinks embedded plane curves to round points*, *J. Diff. Geom.* **26** (1987) 285.

[48] G. Huisken, *Asymptotic behavior for singularities of the mean curvature flow*, *J. Diff. Geom.* **31** (1990) 285.

[49] S. Angenent, *On the formation of singularities in the curve shortening flow*, *J. Diff. Geom.* **33** (1991) 601.

[50] S. Altschuler, *Singularities of the curve shrinking flow for space curves*, *J. Diff. Geom.* **34** (1991) 491.

[51] R. Hamilton, *The Ricci flow on surfaces*, *Contemp. Math.* **71** (1988) 237.

[52] S. Angenent, *Parabolic equations for curves on surfaces: part II. Intersections, blow-up and generalized solutions*, *Ann. Math.* **133** (1991) 171.

[53] I. Bakas, *Renormalization group flows and continual Lie algebras*, *JHEP* **08** (2003) 013 [hep-th/0307154]; *The algebraic structure of geometric flows in two dimensions*, *JHEP* **10** (2005) 038 [hep-th/0507284].

[54] B.C. Low, *Resistive diffusion of force-free magnetic fields in a passive medium*, *Astrophys. J.* **181** (1973) 209; *Resistive diffusion of force-free magnetic fields in a passive medium. II. A nonlinear analysis of the one-dimensional case*, *Astrophys. J.* **184** (1973) 917.

[55] E. Witten, *On string theory and black holes*, *Phys. Rev.* **D 44** (1991) 314;
G. Mandal, A.M. Sengupta and S.R. Wadia, *Classical solutions of two-dimensional string theory*, *Mod. Phys. Lett.* **A 6** (1991) 1685.

[56] D. Kutasov, *Accelerating branes and the string/black hole transition*, hep-th/0509170.

[57] R. Hamilton, *Harnack estimates for the mean curvature flow*, *J. Diff. Geom.* **41** (1995) 215.

[58] U. Abresch and J. Langer, *The normalized curve shortening flow and homothetic solutions*, *J. Diff. Geom.* **23** (1986) 175.

[59] C.L. Epstein and M.I. Weinstein, *A stable manifold theorem for the curve shortening equation*, *Commun. Pure Appl. Math.* **40** (1987) 119.

[60] K. Hashimoto and S. Nagaoka, *Recombination of intersecting D-branes by local tachyon condensation*, *JHEP* **06** (2003) 034 [hep-th/0303204];
F.T.J. Epple and D. Lüst, *Tachyon condensation for intersecting branes at small and large angles*, *Fortschr. Phys.* **52** (2004) 367 [hep-th/0311182].

JHEP06(2007)057

[61] A. Adams, J. Polchinski and E. Silverstein, *Don't panic! Closed string tachyons in ALE space-times*, *JHEP* **10** (2001) 029 [hep-th/0108075];
M. Gutperle, M. Headrick, S. Minwalla and V. Schomerus, *Space-time energy decreases under world-sheet RG flow*, *JHEP* **01** (2003) 073 [hep-th/0211063].

[62] J.W. Dabrowska, A. Khare and U.P. Sukhatme, *Explicit wavefunctions for shape-invariant potentials by operator techniques*, *J. Phys.* **A 21** (1988) L195;
A. Khare and U.P. Sukhatme, *Scattering amplitudes for supersymmetric shape-invariant potentials by operator methods*, *J. Phys.* **A 21** (1988) 501.

[63] W. Magnus and S. Winkler, *Hill's Equation*, Dover, New York (1979)

[64] T. Kwok-Keung Au, *On the saddle point property of Abresch-Langer curves under the curve shortening flow*, math.AP/0102088.

[65] L. Kauffman, *Knots and Physics*, third edition, World Scientific, Singapore (2001).

[66] N. Hungerbühler and K. Smoczyk, *Soliton solutions for the mean curvature flow*, *Diff. Int. Eq.* **13** (2000) 1321.

[67] S. Angenent, *Shrinking doughnuts*, in *Nonlinear diffusion equations and their equilibrium states, 3*, ed. N.G. Lloyd, W.M. Ni, L.A. Peletier and J. Serrin, Birkhäuser, Boston (1992).

[68] I. Affleck and A.W.W. Ludwig, *Universal noninteger 'ground state degeneracy' in critical quantum systems*, *Phys. Rev. Lett.* **67** (1991) 161.

[69] D. Friedan and A. Konechny, *On the boundary entropy of one-dimensional quantum systems at low temperature*, *Phys. Rev. Lett.* **93** (2004) 030402 [hep-th/0312197].

[70] M.R. Gaberdiel, *D-branes from conformal field theory*, hep-th/0201113.

[71] C. Bachas and M. Gaberdiel, *Loop operators and the Kondo problem*, *JHEP* **11** (2004) 065 [hep-th/0411067].

[72] L. Eisenhart, *Riemannian geometry*, Princeton University Press, Princeton, New Jersey (1964).

[73] R.E. Goldstein and D.M. Petrich, *The Korteweg-de Vries hierarchy as dynamics of closed curves in the plane*, *Phys. Rev. Lett.* **67** (1991) 3203;
K. Nakayama, H. Segur and M. Wadati, *Integrability and the motion of curves*, *Phys. Rev. Lett.* **69** (1992) 2603.

JHEP06(2007)057